Article

Probiotic neoantigen delivery vectors for precision cancer immunotherapy

https://doi.org/10.1038/s41586-024-08033-4

Received: 28 September 2023

Accepted: 6 September 2024

Published online: 16 October 2024

Open access

Check for updates

Andrew Redenti[1,2,5], Jongwon Im[2,5], Benjamin Redenti[1], Fangda Li[1], Mathieu Rouanne[1], Zeren Sheng[2], William Sun[2], Candice R. Gurbatri[2], Shunyu Huang[2], Meghna Komaranchath[2], YoungUk Jang[2], Jaeseung Hahn[2], Edward R. Ballister[1,2], Rosa L. Vincent[2], Ana Vardoshivilli[2], Tal Danino[2,3,4] ✉ & Nicholas Arpaia[1,3] ✉

Microbial systems have been synthetically engineered to deploy therapeutic payloads in vivo[1,2]. With emerging evidence that bacteria naturally home in on tumours[3,4] and modulate antitumour immunity[5,6], one promising application is the development of bacterial vectors as precision cancer vaccines[2,7]. Here we engineered probiotic *Escherichia coli* Nissle 1917 as an antitumour vaccination platform optimized for enhanced production and cytosolic delivery of neoepitope-containing peptide arrays, with increased susceptibility to blood clearance and phagocytosis. These features enhance both safety and immunogenicity, achieving a system that drives potent and specific T cell-mediated anticancer immunity that effectively controls or eliminates tumour growth and extends survival in advanced murine primary and metastatic solid tumours. We demonstrate that the elicited antitumour immune response involves recruitment and activation of dendritic cells, extensive priming and activation of neoantigen-specific $CD4^+$ and $CD8^+$ T cells, broader activation of both T and natural killer cells, and a reduction of tumour-infiltrating immunosuppressive myeloid and regulatory T and B cell populations. Taken together, this work leverages the advantages of living medicines to deliver arrays of tumour-specific neoantigen-derived epitopes within the optimal context to induce specific, effective and durable systemic antitumour immunity.

Bacteria support activation of both innate and adaptive immunity through their inherent foreignness and immunostimulatory properties[8]. These features, coupled with the ease to synthetically engineer bacteria for safe delivery of immunomodulatory compounds, make them ideal vectors to augment and direct antitumour immune responses[1,2]. Tumour neoantigens are attractive immunotherapeutic payloads for delivery; these antigenic species are not present in other tissues, pose minimal risk for inducing autoimmunity, and are theoretically excluded from central immunologic tolerance mechanisms[9]. So far, a variety of tumour neoantigen vaccines have demonstrated promising immunologic responses and survival benefit in clinical trials, although benefit remains limited to only a subset of patients[10–12]. In this regard, programming bacteria with genetic directives to release high levels of identified tumour neoantigens thereby provides a system to precisely instruct neoantigen targeting in situ. Here we describe new microbial immunotherapy vectors that stimulate effective and durable tumour antigen-specific immunity and inhibit immunosuppressive mechanisms that may otherwise limit traditional neoantigen vaccines[13].

Engineering microbial cancer vaccines

To enable effective cancer vaccination, we developed an engineered bacterial system in probiotic *Escherichia coli* Nissle 1917 (EcN) to enhance expression, delivery and immune-targeting of arrays of tumour exonic mutation-derived epitopes highly expressed by tumour cells and predicted to bind major histocompatibility complex (MHC) class I and II (Fig. 1a). This system incorporates several key design elements that enhance therapeutic use: (1) optimization of synthetic neoantigen construct form with (2) removal of cryptic plasmids and deletion of Lon and OmpT proteases to increase neoantigen accumulation, (3) increased susceptibility to phagocytosis for enhanced uptake by antigen-presenting cells (APCs) and presentation of MHC class II-restricted antigens, (4) expression of listeriolysin O (LLO) to induce cytosolic entry for presentation of recombinant encoded neoantigens by MHC class I molecules and T helper 1 cell (T_H1)-type immunity and (5) improved safety for systemic administration due to reduced survival in the blood and biofilm formation.

To assemble a repertoire of neoantigens, we conducted exome and transcriptome sequencing of subcutaneous CT26 tumours. Neoantigens were predicted from highly expressed tumour-specific mutations using established methods[14,15], with selection criteria inclusive of putative neoantigens across a spectrum of MHC affinity[16,17]. Given the importance of both MHC class I and MHC class II binding epitopes in antitumour immunity[15,18,19], we integrated a measure of wild-type-to-mutant MHC affinity ratio—termed agretopicity[17,20]—for both epitope types derived from a given mutation, to help estimate

[1]Department of Microbiology & Immunology, Vagelos College of Physicians and Surgeons of Columbia University, New York, NY, USA. [2]Department of Biomedical Engineering, Columbia University, New York, NY, USA. [3]Herbert Irving Comprehensive Cancer Center, Columbia University, New York, NY, USA. [4]Data Science Institute, Columbia University, New York, NY, USA. [5]These authors contributed equally: Andrew Redenti, Jongwon Im. ✉e-mail: td2506@columbia.edu; na2697@cumc.columbia.edu

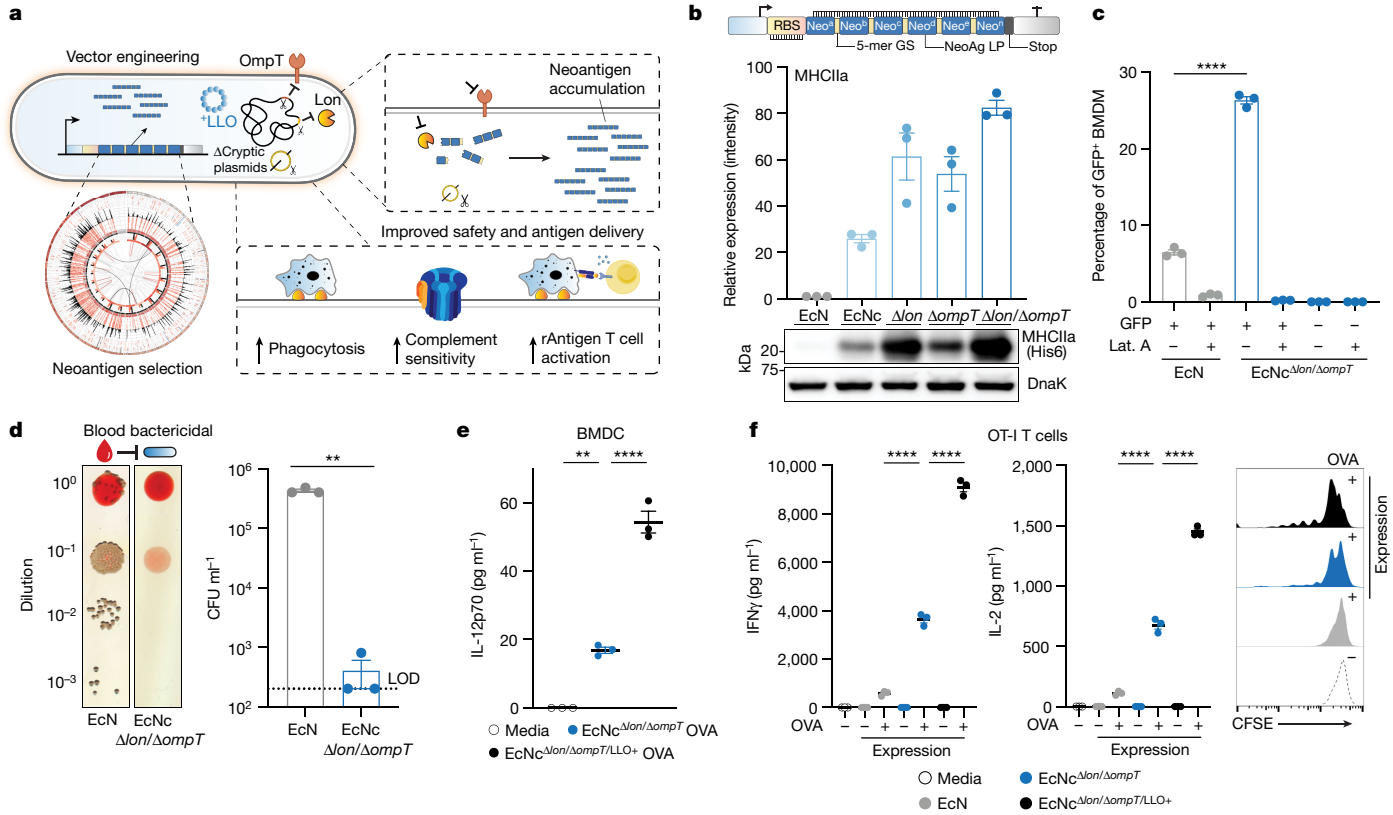

Fig. 1 | Engineering live microbial tumour neoantigen vaccines. a, Design of microbial tumour neoantigen vaccines, with a Circos plot of CT26 mutanome. **b**, Top, an optimized synthetic neoantigen construct schematic. Middle, relative immunoblot chemiluminescent intensity of neoantigen construct MHCIIa expressed from EcN versus derivative strains ($n = 3$ biological replicates per group). Bottom, a representative immunoblot of neoantigen construct MHCIIa expression in a designated strain. **c**, Percentage of GFP$^+$ BMDMs after incubation with EcN or EcNc$^{\Delta lon/\Delta ompT}$ expressing constitutive GFP ($n = 3$ biological replicates per group, $^{****}P < 0.0001$, two-sided unpaired Student's t-test); Lat. A, latrunculin A. **d**, Left, a representative image of EcN or EcNc$^{\Delta lon/\Delta ompT}$ spotted on an LB agar plate after incubation in human blood. Right, a microbial burden in colony-forming units (CFU) per ml (CFU ml^{-1}) ($n = 3$ biological replicates per group, $^{**}P = 0.0039$, two-sided unpaired Student's t-test with Welch's correction). Limit of detection (LOD) was 2×10^2 CFU ml^{-1}. **e**, IL-12p70 quantification in culture supernatants of pulsed BMDCs ($n = 3$ biological replicates per group, $^{**}P = 0.0018$, $^{****}P < 0.0001$, one-way ANOVA with Tukey's multiple comparisons test). **f**, Naive OT-I T cells were incubated with pulsed BMDCs. Left, IFNγ quantification of supernatants of OT-I cultures ($n = 3$ biological replicates per group, $^{****}P < 0.0001$, one-way ANOVA with Tukey's multiple comparisons test). Middle, IL-2 quantification of supernatants of OT-I cultures ($n = 3$ biological replicates per group, $^{****}P < 0.0001$, one-way ANOVA with Tukey's multiple comparisons test). Right, a representative histogram of carboxyfluorescein succinimidyl ester (CFSE) dilution-stimulated OT-I T cells. **b**–**f**, Data are mean ± s.e.m. Gel source data are in Supplementary Figs. 1 and 2.

the ability of adaptive immunity to recognize a neoantigen. Predicted neoantigens were selected from the set of tumour-specific mutations satisfying all criteria, notably encompassing numerous recovered, previously validated CT26 neoantigens[15] (Extended Data Fig. 1a).

We then sought to create a microbial system that could accommodate the production and delivery of diverse sets of neoantigens to lymphoid tissue and the tumour microenvironment (TME). For the purpose of assessing neoantigen production capacity, a prototype gene encoding a synthetic neoantigen construct (NeoAg^P) was created by concatenating long peptides encompassing linked CD4$^+$ and CD8$^+$ T cell mutant epitopes—previously shown as an optimal form for stimulating cellular immunity[21]—derived from CT26 neoantigens (Extended Data Fig. 1b and Extended Data Table 1). The construct was cloned into a stabilized plasmid[22] under constitutive expression and transformed into EcN; however, both immunoblot and enzyme-linked immunosorbent assay (ELISA) assessment showed low production of the prototype construct by EcN across several tested promoters (Extended Data Fig. 1c).

Given the dependency on antigen dosage for establishing an effective and immunodominant antigen-specific immune response[23–25], we developed a system for improved recombinant neoantigen construct production. The incorporation of 5-mer glycine-serine linkers between neoantigen long peptides in the prototype increased expression roughly sixfold (Extended Data Fig. 1c,d). Conversely, expressing only minimal neoepitopes, decreasing the number of neoantigen long peptides in a construct or incorporating 10-mer glycine-serine or immunoprotease-sensitive linkers did not improve production (Extended Data Fig. 1e). To evaluate the capacity of constructs with 5-mer glycine-serine linkers to accommodate production of various neoantigens, and for eventual in vivo testing, we created three more constructs with unique neoantigens from the predicted set, selected on a spectrum of predicted affinity for MHC class I and MHC class II (MHCIa, MHCIIa, MHCI/II^v) (Extended Data Table 1). Neoantigens were grouped on the basis of high predicted affinity for MHC-I (MHCIa) or MHC-II (MHCIIa) or low–moderate affinity for MHC-I or MHC-II (MHCI/II^v). Prototype and new construct expression were evaluated in EcN versus BL21, a strain that harbours chromosomal deletions of the Lon (Δ*lon*) and OmpT (Δ*ompT*) proteases to facilitate recombinant protein production[26]. Unlike BL21, EcN also bears cryptic plasmids that can suppress the copy number of transformed recombinant plasmids[27]. Indeed, on average, BL21 produced tenfold higher levels of neoantigen construct relative to EcN (Extended Data Fig. 1f). Thus, to further enhance construct expression in EcN, we performed sequential synthetic modifications of the microbe. Removal of the EcN cryptic plasmids led to maintenance of roughly 30-fold higher levels of therapeutic plasmid DNA (EcNc) (Extended Data Fig. 2a), with successive deletion of the Lon protease (EcNc$^{\Delta lon}$), OmpT protease (EcNc$^{\Delta ompT}$) or both proteases

(EcNc$^{\Delta lon/\Delta ompT}$) allowing up to 80-fold increased production of synthetic neoantigen constructs relative to the parental EcN strain (Fig. 1b and Extended Data Fig. 2b,c).

As the Lon protease has been connected to capsule and biofilm regulation[28,29], and OmpT with the degradation of complement[30], we tested the susceptibility of the engineered vector EcNc$^{\Delta lon/\Delta ompT}$ to phagocytosis and blood clearance, as well as for its proficiency in biofilm formation. Notably, EcNc$^{\Delta lon/\Delta ompT}$ was fourfold more susceptible to phagocytosis by bone marrow-derived macrophages (BMDMs) relative to EcN (Fig. 1c). Incubation in human blood further revealed a 1000-fold greater sensitivity to blood clearance for EcNc$^{\Delta lon/\Delta ompT}$ versus EcN (Fig. 1d). Moreover, EcNc$^{\Delta lon/\Delta ompT}$ was significantly attenuated in biofilm formation, a major mechanism of microbial resistance to immunity and antimicrobial agents in humans[31] (Extended Data Fig. 2d).

As an antitumour vaccine, the microbial platform must also facilitate presentation of recombinant antigens and activation of APCs. To evaluate the system in this capacity, the model antigen ovalbumin (OVA) was expressed in the cytosol of EcNc$^{\Delta lon/\Delta ompT}$ using a strategy analogous to that used for synthetic neoantigen constructs. BMDMs pulsed with EcNc$^{\Delta lon/\Delta ompT}$ OVA, but not EcN-OVA, presented the H2K^{b}-SIINFEKL complex, indicating efficient processing and cross-presentation of recombinant antigens from EcNc$^{\Delta lon/\Delta ompT}$ (Extended Data Fig. 2e). Furthermore, pulsed BMDMs upregulated MHC class II and CD80, and downregulated PD-L1, demonstrating effective APC activation by EcNc$^{\Delta lon/\Delta ompT}$ expressing a recombinant antigen (Extended Data Fig. 2e,f).

To refine the immune program orchestrated by APCs, we reasoned that constitutive coexpression of LLO—a pH-dependent pore-forming protein derived from *Listeria* that permeabilizes the phagolysosomal membrane—would facilitate cytosolic delivery of encoded neoantigens for presentation to CD8^{+} T cells[32], enhance IL-12 production[33,34] and promote induction of T_H1 immunity[35]. Of note, engineered microbes produced functional LLO, and LLO expression did not affect viability of APCs incubated with LLO-expressing strains (EcNc$^{\Delta lon/\Delta ompT/LLO+}$) or the coexpression of neoantigen constructs (Extended Data Fig. 2g,h). Immunofluorescence microscopy of BMDMs co-incubated with either live EcNc$^{\Delta lon/\Delta ompT}$ OVA or EcNc$^{\Delta lon/\Delta ompT/LLO+}$ OVA confirmed that LLO coexpression enabled recombinant antigen escape into the cytosol (Extended Data Fig. 2i). Bone marrow-derived dendritic cells (BMDCs) pulsed with live EcNc$^{\Delta lon/\Delta ompT/LLO+}$ OVA secreted threefold higher levels of IL-12p70 compared to those pulsed with EcNc$^{\Delta lon/\Delta ompT}$ OVA (Fig. 1e), indicating greater T_H1 instruction by APCs. Moreover, BMDCs pulsed with live EcNc$^{\Delta lon/\Delta ompT/LLO+}$ OVA mediated superior activation of naive OT-I and OT-II T cells, with 2–2.5-fold increased secretion of interferon-γ (IFNγ) and interleukin-2 (IL-2) from both T cell types relative to EcNc$^{\Delta lon/\Delta ompT}$ OVA, and marked proliferation of both OT-I and OT-II T cells (Fig. 1f and Extended Data Fig. 2j). Conversely, BMDCs pulsed with wild-type EcN-OVA induced no measurable proliferation of either T cell type, 13–15-fold lower secretion of IL-2 and IFNγ from OT-I T cells, and no detectable cytokine secretion from OT-II T cells (Fig. 1f and Extended Data Fig. 2j). Taken together, these data suggest recombinant antigens expressed in EcNc$^{\Delta lon/\Delta ompT/LLO+}$ lead to potent antigen-specific activation of both naive cytotoxic and helper T cells, with incorporation of LLO facilitating both enhanced presentation to CD8^{+} T cells and T_H1-type immunity.

Overall, synthetic neoantigen construct optimization and genetic engineering achieved a microbial platform (EcNc$^{\Delta lon/\Delta ompT/LLO+}$) capable of robust production across diverse sets of tumour neoantigens, which was attenuated in immune-resistance mechanisms, effectively taken up by and proficient in activating APCs, and able to drive potent activation of T cells specific for encoded recombinant antigens to support enhanced cellular immunity.

Treatment of colorectal cancer

To assess the in vivo efficacy of the engineered system, BALB/c mice bearing advanced CT26 tumours on a single hind flank received an intratumoural injection of EcN wild-type, EcNc$^{\Delta lon/\Delta ompT}$ or EcNc$^{\Delta lon/\Delta ompT/LLO+}$ strains. These strains were tested either without any neoantigen plasmid (NC), expressing a single neoantigen construct (MHCIa, MHCIIa, MHCI/II$^{\gamma}$), or as a combination of the three neoantigen construct-expressing strains in equal parts: a microbial antitumour vaccine delivering 19 total unique neoantigens (nAg^{19}). Notably, no difference in tumour colonization efficiency was observed for EcNc$^{\Delta lon/\Delta ompT}$ strains compared to wild-type EcN (Extended Data Fig. 3a,b). Whereas intratumoural treatment with wild-type EcN expressing any neoantigen construct did not demonstrate therapeutic benefit (Extended Data Fig. 3c,d), a single intratumoural injection of EcNc$^{\Delta lon/\Delta ompT/LLO+}$ nAg^{19} provided strong antitumour efficacy, with a complete response observed for three out of seven tumours and the combination nAg^{19} more effective than each construct alone (Fig. 2a and Extended Data Fig. 3e–g). Moreover, treatment with EcNc$^{\Delta lon/\Delta ompT}$ and EcNc$^{\Delta lon/\Delta ompT/LLO+}$ strains was well-tolerated, with significantly attenuated body weight change compared to wild-type EcN, and no significant body weight differences compared to PBS treatment over the course of observation (Extended Data Fig. 4a). Direct comparisons of intratumoural treatment with EcNc$^{\Delta lon/\Delta ompT/LLO+}$ nAg^{19} versus EcNc$^{\Delta lon/\Delta ompT}$ nAg^{19} showed that the inclusion of LLO significantly enhanced tumour control and extended survival (Fig. 2a and Extended Data Fig. 4b–d). Assessment of intratumoural IL-12p70 levels demonstrated that inclusion of LLO also significantly enhanced IL-12p70 levels in tumours, suggestive of enhanced T_H1 instruction in vivo (Fig. 2b). Thus, the combination of all synthetic modifications (EcNc$^{\Delta lon/\Delta ompT/LLO+}$ nAg^{19}) synergized to produce a microbial antitumour vaccine with favourable toxicity profile and strong therapeutic effect in vivo.

To evaluate the induction of systemic antitumour immunity after treatment with the microbial neoantigen vaccines, mice with established CT26 tumours on both hind flanks were treated with an injection of microbes into a single tumour. Whereas treatment with EcNc$^{\Delta lon/\Delta ompT/LLO+}$ without neoantigen expression (NC) did not suppress tumour growth, a single injection of EcNc$^{\Delta lon/\Delta ompT/LLO+}$ nAg^{19} induced tumour control and complete regression of two out of six treated and untreated tumours (Extended Data Fig. 4e). Microbial quantification from tumours 14 days after injection showed that microbes colonized treated tumours at high densities, with no bacteria able to be cultured from untreated tumours (Extended Data Fig. 4f). This demonstrates that the engineered neoantigen vaccines stimulate systemic antitumour immunity capable of eliminating distant tumours.

We next evaluated the efficacy of our microbial antitumour vaccination platform following intravenous administration, the preferred route of administration as to circumvent dependence on tumour accessibility. Similar to intratumoural treatment, intravenous administration of EcNc$^{\Delta lon/\Delta ompT/LLO+}$ nAg^{19} to mice with advanced CT26 tumours provided potent antitumour efficacy and survival benefit with minimal body weight alteration (Fig. 2b and Extended Data Fig. 5a–c). After intravenous injection, the engineered microbes persisted at high density within tumours and were cleared rapidly from all other surveyed organs (Fig. 2c and Extended Data Fig. 5d).

Given the potent efficacy observed with intravenous treatment, we compared intravenous treatment with the microbial vaccination system to a standard antitumour vaccination strategy using synthetic long peptide (SLP) vaccination[12]. Mice bearing established hind-flank CT26 tumours received subcutaneous injections of SLP vaccination containing the 19 neoantigens (nAg^{19}-SLP), or intravenous injections of PBS, EcNc$^{\Delta lon/\Delta ompT/LLO+}$ expressing the strong irrelevant xenoantigen OVA or EcNc$^{\Delta lon/\Delta ompT/LLO+}$ nAg^{19}. Compared to SLP vaccination, treatment with EcNc$^{\Delta lon/\Delta ompT/LLO+}$ nAg^{19} significantly reduced tumour growth and extended survival, with complete regression of two of eight tumours in the EcNc$^{\Delta lon/\Delta ompT/LLO+}$ nAg^{19}-treated group (Fig. 2e and Extended Data Fig. 5e,f). Increasing the dose of neoantigen SLPs and adjuvant did not enhance the efficacy of SLP vaccination in further comparison trials (Extended Data Fig. 5g).

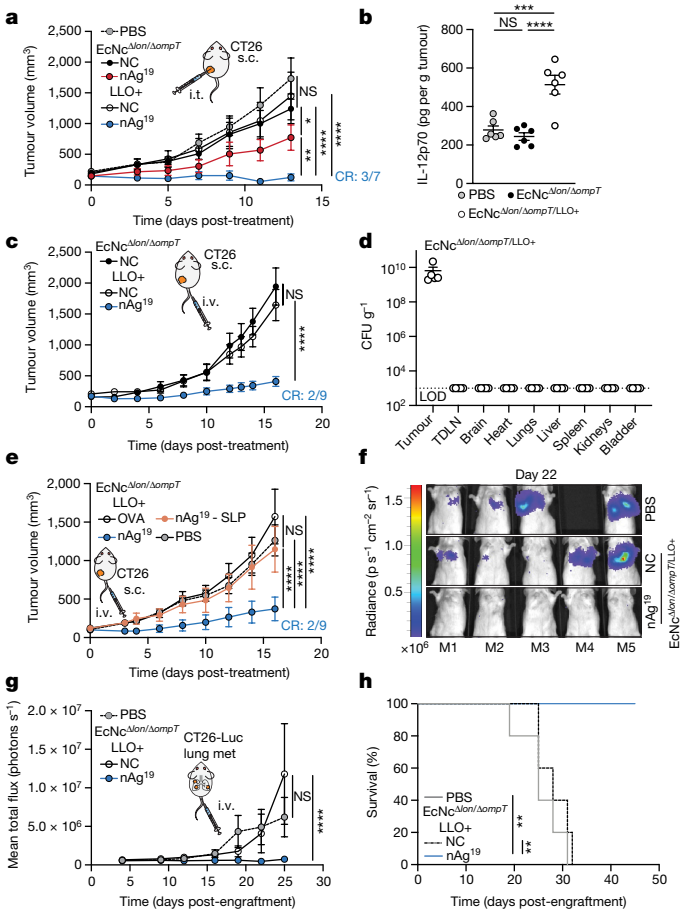

Fig. 2 | Efficacy of microbial tumour neoantigen vaccines in primary and metastatic colorectal carcinoma. a–**e**, BALB/c mice with hind-flank CT26 tumours treated when average tumour volumes were 120–200 mm^3. **a**, Intratumoural (i.t.) treatment on day 0. Tumour growth curves ($n = 5$ mice for PBS and EcNc$^{\Delta lon/\Delta ompT}$ NC, $n = 7$ for other groups, $^*P = 0.0469$, $^{**}P = 0.0096$, $^{****}P < 0.0001$; NS, $P > 0.05$, two-way ANOVA with Tukey's multiple comparisons test). **b**, Intratumoural treatment. Intratumoural IL-12p70 levels ($n = 6$ mice per group, $^{***}P = 0.0004$, $^{****}P < 0.0001$; NS, $P > 0.05$, one-way ANOVA with Tukey's multiple comparisons test). **c**, Intravenous (i.v.) treatment on day 0 and day 8. Tumour growth curves ($n = 9$ mice for nAg^{19}, $n = 8$ for other groups, $^{****}P < 0.0001$; NS, $P > 0.05$, two-way ANOVA with Tukey's multiple comparisons test). **d**, Mice ($n = 5$) received intravenous injection of EcNc$^{\Delta lon/\Delta ompT/LLO+}$. Microbial tissue burden in CFU per gram (CFU g^{-1}), LOD = 1×10^3 CFU g^{-1}. **e**, Intravenous treatment of microbial therapies or PBS, or subcutaneous injections of SLP vaccine every 3–6 days. Tumour growth curves ($n = 8$ mice per group, $^{****}P < 0.0001$; NS, $P > 0.05$, two-way ANOVA with Tukey's multiple comparisons test), **f**–**h**, BALB/c mice with 4 day established CT26-Luc lung metastases. Intravenous treatment every 3–5 days. **f**, Representative lung metastases luminescence. **g**, Mean total flux from lung metastases ($n = 5$ mice per group, $^{****}P > 0.0001$; NS, $P > 0.05$, two-way ANOVA with Dunnett's multiple comparisons test). **h**, Kaplan–Meier survival curve for mice with CT26-Luc lung metastases ($n = 5$ mice per group, $^{**}P = 0.0017$, $^{**}P = 0.0018$, log-rank Mantel–Cox test). **a**–**e**,**g**, Data are mean ± s.e.m. s.c., subcutaneous. CR, complete response.

Having observed robust efficacy in subcutaneous tumours, we then assessed therapeutic efficacy against established metastatic disease. CT26 carcinoma cells with genomically integrated firefly luciferase (CT26-Luc) were injected intravenously, which form rapidly progressive lung metastases traceable by bioluminescence imaging (Extended Data Fig. 5h). Intravenous treatment with PBS, EcNc$^{\Delta lon/\Delta ompT/LLO+}$ without neoantigen expression (NC) or EcNc$^{\Delta lon/\Delta ompT/LLO+}$ nAg^{19} was initiated 4 days after engraftment. We found that engineered microbes colonized metastases-bearing lungs and were not detectable in other tissues (Extended Data Fig. 5i). Microbially treated groups again demonstrated minimal body weight fluctuation, similarly to mice treated with PBS (Extended Data Fig. 5j). Treatment with EcNc$^{\Delta lon/\Delta ompT/LLO+}$ nAg^{19} strongly restrained metastatic growth, with 100% of neoantigen therapeutic-treated mice surviving to 45 days after engraftment, whereas both control groups had completely succumbed to disease (Fig. 2f–h and Extended Data Fig. 5k). This demonstrates both safety and efficacy of intravenously administered EcNc$^{\Delta lon/\Delta ompT/LLO+}$ nAg^{19} in the setting of aggressive, established metastatic disease.

Mechanisms of antitumour immunity

As the engineered microbial neoantigen vaccines are strong immunostimulants and persist within the TME, we reasoned that sustained intratumoural neoantigen production and reduced immunosuppression would facilitate enhanced activation of adaptive immunity to mediate the observed tumour control. To confirm in situ delivery of encoded neoantigens, we intravenously administered EcNc$^{\Delta lon/\Delta ompT/LLO+}$ nAg$^{19\text{-}His}$ (wherein all three neoantigen constructs contain a C-terminal 6×His-tag) and performed immunoblots of tumour and tumour-draining lymph node (TDLN) lysates 2 days following treatment. We observed three His-tagged protein species corresponding to the three encoded neoantigen constructs (Fig. 3a). Immunophenotyping of TDLNs 2 days following intravenous treatment showed significantly higher frequencies of cDC2s in TDLNs of microbial vector-treated mice (Extended Data Fig. 6a). Enhanced frequencies of both CD80$^+$ and CD86$^+$ cDC1s and cDC2s (Fig. 3b,c) were also observed, demonstrating that intravenously delivered microbial vectors recruit and activate dendritic cells within the TDLN. Consistent with delivered neoantigens enhancing T cell activation, ex vivo restimulation of lymphocytes isolated from TDLNs at 8 days post-treatment with phorbol myristate acetate (PMA) and ionomycin showed increased production of IFNγ and TNF by conventional CD4$^+$ (Foxp3$^-$CD4$^+$) and CD8$^+$ T cells in mice treated with EcNc$^{\Delta lon/\Delta ompT/LLO+}$ nAg^{19} versus those treated with PBS or control bacteria (EcNc$^{\Delta lon/\Delta ompT}$) (Extended Data Fig. 6b,c).

Next, to assess the ability for engineered neoantigen therapeutics to drive neoantigen-specific immunity, tumour-infiltrating lymphocytes (TILs) were isolated at 8 days post-treatment and restimulated ex vivo with a pool of synthetic peptides representing the 19 bacterially encoded tumour neoantigens. Flow-cytometric analysis showed increased frequencies of IFNγ secreting conventional Foxp3$^-$CD4$^+$ and CD8$^+$ TILs, demonstrating that treatment with EcNc$^{\Delta lon/\Delta ompT/LLO+}$ nAg^{19} enhanced encoded neoantigen-specific immunity (Fig. 3d). Analysis of TIL reactivity ex vivo demonstrated that several predicted MHC-I and MHC-II binding neoantigens from each neoantigen construct were targeted in EcNc$^{\Delta lon/\Delta ompT/LLO+}$ nAg^{19}-treated mice (Extended Data Fig. 6d). Furthermore, purified TILs from EcNc$^{\Delta lon/\Delta ompT/LLO+}$ nAg^{19}-treated mice were co-incubated with either CT26-Luc or irrelevant tumour cell targets (4T1-Luc) of the same MHC haplotype, demonstrating CT26 tumour cell-specific recognition and killing by generated TILs (Fig. 3e). Compared to peptide stimulation, restimulation with PMA and ionomycin showed even greater levels of IFNγ secreting Foxp3$^-$CD4$^+$ and CD8$^+$ TILs in EcNc$^{\Delta lon/\Delta ompT/LLO+}$ nAg^{19}-treated tumours and IFNγ producing B220$^+$ B cells[36,37], suggestive of epitope spreading and expanded immune activation[38] (Extended Data Fig. 6e,f). Furthermore, we observed increased frequencies of proliferating CD4$^+$ and CD8$^+$ tumour-infiltrating T cells in mice treated with EcNc$^{\Delta lon/\Delta ompT/LLO+}$ nAg^{19} in comparison to treatment with EcNc$^{\Delta lon/\Delta ompT}$ or PBS (Extended Data Fig. 6g). To establish whether microbial neoantigen vaccine treatment generates tumour neoantigen-specific immune memory, we prophylactically vaccinated naive mice with EcNc$^{\Delta lon/\Delta ompT/LLO+}$ OVA or nAg^{19} and grafted CT26 tumours post-vaccination. Tumour growth in mice prophylactically treated with EcNc$^{\Delta lon/\Delta ompT/LLO+}$ nAg^{19} was significantly reduced compared to those treated with EcNc$^{\Delta lon/\Delta ompT/LLO+}$

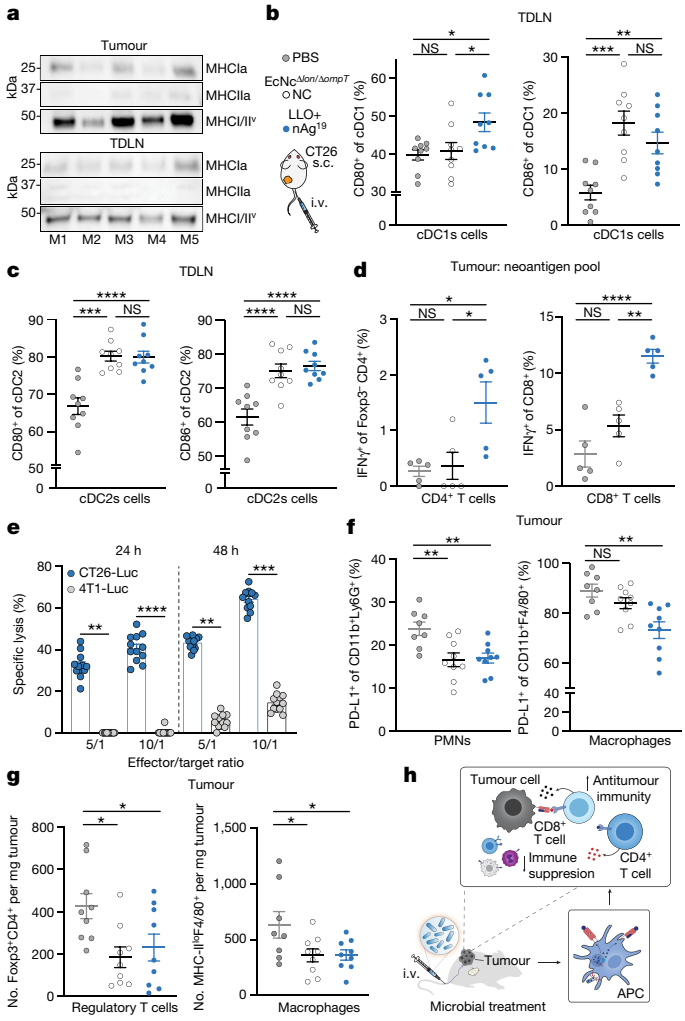

Fig. 3 | Microbial tumour neoantigen vaccines restructure the tumour immune microenvironment. a, Immunoblot of tumours ($n = 5$) and TDLNs ($n = 5$). **b**, Left, the percentage CD80^{+} of cDC1s (*$P = 0.0189$, *$P = 0.0415$; NS, $P > 0.05$). Right, the percentage CD86^{+} of cDC1s (**$P = 0.0061$, ***$P = 0.0002$; NS, $P > 0.05$). **c**, Left, the percentage CD80^{+} of cDC2s (****$P < 0.0001$; NS, $P > 0.05$). Right, the percentage CD86^{+} of cDC2s (***$P = 0.0001$, ****$P < 0.0001$; NS, $P > 0.05$). **d**, Left, the frequency of IFNγ^{+}Foxp3^{-}CD4^{+} ($n = 5$ mice per group, *$P = 0.0238$, *$P = 0.0147$; NS, $P > 0.05$). Right, the frequency of IFNγ^{+}CD8^{+} T cells ($n = 5$ mice per group, **$P = 0.0015$, ****$P < 0.0001$; NS, $P > 0.05$). **e**, CT26 TILs, specific lysis ($n = 12$ mice, **$P = 0.0023$, **$P = 0.0027$, ***$P = 0.001$, ****$P < 0.0001$; NS, $P > 0.05$, Kruskal–Wallis test with Dunn's multiple comparisons test). **f**, Left, the percentage PD-L1^{+} of Ly6G^{+}CD11b^{+} ($n = 8$ mice for PBS, $n = 9$ for other groups, **$P = 0.0037$, **$P = 0.0059$). Right, the percentage PD-L1^{+} of CD11b^{+}F4/80^{+} ($n = 8$ mice for PBS, $n = 9$ for all other groups, **$P = 0.0010$; NS, $P > 0.05$). PMNs, polymorphonuclear cells. **g**, Left, the number of Foxp3^{+}CD4^{+} T cells mg^{-1} ($n = 9$ mice per group *$P = 0.0131$, *$P = 0.0241$). Right, the number of MHC-II^{lo}F4/80^{+} CD11b^{+} macrophages per mg ($n = 8$ mice for PBS, $n = 9$ for other groups, *$P = 0.0385$, *$P = 0.0407$). **h**, Immunologic mechanism. **b**–**d**,**f**,**g**, One-way ANOVA with **a**–**d**, Tukey's, **f**, Dunnett's or **g**, left, Holm–Šídák's or right, Dunnett's multiple comparisons test. **b**,**c**, $n = 9$ mice per group. **b**–**g**, Data are mean ± s.e.m. Gel source data are in Supplementary Fig. 2.

OVA (Extended Data Fig. 6h). As validation of immune memory formation in tumour-bearing hosts, no tumour growth was observed on rechallenge of mice that had cleared CT26 tumours after EcNc$^{\Delta lon/\Delta ompT/LLO+}$ nAg[19] treatment (Extended Data Fig. 6i). Together, these experiments indicate generation of tumour neoantigen-specific T cells that are proficient in tumour cell killing and establish durable immune memory.

Beyond induction of tumour antigen-specific T cell responses, treatment with EcNc$^{\Delta lon/\Delta ompT/LLO+}$ nAg[19] resulted in reduced frequencies of tumour-resident immunosuppressive PD-L1^{+}Ly6G^{+} polymorphonuclear cells and PD-L1^{+}F4/80^{+} macrophages[39,40] (Fig. 3f). Bacteria-treated groups further showed reduced numbers and frequencies of Foxp3^{+}CD4^{+} regulatory T cells and MHC-II^{lo}F4/80^{+} tumour-associated macrophages (Fig. 3g and Extended Data Fig. 6j), two cell populations known for their roles in inhibiting antitumour immunity[41,42]. Moreover, within TDLNs of the neoantigen therapeutic-treated group, myeloid immunophenotyping showed a reduction of PD-L1 on cDC1s and cDC2s populations (Extended Data Fig. 6k), which has been shown to facilitate antitumour immunity[43]. In summary, intravenously delivered microbial neoantigen therapeutics sustain neoantigen production and availability in lymphoid tissue in vivo, recruit and activate dendritic cells, stimulate both neoantigen-specific and broad adaptive immunity, and reduce immunosuppression within the TME, shaping a more effective environment for productive antitumour immunity (Fig. 3h).

Treatment of melanoma

Neoantigens are generally unique to the individual tumour[9], thus vaccination platforms must be able to flexibly incorporate and deliver diverse sets of neoantigens on the basis of the unique mutations present in a particular tumour. To evaluate the suitability of our engineered microbial platform in this regard, we performed paired exome and transcriptome sequencing on a second, more aggressive tumour cell type (B16F10 melanoma) grown orthotopically in C57BL/6 mice and designed tumour-specific therapeutics (Fig. 4a). We applied an equivalent neoantigen prediction algorithm as performed for CT26 and identified numerous putative B16F10-specific neoantigens, including many that had previously been validated by others[15] (Extended Data Fig. 7a). A set of seven constructs were devised from neoantigens of varying imputed MHC-I and MHC-II affinities, with each construct containing six unique predicted neoantigens (Extended Data Table 2) and confirmed to be robustly expressed by EcNc$^{\Delta lon/\Delta ompT/LLO+}$ (Fig. 4a and Extended Data Fig. 7b).

We then sought to test the antitumour efficacy of our therapeutics against advanced B16F10 tumours. When established orthotopic tumours were injected with microbial therapeutics intratumourally, tumours grew progressively after treatment with EcNc$^{\Delta lon/\Delta ompT/LLO+}$ OVA, whereas treatment with the equal-parts combination of all seven construct-expressing strains—encompassing 42 unique B16F10 neoantigens (nAg[42])—significantly repressed growth over the same time course (Fig. 4b). Similarly, intravenous treatment with EcNc$^{\Delta lon/\Delta ompT/LLO+}$ nAg[42] potently restrained orthotopic tumour growth, with 72% of nAg[42]-treated mice alive 50 days post-tumour engraftment, whereas all control group mice succumbed to malignancy by day 24 or 30 (Fig. 4c,d and Extended Data Fig. 7c). Treatment with intravenous microbial vaccines again induced no significant body weight change compared to PBS-treated mice (Extended Data Fig. 7d).

To evaluate the tissue biodistribution of the microbial neoantigen vaccines after systemic administration in this setting, we surveyed organs after intravenous injection of EcNc$^{\Delta lon/\Delta ompT/LLO+}$ nAg[42]. As we observed for BALB/c mice with CT26 tumours, live microbial vectors specifically colonized the B16F10 tumour at high density without detectable presence in any other organs examined (Fig. 4e). To confirm that the microbial B16F10 neoantigen vaccine generated T cells capable of direct tumour cell killing, we treated tumour-free C57BL/6 mice intravenously with microbial therapeutics and co-incubated purified splenic T cells with B16F10 tumour cells in vitro. Indeed, T cells from mice treated intravenously with EcNc$^{\Delta lon/\Delta ompT/LLO+}$ nAg[42] but not EcNc$^{\Delta lon/\Delta ompT/LLO+}$ OVA demonstrated enhanced killing of B16F10 tumour cells (Fig. 4f). These data verify tumour-specific colonization and antigen-specific T cell induction by microbial neoantigen vaccines in

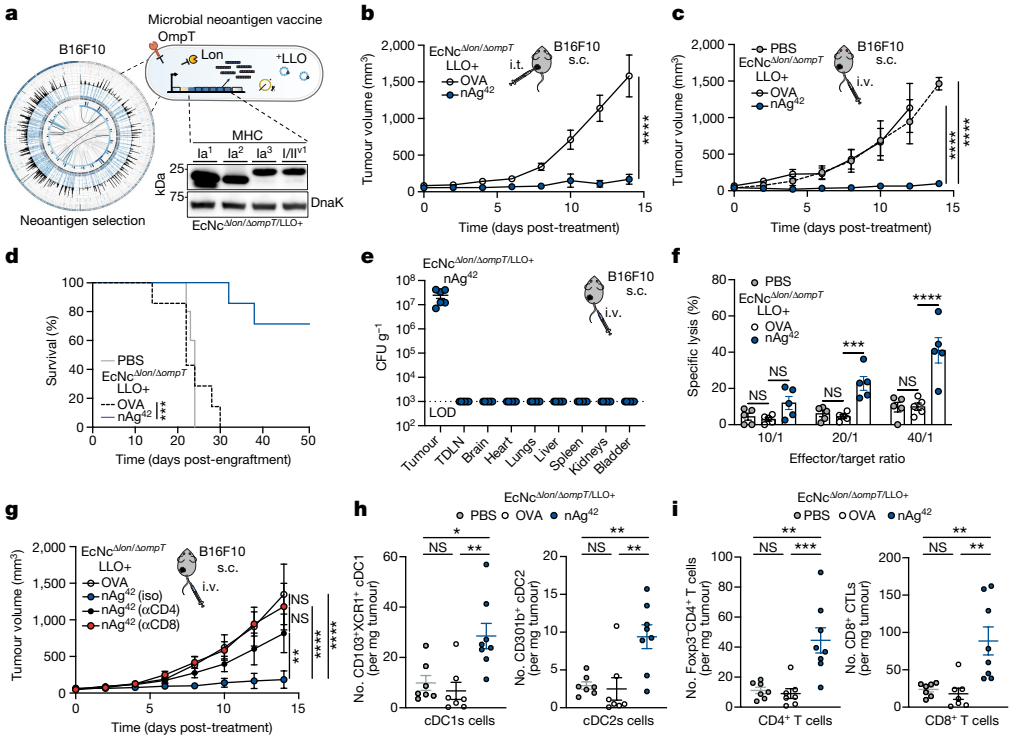

Fig. 4 | Microbial antitumour vaccine efficacy in orthotopic melanoma. **a**, Melanoma therapeutic design. Left, a Circos plot, mutanome B16F10. Right, an immunoblot with neoantigen constructs. **b**–**e**,**g**–**i**, C57BL/6 mice with orthotopic B16F10 tumours treated starting 9 days post-engraftment. **b**, Intratumoural treatment every 3–5 days. Tumour growth curves ($n = 7$ mice per group, $^{****}P < 0.0001$; NS, $P > 0.05$). **c**, Intravenous treatment every 3–5 days. Tumour growth curves ($^{****}P < 0.0001$; NS, $P > 0.05$). **d**, Kaplan–Meier survival curves, mice from **c** ($^{***}P = 0.0001$, log-rank Mantel–Cox test). **e**, Intravenous treatment, EcNc$^{\Delta lon/\Delta ompT/LLO+}$ nAg^{42} ($n = 6$ mice). Microbial CFU g^{-1}, LOD = 1×10^3 CFU g^{-1}. **f**, Purified splenic T cells, specific lysis B16F10-Luc ($n = 5$ mice per group, $^{***}P = 0.001$, $^{****}P < 0.0001$; NS, $P > 0.05$). **g**, Intravenous treatment every 3–5 days. Tumour growth curves ($n = 6$ mice for OVA, $n = 7$ for isotype, $n = 8$ for other groups, $^{**}P = 0.0082$, $^{****}P < 0.0001$; NS, $P > 0.05$). **h**,**i**, Intravenous treatment on days 9 and 12. **h**, Left, the number of CD103$^+$XCR1$^+$ cDC1 per mg ($^*P = 0.0103$, $^{**}P = 0.0030$; NS, $P > 0.05$). Right, the number of CD301b$^+$ cDC2 per mg ($^{**}P = 0.0038$, $^{**}P = 0.0064$; NS, $P > 0.05$). **i**, Left, the number of Foxp3$^-$CD4$^+$ T cells per mg ($^{**}P = 0.0015$, $^{***}P = 0.0008$; NS, $P > 0.05$). Right, the number of CD8$^+$ T cells mg^{-1} ($^{**}P = 0.0022$, $^{**}P = 0.0047$; NS, $P > 0.05$). **b**,**c**,**g**, two-way ANOVA, or **f**,**h**,**i**, one-way ANOVA, with **b**, Šídák's or **c**,**f**–**i**, Tukey's multiple comparisons test. **h**,**i**, $n = 8$ mice for nAg^{42}, $n = 7$ for other groups. **c**,**d**, $n = 5$ mice for PBS, $n = 7$ for other groups. **b**,**c**,**e**–**i**, Data are mean ± s.e.m. Gel source data are in Supplementary Fig. 2.

B16F10 melanoma. To assess the dependency of antitumour efficacy on CD4$^+$ and CD8$^+$ T cells in vivo, we depleted either CD4$^+$ or CD8$^+$ T cells from mice treated intravenously with EcNc$^{\Delta lon/\Delta ompT/LLO+}$ nAg^{42}. We found that depletion of either CD4$^+$ or CD8$^+$ T cells ablated therapeutic efficacy, indicating that both conventional CD4$^+$ and cytotoxic CD8$^+$ T cells are required for productive antitumour immunity in vivo (Fig. 4g and Extended Data Fig. 7e).

Immunity and metastases in melanoma

To characterize the immunologic changes associated with antitumour efficacy in this tumour model, we performed immunophenotyping of orthotopic B16F10 tumours 8 days post-intravenous microbial treatment. Tumours treated intravenously with EcNc$^{\Delta lon/\Delta ompT/LLO+}$ nAg^{42} had significantly higher numbers and frequencies of cDC1s and cDC2s, conventional CD4$^+$ and cytotoxic CD8$^+$ T cells, natural killer (NK) cells and inflammatory monocytes (Fig. 4h,i and Extended Data Fig. 7f–j).

Analyses of the intratumoural lymphoid compartment showed enhanced expression of CD69 on Foxp3$^-$CD4$^+$ and CD8$^+$ TILs, and significantly increased frequencies of IFNγ secreting conventional Foxp3$^-$CD4$^+$ and cytotoxic CD8$^+$ TILs after restimulation with PMA and ionomycin in EcNc$^{\Delta lon/\Delta ompT/LLO+}$ nAg^{42}-treated tumours, indicating enhanced T cell activation and effector cytokine production within the TME (Fig. 5a and Extended Data Fig. 8a). Tumour-infiltrating Foxp3$^-$CD4$^+$ and CD8$^+$ T cells and NK cells also expressed significantly higher levels of Granzyme-B after EcNc$^{\Delta lon/\Delta ompT/LLO+}$ nAg^{42} treatment, suggestive of amplified cytolytic function (Fig. 5b,c). Consistent with enduring activity of antitumour immunity, we also observed higher levels of proliferating tumour-infiltrating CD4$^+$ and CD8$^+$ T cells and NK cells as assessed by Ki-67 staining (Extended Data Fig. 8b).

In addition to the enhanced activation of tumour-infiltrating T and NK cells, treatment with EcNc$^{\Delta lon/\Delta ompT/LLO+}$ nAg^{42} significantly reduced TIM-1 expression by tumour-infiltrating CD19$^+$ B cells and thus the frequency of regulatory TIM-1$^+$ B cells—an important immunosuppressive cell population in the B16F10 model[44]—and increased B cell proliferation (Fig. 5d and Extended Data Fig. 8c). Moreover, EcNc$^{\Delta lon/\Delta ompT/LLO+}$ nAg^{42} vaccination reduced the frequency of immunosuppressive Foxp3$^+$ regulatory T cells, myeloid-derived suppressor cells (MDSCs) and MHC-II^{lo} macrophages within tumours (Fig. 5e and Extended Data Fig. 8d). Infiltrating monocytes and dendritic cells in EcNc$^{\Delta lon/\Delta ompT/LLO+}$ nAg^{42}-treated tumours showed increased expression of MHC-II (Extended Data Fig. 8e), suggestive of enhanced antigen presentation capacity. Overall, these data demonstrate that intravenous microbial tumour neoantigen vaccination mediates immunologic restructuring within the melanoma TME, recruiting APCs and activating NK cells, and CD4$^+$ and CD8$^+$ T cells while diminishing immunosuppressive cell populations.

Given the robust antitumour efficacy induced by intravenous vaccination in orthotopic B16F10, we investigated the efficacy of EcNc$^{\Delta lon/\Delta ompT/LLO+}$ nAg^{42} in established, systemic B16F10-Luc metastases (Extended Data Fig. 8f). Whereas systemic metastases rapidly progressed in PBS or EcNc$^{\Delta lon/\Delta ompT/LLO+}$ OVA treated mice, EcNc$^{\Delta lon/\Delta ompT/LLO+}$ nAg^{42} strongly inhibited metastatic growth (Fig. 5f,g and Extended Data Fig. 8g,h).

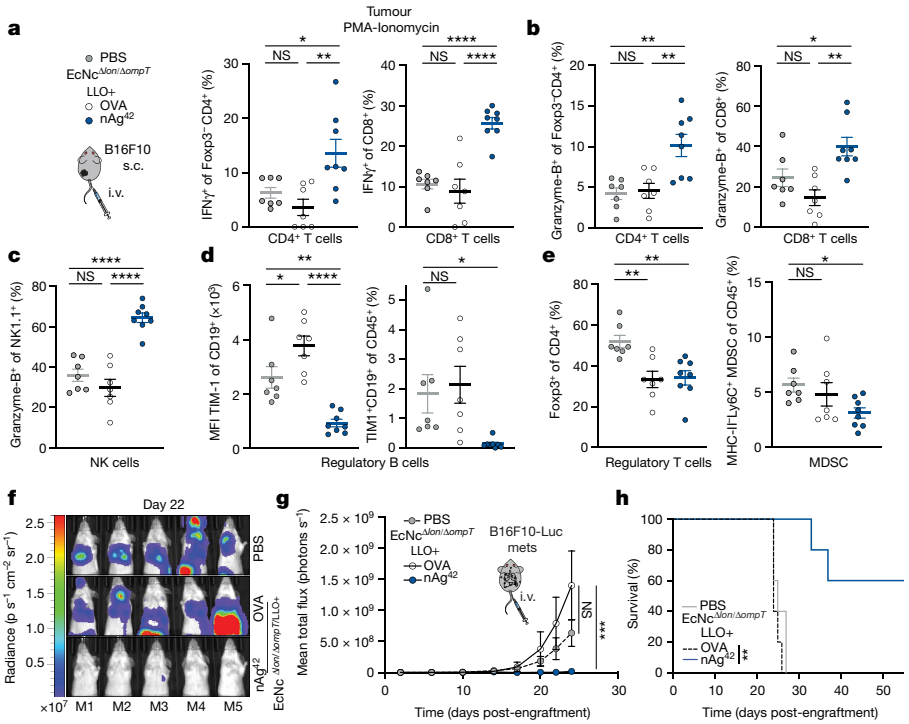

Fig. 5 | Microbial neoantigen vectors restructure the tumour immune microenvironment and suppress established metastatic melanoma. **a**–**e**, Mice with orthotopic B16F10 received an intravenous treatment on day 9 and 12 post-engraftment. **a**, Left, experimental schematic. Middle, the frequency of IFNγ$^+$Foxp3$^-$CD4$^+$ post-stimulation (*P = 0.0335, **P = 0.0040; NS, P > 0.05). Right, the frequency of IFNγ$^+$CD8$^+$ T cells (****P < 0.0001; NS, P > 0.05). **b**, Left, the frequency of Granzyme-B$^+$Foxp3$^-$CD4$^+$ (**P = 0.0024, **P = 0.0041; NS, P > 0.05). Right, the frequency of Granzyme-B$^+$ CD8$^+$ T cells (*P = 0.0495, **P = 0.0014; NS, P > 0.05). **c**, Frequency of Granzyme-B$^+$NK1.1$^+$ NK cells (****P < 0.0001; NS, P > 0.05). **d**, Left, the median fluorescence intensity (MFI) of TIM-1 on CD19$^+$ B cells (*P = 0.0457, **P = 0.0029, ****P < 0.0001). Right, the frequency of TIM-1$^+$CD19$^+$ B cells of CD45$^+$ cells (*P = 0.0442; NS, P > 0.05). **e**, Left, the frequency of Foxp3$^+$CD4$^+$ T cells of CD4$^+$ cells (**P = 0.0035, **P = 0.0038). Right, the frequency of MHCII$^-$Ly6c$^+$ MDSCs of CD45$^+$ cells (*P = 0.0440; NS, P > 0.05). **f**–**h**, C57BL/6 mice (n = 5 mice per group) with 2-day established B16F10-Luc systemic metastases. Intravenous treatment every 3–5 days. **f**, Representative systemic metastases luminescence. **g**, Mean total flux from systemic metastases (***P > 0.0003; NS, P > 0.05, two-way ANOVA with Dunnett's multiple comparisons test). **h**, Kaplan–Meier survival curve for mice with B16F10-Luc systemic metastases (**P = 0.0015, log-rank Mantel–Cox test). **a**–**e**, One-way ANOVA with **a**–**c**, Tukey's, **d**, left, Tukey's or right, Dunnett's and **e**, Dunnett's multiple comparisons test. **a**–**e**, n = 8 mice for nAg^{42}, n = 7 for other groups. **a**–**e**,**g**, Data are mean ± s.e.m.

Treatment with EcNc$^{\Delta lon/\Delta ompT/LLO+}$ nAg^{42} significantly extended survival, with 60% of mice surviving to 55 days with no detectable metastases, whereas all control treated mice had died by day 27 (Fig. 5h). Again, treatment was well tolerated, with no significant weight change relative to PBS (Extended Data Fig. 8i). These data demonstrate that the microbial tumour neoantigen vaccination system stimulates productive antitumour immunity in vivo after intravenous administration in established, systemic metastatic melanoma.

Discussion

Through microbial engineering, we couple the tumour-homing and immunostimulatory nature of bacteria with precise instructions for coordinated adaptive immunity towards tumour neoantigens, achieving a platform capable of mediating control and eradication of advanced solid tumours.

Bioinformatic-based identification of neoantigens that are both immunogenic and able to generate T cells capable of tumour cell killing remains a challenge. Predicted MHC-binding affinity is a frequently used criterion in neoantigen identification, as analyses of MHC-I binding epitopes from viruses showed that immunogenic epitopes usually possess less than 500 nM affinity, but most show less than 50–200 nM affinity[45]. Whereas many immunogenic tumour neoantigens similarly show strong MHC-binding affinity (less than 50–500 nM)[12,20], only a small fraction of predicted strong binding tumour neoepitopes are immunogenic[20], and studies have revealed presentation, immunogenicity and TIL reactivity for neoantigens with low binding affinity (greater than 500 nM)[17,46,47]. A detailed analysis of MHC-I binding neoepitopes from human tumours showed that of the 10.5% of neoepitopes with more than 500 nM affinity, 50% contained cysteine residues, suggesting that low-affinity neoantigens may possess distinct characteristics[48]. Further criteria have been proposed to aid neoantigen identification, including differential binding affinity of the neoepitope versus corresponding wild-type epitope[17,20], variant allele fraction of the mutation[14] and expression level of the mutation-containing gene[15]; however, no standardized prediction algorithm has been identified[20]. Although we recognize the neoantigen prediction methods we use may have limitations, in this study, we used a combination of prediction criteria and primarily selected high-affinity neoantigens, with the incorporation of some low-affinity neoantigens.

We found that antigen sets encompassing both predicted MHC-I and MHC-II binding neoantigens mediated antitumour efficacy. Indeed, enhanced frequencies of neoantigen-specific CD4$^+$ and CD8$^+$ T cells were observed, MHC-I and MHC-II binding neoantigens were targeted by TILs in immunized mice, and both CD4$^+$ and CD8$^+$ T cells were required for efficacy of the microbial vaccination system in vivo. This agrees with the critical role of both CD4$^+$ and CD8$^+$ T cells in effective antitumour immunity, and the expanding set of verified MHC-I- and MHC-II-dependent neoantigens recognized across tumours[12,15,18,46,47]. Together, these results support the targeting of both MHC-I and MHC-II binding tumour neoantigens in antitumour immunotherapies.

We show that across distinct tumour models and genetic backgrounds, the antitumour effect of vaccination is accompanied by broad modulation of the immune compartment within the TME. The coordinated regulation of APCs, reduction of immunosuppressive myeloid, regulatory T and B cell populations, and activation of NK cells and $CD4^+$ and $CD8^+$ T cells together indicate the advantage of precisely engineered microbial platforms as next-generation antitumour vaccines that align several arms of immunity[13]. In agreement with previous reports regarding synthetic peptide, adenoviral and messenger RNA (mRNA) neoantigen vaccines[49–51], we did not observe suppression of established CT26 tumour growth on SLP vaccination. By contrast, engineered microbial vaccines significantly reduced growth and achieved a portion of complete responses. This is consistent with a model whereby microbial vectors enable direct modulation of innate and adaptive immunity and sustained neoantigen delivery within the TME to promote effective therapeutic vaccination of established tumours.

The unique ability of microbial vaccines to directly remodel the TME may promote synergy with other forms of immunotherapy. Adoptive T cell therapy (ACT) has resulted in regression of advanced malignancy in a subset of patients, although solid tumours often show resistance[52]. Previous murine studies demonstrated that target-antigen vaccination amplifies ACT efficacy in solid tumours when targeting a carcinoembryonic antigen (claudin-6) with chimeric antigen receptor T (CAR-T) cell therapy[53]. However, in a human solid tumour trial the effect of combining claudin-6 vaccination with CAR-T cell therapy was unclear compared with CAR-T cell monotherapy[54]. Solid tumour resistance mechanisms to T cell-mediated immunotherapies often occur within the TME: restricted antigen availability, reduced APC infiltration and function, antitumour immune cell exclusion, upregulation of immunoinhibitory ligands and enrichment of immunosuppressive populations[55]. As the microbial neoantigen vectors locally increase neoantigen density, recruit and activate dendritic cells and $CD4^+$ and $CD8^+$ T cells, and reduce immunosuppressive populations and ligands within the TME, combination with ACT may oppose these resistance mechanisms and provide synergistic benefit.

Through extra programming of the microbial vectors and rational incorporation of other immunotherapeutics, this system may achieve reliable eradication of established solid tumours and metastases through precision cancer immunotherapy using living antitumour vaccines.

Online content

Any methods, additional references, Nature Portfolio reporting summaries, source data, extended data, supplementary information, acknowledgements, peer review information; details of author contributions and competing interests; and statements of data and code availability are available at https://doi.org/10.1038/s41586-024-08033-4.

1. Canale, F. P. et al. Metabolic modulation of tumours with engineered bacteria for immunotherapy. *Nature* **598**, 662–666 (2021).
2. Chen, Y. E. et al. Engineered skin bacteria induce antitumor T cell responses against melanoma. *Science* **380**, 203–210 (2023).
3. Nejman, D. et al. The human tumor microbiome is composed of tumor type-specific intracellular bacteria. *Science* **368**, 973–980 (2020).
4. Pawelek, J. M., Low, K. B. & Bermudes, D. Tumor-targeted *Salmonella* as a novel anticancer vector. *Cancer Res.* **57**, 4537–4544 (1997).
5. Naghavian, R. et al. Microbial peptides activate tumour-infiltrating lymphocytes in glioblastoma. *Nature* https://doi.org/10.1038/s41586-023-06081-w (2023).
6. Kalaora, S. et al. Identification of bacteria-derived HLA-bound peptides in melanoma. *Nature* **592**, 138–143 (2021).
7. Stark, J. C. et al. On-demand biomanufacturing of protective conjugate vaccines. *Sci. Adv.* **7**, eabe9444 (2021).
8. Iwasaki, A. & Medzhitov, R. Control of adaptive immunity by the innate immune system. *Nat. Immunol.* **16**, 343–353 (2015).
9. Schumacher, T. N. & Schreiber, R. D. Neoantigens in cancer immunotherapy. *Science* **348**, 69–74 (2015).
10. Sahin, U. et al. Personalized RNA mutanome vaccines mobilize poly-specific therapeutic immunity against cancer. *Nature* **547**, 222–226 (2017).
11. Rojas, L. A. et al. Personalized RNA neoantigen vaccines stimulate T cells in pancreatic cancer. *Nature* **618**, 144–150 (2023).
12. Ott, P. A. et al. An immunogenic personal neoantigen vaccine for patients with melanoma. *Nature* **547**, 217–221 (2017).
13. Sellars, M. C., Wu, C. J. & Fritsch, E. F. Cancer vaccines: building a bridge over troubled waters. *Cell* **185**, 2770–2788 (2022).
14. Hundal, J. et al. pVACtools: a computational toolkit to identify and visualize cancer neoantigens. *Cancer Immunol. Res.* **8**, 409–420 (2020).
15. Kreiter, S. et al. Mutant MHC class II epitopes drive therapeutic immune responses to cancer. *Nature* **520**, 692–696 (2015).
16. Lee, M. Y., Jeon, J. W., Sievers, C. & Allen, C. T. Antigen processing and presentation in cancer immunotherapy. *J. Immunother. Cancer* **8**, e001111 (2020).
17. Duan, F. et al. Genomic and bioinformatic profiling of mutational neoepitopes reveals new rules to predict anticancer immunogenicity. *J. Exp. Med.* **211**, 2231–2248 (2014).
18. Alspach, E. et al. MHC-II neoantigens shape tumour immunity and response to immunotherapy. *Nature* **574**, 696–701 (2019).
19. Kruse, B. et al. $CD4^+$ T cell-induced inflammatory cell death controls immune-evasive tumours. *Nature* **618**, 1033–1040 (2023).
20. Wells, D. K. et al. Key parameters of tumor epitope immunogenicity revealed through a consortium approach improve neoantigen prediction. *Cell* **183**, 818–834.e13 (2020).
21. Zwaveling, S. et al. Established human papillomavirus type 16-expressing tumors are effectively eradicated following vaccination with long peptides. *J. Immunol.* **169**, 350–358 (2002).
22. Fedorec, A. J. H. et al. Two new plasmid post-segregational killing mechanisms for the implementation of synthetic gene networks in *Escherichia coli*. *iScience* **14**, 323–334 (2019).
23. Zinkernagel, R. M. et al. Antigen localisation regulates immune responses in a dose- and time-dependent fashion: a geographical view of immune reactivity. *Immunol. Rev.* **156**, 199–209 (1997).
24. Henrickson, S. E. et al. T cell sensing of antigen dose governs interactive behavior with dendritic cells and sets a threshold for T cell activation. *Nat. Immunol.* **9**, 282–291 (2008).
25. Yewdell, J. W. & Bennink, J. R. Immunodominance in major histocompatibility complex class I-restricted T lymphocyte responses. *Annu. Rev. Immunol.* **17**, 51–88 (1999).
26. Daegelen, P., Studier, F. W., Lenski, R. E., Cure, S. & Kim, J. F. Tracing ancestors and relatives of *Escherichia coli* B, and the derivation of B strains REL606 and BL21(DE3). *J. Mol. Biol.* **394**, 634–643 (2009).
27. Kan, A., Gelfat, I., Emani, S., Praveschotinunt, P. & Joshi, N. S. Plasmid vectors for in vivo selection-free use with the probiotic *E. coli* Nissle 1917. *ACS Synth. Biol.* **10**, 94–106 (2021).
28. Russo, T. A. & Singh, G. An extraintestinal, pathogenic isolate of *Escherichia coli* (O4/K54/H5) can produce a group 1 capsule which is divergently regulated from its constitutively produced group 2, K54 capsular polysaccharide. *J. Bacteriol.* **175**, 7617–7623 (1993).
29. Niba, E. T. E., Naka, Y., Nagase, M., Mori, H. & Kitakawa, M. A genome-wide approach to identify the genes involved in biofilm formation in *E. coli*. *DNA Res.* **14**, 237–246 (2007).
30. Riva, R., Korhonen, T. K. & Meri, S. The outer membrane protease PgtE of *Salmonella enterica* interferes with the alternative complement pathway by cleaving factors B and H. *Front. Microbiol.* **6**, 63 (2015).
31. Lewis, K. Riddle of biofilm resistance. *Antimicrob. Agents Chemother.* **45**, 999–1007 (2001).
32. Higgins, D. E., Shastri, N. & Portnoy, D. A. Delivery of protein to the cytosol of macrophages using *Escherichia coli* K-12. *Mol. Microbiol.* **31**, 1631–1641 (1999).
33. Wallecha, A. et al. Listeria monocytogenes-derived listeriolysin O has pathogen-associated molecular pattern-like properties independent of its hemolytic ability. *Clin. Vaccine Immunol.* **20**, 77–84 (2013).
34. Kang, S.-J., Liang, H.-E., Reizis, B. & Locksley, R. M. Regulation of hierarchical clustering and activation of innate immune cells by dendritic cells. *Immunity* **29**, 819–833 (2008).
35. Yamamoto, K. et al. Listeriolysin O, a cytolysin derived from Listeria monocytogenes, inhibits generation of ovalbumin-specific Th2 immune response by skewing maturation of antigen-specific T cells into Th1 cells. *Clin. Exp. Immunol.* **142**, 268–274 (2005).
36. Harris, D. P. et al. Reciprocal regulation of polarized cytokine production by effector B and T cells. *Nat. Immunol.* **1**, 475–482 (2000).
37. Ding, Q., Mohib, K., Kuchroo, V. K. & Rothstein, D. M. TIM-4 identifies IFN-γ-expressing proinflammatory B effector 1 cells that promote tumor and allograft rejection. *J. Immunol.* **199**, 2585–2595 (2017).
38. Vanderlugt, C. L. & Miller, S. D. Epitope spreading in immune-mediated diseases: implications for immunotherapy. *Nat. Rev. Immunol.* **2**, 85–95 (2002).
39. Gabrilovich, D. I., Ostrand-Rosenberg, S. & Bronte, V. Coordinated regulation of myeloid cells by tumours. *Nat. Rev. Immunol.* **12**, 253–268 (2012).
40. He, G. et al. Peritumoural neutrophils negatively regulate adaptive immunity via the PD-L1/PD-1 signalling pathway in hepatocellular carcinoma. *J. Exp. Clin. Cancer Res.* **34**, 141 (2015).
41. Tanaka, A. & Sakaguchi, S. Regulatory T cells in cancer immunotherapy. *Cell Res.* **27**, 109–118 (2017).
42. Wang, B. et al. Transition of tumor-associated macrophages from MHC class II(hi) to MHC class II(low) mediates tumor progression in mice. *BMC Immunol.* **12**, 43 (2011).
43. Peng, Q. et al. PD-L1 on dendritic cells attenuates T cell activation and regulates response to immune checkpoint blockade. *Nat. Commun.* **11**, 4835 (2020).
44. Bod, L. et al. B-cell-specific checkpoint molecules that regulate anti-tumour immunity. *Nature* **619**, 348–356 (2023).
45. Sette, A. et al. The relationship between class I binding affinity and immunogenicity of potential cytotoxic T cell epitopes. *J. Immunol.* **153**, 5586–5592 (1994).
46. Bassani-Sternberg, M. et al. Direct identification of clinically relevant neoepitopes presented on native human melanoma tissue by mass spectrometry. *Nat. Commun.* **7**, 13404 (2016).
47. Tran, E. et al. Immunogenicity of somatic mutations in human gastrointestinal cancers. *Science* **350**, 1387–1390 (2015).
48. Sachs, A. et al. Impact of cysteine residues on MHC binding predictions and recognition by tumor-reactive T cells. *J. Immunol.* **205**, 539–549 (2020).

49. Arbelaez, C. A. et al. A nanoparticle vaccine that targets neoantigen peptides to lymphoid tissues elicits robust antitumor T cell responses. *NPJ Vaccines* **5**, 106 (2020).
50. D'Alise, A. M. et al. Adenoviral vaccine targeting multiple neoantigens as strategy to eradicate large tumors combined with checkpoint blockade. *Nat. Commun.* **10**, 2688 (2019).
51. Salomon, N. et al. A liposomal RNA vaccine inducing neoantigen-specific $CD4^+$ T cells augments the antitumor activity of local radiotherapy in mice. *OncoImmunology* **9**, 1771925 (2020).
52. Rosenberg, S. A. et al. Durable complete responses in heavily pretreated patients with metastatic melanoma using T-cell transfer immunotherapy. *Clin. Cancer Res.* **17**, 4550–4557 (2011).
53. Reinhard, K. et al. An RNA vaccine drives expansion and efficacy of claudin-CAR-T cells against solid tumors. *Science* **367**, 446–453 (2020).
54. Mackensen, A. et al. CLDN6-specific CAR-T cells plus amplifying RNA vaccine in relapsed or refractory solid tumors: the phase 1 BNT211-01 trial. *Nat. Med.* **29**, 2844–2853 (2023).
55. O'Donnell, J. S., Teng, M. W. L. & Smyth, M. J. Cancer immunoediting and resistance to T cell-based immunotherapy. *Nat. Rev. Clin. Oncol.* **16**, 151–167 (2019).

Methods

Cell lines

The B16F10 melanoma (ATCC CRL-6475), CT26 colon carcinoma (ATCC CRL-2638) and 4T1 breast cancer (ATCC CRL-2539) authenticated cell lines were purchased directly from ATCC. CT26-Luc, B16F10-Luc and 4T1-Luc cells were lentivirally transduced with luciferase. Cells were confirmed mycoplasma free. Cells were cultured in incubators at 37 °C with atmosphere of humidified 5% CO_2. B16F10 and B16F10-Luc cells were grown in DMEM supplemented with 10% (vol/vol) fetal bovine serum (FBS), 1× GlutaMax, 1% (vol/vol) MEM non-essential amino acids solution (Gibco-11140050) and 100 U ml^{-1} penicillin–streptomycin. CT26, CT26-Luc, 4T1 and 4T1-Luc cells were grown in Roswell Park Memorial Institute medium (RPMI-1640) supplemented with 10% (vol/vol) FBS, 1× GlutaMax, 1% (vol/vol) MEM non-essential amino acids solution and 100 U ml^{-1} penicillin–streptomycin. No commonly misidentified cell lines were used in this study.

Exome sequencing

Paired tumour and tail DNA from BALB/c mice bearing subcutaneous CT26 tumours or C57BL/6 mice bearing subcutaneous B16F10 tumours was extracted in triplicate ($n = 3$ mice per tumour line) using Qiagen DNeasy Blood & Tissue Minikit following the manufacturer's instructions. Exome capture from mouse tumour and tail DNA triplicates was conducted using Agilent SureSelectXT All Exon kit for target enrichment DNA library preparation[56], according to the manufacturer's instructions (Agilent). Genomic DNA was fragmented by acoustic shearing with a Covaris S220 instrument. Fragmented DNAs were cleaned, end-repaired and adenylated at the 3′ end. Adaptors were ligated to DNA fragments, and adaptor-ligated DNA fragments enriched with limited-cycle PCR. Adaptor-ligated DNA fragments were validated using Agilent TapeStation (Agilent) and quantified using Qubit 2.0 Fluorometer (ThermoFisher Scientific) and Real-Time PCR (KAPA Biosystems). Sequencing libraries were clustered onto a lane of a flow cell. After clustering, the flow cell was loaded on an Illumina HiSeq4000 Instrument per the manufacturer's instructions. Samples were sequenced using 2 × 150 bp paired end configuration. Image analysis and base calling was conducted by the HiSeq Control Software. Raw sequence data (.bcl files) generated from Illumina HiSeq was converted into fastq files and de-multiplexed using Illumina bcl2fastq2.17. Sequence reads were trimmed to remove adaptor sequences and nucleotides with poor quality using Trimmomatic v.0.39 (ref. 57). Trimmed reads were aligned to the GRCm38 reference genome using the Illumina Dragen Bio-IT platform. Alignments were sorted and PCR or optical duplicates marked for generation of BAM files. Somatic single-nucleotide variants and insertion or deletion (indel) variants were called using Illumina Dragen[58] and GATK Mutect2 (ref. 59). All variants from paired-normal tissue and murine variants from the dbSNP database[60] were removed during the process. VCF files were left aligned and normalized, with splitting of multiallelic sites into several sites using bcftools v.1.13 (ref. 61). Only tumour-specific variants called by both algorithms were used for further analysis.

RNA sequencing

Tumour RNA from BALB/c mice bearing subcutaneous CT26 tumours or C57BL/6 mice bearing subcutaneous B16F10 tumours was extracted in triplicate using Qiagen RNeasy Minikit as per the manufacturer's instructions. Extracted RNA samples were quantified using Qubit 2.0 Fluorometer (Life Technologies) and RNA integrity checked using Agilent TapeStation 2400 (Agilent). RNA sequencing libraries were prepared using the NEBNext Ultra RNA library Prep Kit for Illumina as per the manufacturer's instructions (New England Biolabs). mRNAs were enriched with Oligo(dT) beads. Enriched mRNAs were fragmented for 15 min at 94 °C. First- and second-strand complementary DNAs (cDNAs) were synthesized subsequently. cDNA fragments were end-repaired and adenylated at 3′ ends, and universal adaptors ligated to cDNA fragments, followed by index addition and library enrichment by limited-cycle PCR. Sequencing libraries were validated on Agilent TapeStation (Agilent), and quantified using Qubit 2.0 Fluorometer (Invitrogen) and quantitative PCR (qPCR) (KAPA Biosystems). Library loading, sequencing and read trimming were done as described above. Trimmed reads were aligned to the mm10 reference using STAR aligner v.2.5.2b (ref. 62). Unique gene hit counts were calculated using feature counts from Subread Package v.1.5.2. Unique reads that fell within exon regions were counted. The gene hit counts table was used for expression analysis using DESeq2 v.1.20.0 (ref. 63).

Neoantigen prediction and selection

Mutation-specific RNA expression and allele fraction were added to somatic VCF files using Bam-readcount[64] and VAtools (http://vatools.org). Somatic VCFs were annotated with The Ensembl Variant Effect Predictor (VEP Ensembl v.104)[65]. Only PASS variants from VCFs were considered. Annotated VCFs were analysed using pVac-Seq for neoepitope discovery[14]. MHC-I affinities were predicted with NetMHCpan v.4.1 (ref. 66) and NetMHC v.4.0 (ref. 67), and MHC-II affinities were predicted with NetMHCIIpan v.4.1 (ref. 68) and NNalign v.2.0 (ref. 69). Exonic mutation-derived long peptides based on single-nucleotide polymorphisms (SNP) or indels predicted to generate mutant MHC-binding peptides were first filtered on the basis of the set of minimum criteria: (1) present in all tumour sample triplicates (DNA variant allele fraction ≥ 0.05) and none of the normal tissue triplicates, (2) non-synonymous mutation resulting from either SNP or indel, (3) confirmed exonic mutation transcription (RNA variant allele fraction ≥ 0.05) and gene expression by RNA sequencing in tumour sample triplicate (transcripts per million ≥ 1), (4) at least one predicted MHC-I or MHC-II binding epitope and (5) MHC-I or MHC-II differential binding affinity[17,20] (wild-type half-maximum inhibitory concentration (IC_{50})/mutant IC_{50}) ≥ 1.2. Predicted neoantigens fulfilling all previous criteria were then prioritized for inclusion and selected according to the following hierarchy: (1) high predicted affinity (MHC-I or MHC-II $IC_{50} \leq 500$ nM), (2) moderate predicted affinity (MHC-I or MHC-II IC_{50} 500–1,000 nM) and (3) low predicted affinity (MHC-I or MHC-II IC_{50} 1,000–5,000 nM) (Extended Data Tables 1 and 2).

Strains and plasmids

Plasmids were constructed using restriction-enzyme mediated and Gibson assembly cloning methods. Neoantigen construct iterations were designed and created as Geneblocks (IDT) encoding a constitutive promoter and 5′ untranslated region (UTR) containing selected ribosome-binding site, followed by coding region composed of mutant-residue containing long peptides connected in tandem or by various linkers as indicated. 5′ BamHI and 3′ XbaI restriction endonuclease sites were added to constructs. Coding sequences were codon optimized for *E. coli*. Constructs were cloned between BamHI and XbaI restriction sites on a stabilized p246-*lux*CDABE plasmid where *lux*CDABE had been cloned out[22], and flanked by 3′ λ-phage transcription terminator, with high-copy pUC origin. For protein expression assessment studies, the codon sequence for a 6×-Histidine Tag (HisTag) was added immediately before the stop codon within the neoantigen construct coding sequence by PCR amplification of full construct plasmids with oligonucleotide containing 6×-HisTag sequence followed by kinase, ligase, DpnI enzyme mix protocol (NEB). Neoantigen construct plasmids were transformed into chemically competent *E. coli* DH5α or BL21(DE3) (New England Biolabs), or electrocompetent EcN parental strain or genetic derivatives. The parental EcN strain and all derivatives used in this study harbour an integrated *luxCDABE* cassette within the genome, which also contains an erythromycin resistance gene[70]. Plasmid encoding constitutive LLO was constructed by cloning in the hok/sok stabilization system to pCG02-p15a backbone[71], PCR amplification of backbone with SLC cloned out, and Gibson assembly

of Geneblock encoding LLO under constitutive promoter and 5′ UTR containing selected ribosome-binding site. Constitutive LLO plasmids were transformed into electrocompetent EcN parental and genetic derivative strains. Strains were cultured in Luria-Bertani (LB) medium with antibiotics for plasmid retention (pUC:kanamycin 50 μg ml^{-1}, p15a:spectinomycin 50 μg ml^{-1}) in a 37 °C orbital incubator.

Construction of cryptic plasmid-cured EcN

EcN cryptic plasmids were cured with Cas9-mediated double-strand break, as described previously[27]. Briefly, EcN was transformed with pFREE or pCryptDel4.8 to cure the cryptic plasmids pMUT1 or pMUT2, respectively. The transformants were grown overnight and diluted 1:1,000 the next day into fresh LB containing 0.2% rhamnose and 0.43 μM anhydrotetracycline. After 24 h of incubation, the culture was streaked onto LB plates without antibiotics and incubated overnight in a 30 °C incubator. Colonies were screened with colony PCR to verify the loss of cryptic plasmids.

Construction of genetic knockout strains

Genetic knockouts were performed using the lambda red recombination system[72]. In brief, EcNc was transformed with pKD46. Transformants were grown at 30 °C in LB with ampicillin and L-arabinose, then made electrocompetent. The chloramphenicol resistance cassette with corresponding overhangs for each target gene for deletion was prepared by PCR amplification of pKD3. Electroporation was performed using 100 μl of competent cells and 50–300 ng amplified DNA. After 2 h of recovery, cells were plated on LB agar containing chloramphenicol and incubated at 37 °C overnight. Target gene deletion was verified by colony PCR. For excision of the antibiotic resistance marker, pCP20 was transformed, and the transformants were plated on fresh LB plates containing ampicillin and incubated at 30 °C overnight. Selected colonies were then inoculated onto fresh LB plates without antibiotics and cultured at 43 °C overnight for induction of flippase and plasmid curing. Clones were subsequently screened for loss of antibiotic resistance.

qPCR for PCN

Copy number variant plasmids were constructed from a high-copy pUC-GFP[22] plasmid. The plasmid backbone excluding the pUC origin was PCR-amplified and Gibson assembled with sc101*, p15A or ColE1 origin of replication insert. The respective inserts were prepared from PCR amplification of template plasmid pCG02_sc101*, pCG02_p15A or pTH05_ColE1. Plasmid copy number (PCN) was determined as reported previously[22], in which the relative abundance of plasmid DNA compared to genomic DNA is measured by qPCR. Briefly, strains with the plasmid of interest were grown at 37 °C overnight in fresh LB with appropriate antibiotics. Cells were collected by centrifugation at 3,000*g* at 4 °C for 10 min, the supernatant removed and the cell pellet resuspended in distilled water for optical density measurement at 600 nm (OD_{600}) equal to 1. Resuspended cells were fivefold serially diluted. Samples were denatured at 95 °C for 10 min and 2 μl of each sample dilution was added into 18 μl of NEB Luna Universal qPCR Master Mix in each well of a 96-well plate. Then 25-fold diluted samples were used for the measurement of crossing point values: the cycle number when amplified sample fluorescence exceeds the background. Fivefold diluted samples were used for generation of the standard curve for PCR efficiency (*E*). *E* was defined from the slope (*S*) of each standard curve with the equation $E = 5(-1/S)$ and PCN was determined with the equation PCN = $(E_G^{CTG})/(E_P^{CTP})$, where respective values for genomic DNA are denoted by a subscript G and plasmid DNA by subscript P.

Immunoblot and ELISA

For immunoblot and ELISA, a C-terminal 6×-HisTag was attached to each neoantigen construct. Strains expressing neoantigen construct with C-terminal 6×-HisTag were grown overnight in LB media with appropriate antibiotics. Equalization of OD_{600} measurement to match colony-forming units (CFU) per ml (CFU ml^{-1}) between all cultures was done before all sample processing. CFU-matched cultures were centrifuged at 3,000*g* at 4 °C for 10 min. For immunoblot, samples were resuspended in B-PER lysis reagent (ThermoFisher Scientific) containing 250 U ml^{-1} benzonase nuclease (Millipore Sigma) and 1 U ml^{-1} rLysozyme (Millipore Sigma) and placed on an orbital shaker for 15 min at room temperature. Samples were centrifuged at 10,000*g* for 20 min at 4 °C to separate soluble and insoluble fractions or total lysate used directly. Processed samples were mixed with SDS-loading buffer with 5 mM dithiothreitol, boiled and subject to immunoblot analysis. For relative quantification of immunoblot chemiluminescent intensity, target protein bands on the same blot were normalized to the loading control band DnaK for the same sample. DnaK loading controls were always run on the same gel as target proteins. Normalized values were divided to provide relative intensity values. Mouse anti-6×His (αTHE) was purchased from GenScript, mouse anti-DnaK was purchased from Abcam (8E2/2). αTHE and 8E2/2 antibodies were used at 1:5,000 dilution.

For HisTag ELISA, samples were resuspended in ice-cold PBS containing HALT protease inhibitor cocktail (ThermoFisher Scientific). Samples were sonicated on ice for 2 min total time. Sonicated samples were centrifuged at 10,000*g* for 20 min at 4 °C. Soluble sample fractions were analysed using GenScript HisTag ELISA Detection Kit as per the manufacturer's instructions.

For ex vivo immunoblot analysis, BALB/c mice bearing established hind-flank CT26 tumours were injected intravenously with the EcNc$^{\Delta lon/\Delta ompT/LLO+}$ nAg$^{19\text{-}His}$ strain cocktail that contains all three neoantigen constructs, in which each construct (MHCIa, MHCIIa and MHCI/II$^{\gamma}$) contained a C-terminal 6×-HisTag. Then 48 h after treatment, tumours and TDLNs were extracted from mice and placed in B-PER lysis reagent (ThermoFisher Scientific) with 250 U ml^{-1} benzonase nuclease (Millipore Sigma), and homogenized using a gentleMACS tissue dissociator (Miltenyi Biotec, C-tubes). Tissue homogenate was sonicated on ice for 3 min. Sonicated samples were centrifuged at 10,000*g* for 20 min at 4 °C to separate soluble and insoluble fractions, and fractions subsequently resuspended and diluted in lysis buffer. Sample fractions were mixed with SDS-loading buffer with 5 mM dithiothreitol, boiled and subject to immunoblot analysis.

For ex vivo IL-12p70 ELISA analysis, BALB/c mice bearing established hind-flank CT26 tumour were injected intratumourally with PBS, EcNc$^{\Delta lon/\Delta ompT}$ or EcNc$^{\Delta lon/\Delta ompT/LLO+}$. Then 4–24 h after treatment, tumours were extracted and placed in ice-cold PBS containing HALT protease inhibitor cocktail without dimethylsulfoxide (DMSO) (ThermoFisher Scientific). Tumours were homogenized using a gentleMACS tissue dissociator (Miltenyi Biotec, C-tubes), and centrifuged at 3,000*g* for 10 min at 4 °C. The supernatant was then collected and centrifuged at 10,000*g* for 20 min at 4 °C to separate soluble and insoluble fractions. IL-12p70 in soluble sample fractions was analysed using the Mouse IL-12p70 Quantikine ELISA Kit (R&D systems) according to the manufacturer's instructions.

Blood bactericidal assay

EcN wild-type or EcNc$^{\Delta lon/\Delta ompT}$ were cultured overnight in LB media without antibiotics. Cultures were centrifuged at 3,000*g* for 10 min, resuspended in 1 ml of ice-cold sterile PBS and normalized to $OD_{600} = 1$. Then 50 μl of $OD_{600} = 1$ microbe suspension was added to 1 ml of single donor human whole blood (Innovative Research) in triplicate and incubated in a 37 °C stationary incubator. After 2 h of incubation, a sample was taken from each blood–microbe mixture and serial dilution was prepared in PBS. Dilutions were plated on LB agar with erythromycin (25 μg ml^{-1}). After incubation overnight at 37 °C, colonies were quantified by spot-forming assay and CFU ml^{-1} blood was calculated.

Biofilm assay

Biofilm formation assays were conducted as described previously[73]. Briefly, EcN wild-type, cryptic plasmid-cured (EcNc), Lon knockout

(EcNc$^{\Delta lon}$), OmpT knockout (EcNc$^{\Delta ompT}$) or double protease knockout (EcNc$^{\Delta lon/\Delta ompT}$) were cultured for 48 h in LB media with 25 μg ml^{-1} erythromycin in borosilicate glass tubes in a 30 °C stationary incubator, with tube caps wrapped with parafilm to prevent evaporation. At 48 h, cultures were discarded and borosilicate tubes were washed three times with PBS. Tubes were inverted and allowed to dry for 6 h. Biofilms left on borosilicate tubes were stained with 0.1% (vol/vol) crystal violet for 15 min. Crystal violet stain was discarded and tubes washed three times with PBS, then inverted and allowed to dry overnight. Crystal violet-stained biofilms were dissolved with 95% ethanol and transferred to 96-well plates for measurement of absorbance at 590 nm.

Phagocytosis assay

Bacterial phagocytosis assays were adapted from previous work[74]. Culture and isolation of murine BMDMs was performed as described previously[75]. Bulk femoral bone marrow cells from BALB/c or C57BL/6 mice were cultured on 15 cm non-treated cell culture Petri dishes in RPMI with 20% FBS, 25 ng ml^{-1} M-CSF (R&D Systems) and 100 U ml^{-1} penicillin–streptomycin. Media was replaced with fresh media after 4 days of culture. After 7 days of culture, plates were washed with PBS and adherent macrophages were dissociated using trypsin-EDTA. Macrophages were washed in PBS, resuspended at a density of 2×10^5 cells per ml in media and 1 ml transferred to each well of 24-well plates. The 24-well plates were incubated overnight in a 37 °C incubator with humidified 5% CO_2. EcN wild-type or EcNc$^{\Delta lon/\Delta ompT}$, with or without a constitutive green-fluorescent protein (GFP)-expressing plasmid were cultured overnight in LB media with appropriate antibiotics. Bacterial cultures were centrifuged at 3,000*g* for 10 min, washed three times with sterile PBS and resuspended at a density of 4×10^8 bacteria per ml in sterile PBS. Media from wells containing adherent macrophages was aspirated, wells washed three times with PBS and 1 ml of RPMI with 5% mouse serum added to each well. Latrunculin A was added at a concentration of 1 μM to selected wells to inhibit phagocytosis. Next, 2×10^7 CFU of microbes were added to each well with each condition tested in triplicate. Microbial strains were incubated with BMDMs for 30 min in a 37 °C incubator at 20 rpm. After 30 min, media was aspirated and wells were washed six times with sterile ice-cold PBS. Adherent macrophages were dissociated using non-enzymatic cell dissociation buffer (Gibco), resuspended in fluorescence-activated cell sorting (FACS) buffer (PBS containing 2% FBS, 2 mM EDTA and 0.09% sodium azide) and analysed by flow cytometry.

In vitro BMDM activation

BMDMs were cultured as described above for phagocytosis assays. BMDMs were washed in PBS, resuspended at a density of 2×10^5 ml^{-1} in media and 1 ml transferred to each well of 24-well plates. The 24-well plates were incubated overnight in a 37 °C incubator with humidified 5% CO_2. Wild-type EcN or EcNc$^{\Delta lon/\Delta ompT}$ with constitutive expression of OVA from a pUC origin plasmid were cultured overnight in LB media with appropriate antibiotics. Cultures were centrifuged at 3,000*g* for 10 min, washed three times with PBS and resuspended at a density of 4×10^8 bacteria ml^{-1} in sterile PBS. Media from wells containing macrophages was aspirated, wells were washed three times with PBS and 1 ml of RPMI with 5% mouse serum was added to each well. Next, 1×10^7 live microbes were added to each well, with each condition replicated in triplicate. Live microbial strains were incubated with BMDMs for 6 h in a 37 °C incubator. After 6 h, media was aspirated and wells were washed six times with sterile ice-cold PBS. Adherent macrophages were dissociated using non-enzymatic cell dissociation buffer (Gibco), resuspended in FACS buffer and analysed by flow cytometry. DRAQ7 cell viability reagent was used to exclude dead cells (diluted 1:1,000 in FACS buffer). Extracellular antibodies for BMDM activation panel included CD80 (catalogue no. 16-10A1, Biolegend), MHC-II (catalogue no. M5/114.15.2, Biolegend), PD-L1 (catalogue no. 10F.9G2, Biolegend) and H2K^b-SIINFEKL (catalogue no. 25-D1.16, Biolegend), each used at 1:200 dilution.

In vitro BMDC stimulation

BMDC isolation and culture from mouse bone marrow was adapted from previous methods[76]. BMDCs from C57BL/6 mice were cultured on 15 cm non-treated cell culture Petri dishes in RPMI with 20% FBS, 20 ng ml^{-1} GM-CSF (Biolegend) and 100 U ml^{-1} penicillin–streptomycin. Every 1–2 days for the first 4 days, plates were gently washed and non-adherent granulocytes removed by aspirating 50% of the culture media with subsequent replacement of fresh media. On day 4, media was aspirated completely and replaced with fresh culture media with 20 ng ml^{-1} GM-CSF. On day 6, BMDC plates were washed with PBS and loosely adherent and non-adherent cells collected. Cells were centrifuged at 300*g* for 5 min, resuspended in fresh culture media and replated on 15 cm non-treated cell culture Petri dishes. On days 7–8, plates were washed with PBS and loosely adherent and non-adherent cells were collected. Cells were centrifuged at 300*g* for 5 min, resuspended in fresh culture media at a density of 2.5×10^5 ml^{-1} and 200 μl was transferred to 96-well plates and incubated overnight in a 37 °C incubator. The next day, media from wells containing BMDCs was aspirated, and 1 ml of RPMI with 5% mouse serum was added to each well. BMDCs were pulsed with live bacteria at an multiplicity of infection of 10 for 2 h. Plates were centrifuged at 300*g* for 5 min, media aspirated and replaced with fresh RPMI with 10% FBS, 10 μg ml^{-1} gentamicin and 100 U ml^{-1} penicillin–streptomycin. Gentamicin concentration was increased to 40 μg ml^{-1} after 2–4 h. Plates were incubated for 5–48 h in a 37 °C incubator, at which time the supernatant was assessed for IL-12p70 using the Mouse IL-12p70 Quantikine ELISA Kit (R&D systems) according to the manufacturer's instructions.

OT-I and OT-II T cell stimulation and proliferation

BMDCs were cultured as above, resuspended at a density of 2.5×10^5 ml^{-1} and 5×10^4 BMDCs transferred to 96-well plates and incubated overnight in a 37 °C incubator. The next day, media from wells containing BMDCs was aspirated, and 1 ml of RPMI with 5% mouse serum was added to each well. BMDCs were pulsed with 2×10^6 CFU of the respective bacterial strain for 2.5 h, plates were centrifuged at 300*g* for 5 min, media aspirated and replaced with fresh RPMI with 10% FBS and 10 μg ml^{-1} gentamicin and 100 U ml^{-1} penicillin–streptomycin. Gentamicin concentration was increased to 40 μg ml^{-1} after 2–4 h. Spleens from naive OT-I and OT-II mice were extracted, filtered through 100 μm cell strainers and washed in complete RPMI (RPMI-1640 supplemented with 10% (vol/vol) FBS, 1× GlutaMax, 1% (vol/vol) MEM non-essential amino acids solution (Gibco-11140050) and 100 U ml^{-1} penicillin–streptomycin). OT-I and OT-II T cells were isolated from single-cell suspensions of spleens from the respective transgenic mouse using the EasySep Mouse T Cell Isolation Kit (StemCell Technologies) according to the manufacturer's instructions. Purified OT-I and OT-II T cells were resuspended in T cell media (complete RPMI supplemented with 50 μM β-mercaptoethanol) at a density of 5×10^5 ml^{-1} and 5×10^4 T cells incubated with 5×10^4 BMDCs pulsed with the respective microbial strains. For cytokine secretion assessment, T cells were incubated with BMDCs for 24 h, at which time supernatant was assessed for IFNγ and IL-2 using Mouse IFNgamma Quantikine ELISA Kit and Mouse IL-2 Quantikine ELISA Kit (R&D systems) according to the manufacturer's instructions.

Carboxyfluorescein succinimidyl ester (CFSE) proliferation assays were conducted as previously described[77]. Here, 1×10^7 OT-I or OT-II T cells were resuspended in 1 ml of room temperature PBS, and 1 μl of 5 mM CFSE (Biolegend) was added. T cells were incubated in CFSE solution for 5 min at room temperature protected from light, after which time staining was quenched by adding ten times the staining volume of cell culture media. T cells were centrifuged at 300*g* for 5 min, resuspended in T cell media at a density of 5×10^5 ml^{-1} and incubated for an extra 10 min at room temperature. Then 5×10^4 T cells were incubated with 5×10^4 BMDCs pulsed with the respective live microbial strains. At 48 h, 50% of the media from each well was gently aspirated so as to not

disturb any cells, and replaced with fresh T cell media. At 72–96 h, OT-I and OT-II T cells were collected and analysed by flow cytometry. DRAQ7 cell viability reagent was used to exclude dead cells (diluted 1:1,000 in FACS buffer). Extracellular antibody staining for CFSE assays included antimouse CD3 (catalogue no. 17A2, Biolegend), used at 1:200 dilution.

Listeriolysin haemolytic activity assay

Sheep red blood cell (RBC) lysis by bacterial lysate was performed as described previously[78]. Briefly, bacteria were grown overnight in fresh LB containing appropriate antibiotics. Cultures were centrifuged at 3,000*g* for 10 min, supernatants discarded and the cell pellet resuspended to $OD_{600} = 8$ in 0.1% (w/w) bovine serum albumin (BSA) in sterile PBS titrated to pH of 5.25 with 1 M HCl. Bacteria were sonicated for 2 min. After sonication, the soluble fraction was isolated by centrifugation at 10,000*g* at 4 °C for 20 min. Sheep RBCs were washed three times with PBS and resuspended at a final concentration of 6×10^8 ml^{-1} in 0.1% (w/w) BSA in PBS titrated to pH of 5.25. Equal parts of bacterial lysate soluble fraction and sheep RBC suspension were mixed and incubated for 15 min at 37 °C. After incubation RBC mixtures were centrifuged at 1,000*g* for 1 min at 4 °C and supernatant absorbance at 541 nm was then measured to quantify RBC lysis.

Listeriolysin cytosolic access assay

BMDMs were cultured as described above for phagocytosis assays. BMDMs were washed in PBS, resuspended at a density of 2.5×10^5 ml^{-1} in media, 100 ml transferred to wells of an eight-well Lab-Tek Chamber Slide system (ThermoFisher) and incubated overnight in a 37 °C incubator. The next day, media from wells containing BMDMs was aspirated, and 1 ml of complete RPMI without antibiotics was added to each well. BMDMs were then pulsed with 1.25×10^6 CFU of the respective bacterial strain for 60 min. After the designated time media from each well was aspirated, wells were washed four times with PBS and media was replaced with fresh RPMI with 10% FBS and 40 μg ml^{-1} gentamicin and incubated in a stationary 37 °C incubator. After either 30 or 60 min of more incubation, media was aspirated and wells washed four times with ice-cold PBS. Then 100 ml of 100% methanol at −80 °C was then added to each well for fixation and allowed to incubate at room temperature for 10 min. Methanol was then removed, 100 ml of ice-cold PBS added to each well and slides incubated at 4 °C. Cells were permeabilized with 0.5% Triton X in PBS for 10 min. Blocking solution in 10% heat-inactivated horse serum and 3% BSA was added to each well for 30 min. After washing three times, primary antibodies in 1% heat-inactivated horse serum and 1% BSA were incubated overnight at 4 °C in a humidified chamber. The next day, slides were washed with PBS three times for 10 min each and secondary antibodies were applied for 1 h at room temperature in the dark. DAPI (4′6-diamidino-2-phenylindole) was applied as part of the secondary antibody cocktail for nuclear staining. Slides were washed in PBS three times before mounting coverslips with DAKO gel and stored at 4 °C until immunofluorescence analysis. Anti-ovalbumin (catalogue no. EPR27117-90, Abcam) and anti-CD11b (catalogue no. M1/70, Abcam) primary antibodies were used for staining, both at 1:200 dilution.

Animal experiments

All animal experiments were approved by the Institutional Animal Care and Use Committee (Columbia University, protocol AABQ5551). The 6–7-week-old female BALB/c, C57BL/6 and B6(Cg)-Tyrc-2J/J (Jackson Laboratories) mice were kept in accordance with all rules for animal research at Columbia University. Mice were housed in a facility with a 12 h light–dark cycle, and provided unrestricted access to both food and water. The housing facility was maintained at 21–24 °C, and kept at 40–60% humidity. Sample size was determined on the basis of our previous studies and/or pilot experiments. For subcutaneous tumour models: 5×10^6 CT26 cells in 100 μl of sterile PBS were inoculated subcutaneously on the hind flank of BALB/c mice, or 5×10^5 B16F10 melanoma cells in 100 μl of sterile PBS subcutaneously on the hind flank (orthotopic) of C57BL/6 mice using a 26G needle on a 1 cc syringe. CT26 tumours were allowed to establish as indicated for each experiment, and mice were distributed between groups to equate the average starting tumour volume before treatment. B16F10 orthotopic tumours were allowed to establish for 9 days, and initial average tumour volume equated between groups before treatment. Tumour dimensions were measured unblinded with a calliper every 1–3 days for calculating tumour volumes using the equation $(a^2 \times b)/2$ (a is width, b is length, where width is the smaller dimension). Group tumour sizes were computed as mean ± s.e.m. Body weight was measured each time tumour measurements were taken. Animals were euthanized when any of the following criteria were met: tumour burden greater than 2 cm in the largest dimension for any subcutaneous tumour, greater than 20% body weight loss, as otherwise recommended by veterinary staff or when showing clinical signs of impaired health. To examine the requirement of individual T cell populations for the efficacy of the microbial neoantigen vaccines, mice were injected intraperitoneally with 200 μg (in 100 μl of InVivoPure pH 6.5 buffer, BioXcell) of antimouse CD4 (clone GK1.5, BioXcell), 200 μg (in 100 μl of InVivoPure pH 7.0 buffer, BioXcell) of antimouse CD8β (clone Ly-3.2, BioXcell) or 200 μg (in 100 μl of InVivoPure pH 7.0 buffer, BioXcell) of IgG1 isotype control (clone HRPN, BioXcell) beginning 2 days before the initiation of therapeutic treatment and every 2–3 days thereafter until study endpoint.

In prophylactic vaccination studies, BALB/c mice received an intravenous injection of either EcNc$^{\Delta lon/\Delta ompT/\mathrm{LLO}^+}$ OVA or EcNc$^{\Delta lon/\Delta ompT/\mathrm{LLO}^+}$ nAg[19] every 3–5 days for a total of four injections. Four days after the final injection, 1×10^6 CT26 cells in 100 μl of sterile PBS were inoculated subcutaneously on the hind flank. In rechallenge studies, BALB/c mice that had cleared subcutaneous CT26 tumours on a single hind flank were engrafted with 1×10^6 CT26 cells on the opposite hind flank 100 days after tumour clearance. Age-matched naive BALB/c mice were engrafted with 1×10^6 of the same CT26 cells on a single hind flank as controls.

For therapeutic studies in systemic metastases models, 5×10^5 CT26-Luc cells or 1.5×10^5 B16F10-Luc cells were injected in 100 μl of sterile PBS through the lateral tail vein with a 27G needle on 1 cc syringe. Metastases were allowed to establish for 4 days in Balb/C mice before treatment for CT26-Luc, and for 2 days in C57BL/6 albino mice (B6(Cg)-Tyrc-2J/J) for B16F10-Luc. Mice were randomly distributed between groups after metastases engraftment and before treatment. For in vivo luminescence tracking of metastases burden, mice were injected intraperitoneally with 125 μl of aqueous solution of D-Luciferin (50 mg ml^{-1}) 6 min before imaging, and placed under isoflurane anaesthesia for imaging using an in vivo imaging system (IVIS), with exposure time set to 6 min. Total flux from the lungs (CT26-Luc) or body (B16F10-Luc) was used to quantify tumour burden. For evaluation of lung metastases burden at the timepoint of treatment initiation, mice were injected intraperitoneally with 250 μl of aqueous solution of D-Luciferin (50 mg ml^{-1}) 6 min before imaging and placed under isoflurane anaesthesia for imaging using an IVIS with exposure time set to 10 min. After in vivo IVIS analysis, mice were then re-injected with 100 μl of aqueous solution of D-luciferin (50 mg ml^{-1}) and lungs were extracted for ex vivo IVIS imaging with exposure time set to 2 min.

No formal blinding was done for in vivo experiments. For all animal experiments, intratumoural treatments were injected directly into the tumour core with care to not allow leakage of any therapeutic solution. Intravenous treatments were injected through the lateral tail vein, with care not to allow leakage of any therapeutic solution.

SLP vaccination

The formulation and administration of SLP vaccines was adapted from previous studies[15,79,80]. Each dose contained either 20 μg of each 29-mer CT26 neoantigen peptide (19 neoantigens, 380 μg of total peptide per dose) and 50 μg of poly I:C in 200 μl of 10% DMSO/90% PBS (vol/vol) in Fig. 2e and Extended Data Fig. 5e,f, or 25 μg of each 29-mer CT26 neoantigen peptide (19 neoantigens, 475 μg total peptide per dose) and 100 μg

of poly I:C in 200 µl of 10% DMSO /90% PBS (vol/vol) in Extended Data Fig. 5g. Therapeutic SLP vaccinations were administered subcutaneously to BALB/c mice with established hind-flank CT26 tumours on the contralateral hind flank using a 29G needle. SLP vaccine groups were treated on the same days as microbial therapeutic groups.

Ex vivo lung histology

Explanted lungs from BALB/C mice bearing CT26-Luc metastases or C57BL/6 albino mice (B6(Cg)-Tyrc-2J/J) bearing B16F10-Luc metastases were washed three times in PBS and placed in 10% formalin. After at least 24 h of fixation, lungs were transferred to 70% ethanol and subsequently embedded in paraffin. Then 50 µm consecutive sections were stained with haematoxylin and eosin. Lung sections were analysed for the presence of tumour foci.

Microbial administration for in vivo experiments

For therapeutic administration, bacterial strains were grown overnight in fresh LB media containing the appropriate antibiotics. Overnight cultures were centrifuged at 3,000*g* at 4 °C for 10 min and washed three times with ice-cold sterile PBS. Microbes were delivered intratumourally at a concentration of 5×10^8 CFU ml^{-1} in sterile PBS, with 20 µl of injected using a 1 cc syringe with a 29G needle. For intravenous treatment, 100 µl of microbes were delivered at a concentration of 1×10^8 CFU ml^{-1} in sterile PBS, through the lateral tail vein using a 1 cc syringe with a 29G needle.

Biodistribution and in vivo bacterial dynamics

For biodistribution experiments, BALB/c mice bearing established hind-flank CT26 or lung metastatic CT26-Luc tumours were injected intravenously with 100 µl of 1×10^8 CFU ml^{-1} EcNc$^{\Delta lon/\Delta ompT/\mathrm{LLO}+}$. Then 96–120 h after a single i.v. injection for hind-flank tumours or at endpoint for lung metastases, tumours or tumour-bearing lungs and other organs were extracted from mice, weighed and homogenized using a gentleMACS tissue dissociator (Miltenyi Biotec, C-tubes). Homogenates were serially diluted in sterile PBS and plated on LB agar plates at 37 °C overnight. Colonies were quantified per organ and computed as CFU per gram of tissue (CFU g^{-1}). For tracking bacterial colonization of subcutaneous tumours by microbial luminescence, tumour-bearing mice treated intratumourally or intravenously with wild-type EcN parental strain or genetic derivates were imaged using IVIS at various time points. For abscopal experiments, treated and untreated tumours were harvested 14 days after a single intratumoural bacterial injection.

Ex vivo T cell killing assay

For B16F10-Luc specific killing, naive tumour-free C57BL/6 mice were injected intravenously every 4 days with PBS, EcNc$^{\Delta lon/\Delta ompT/\mathrm{LLO}+}$ OVA or nAg[42] for a total of four doses. Five days after the final dose spleens from treated mice were extracted, filtered through 100 µm cell strainers and washed in complete RPMI. T cells were isolated from single-cell suspensions of spleens from the respective mouse using the EasySep Mouse T Cell Isolation Kit (StemCell Technologies) according to the manufacturer's instructions. Purified T cells were resuspended in T cell media for use in the specific lysis assay.

The luciferase-based killing assay was adapted from previous methods[81]. B16F10-Luc target cells were grown for 48 h in the presence of 100 U ml^{-1} murine IFNγ. Target cells were gathered and plated at 1×10^4 cells per well in a 96-well plate. After 12 h, T cells were added to each well to achieve designated effector-to-target ratios (10:1, 20:1 or 40:1). After 42 h of co-incubation, 50 U ml^{-1} IL-2 was added to all wells.

For CT26-Luc versus 4T1-Luc luciferase-based specific killing assay: BALB/c mice with established hind-flank CT26 tumours were treated intravenously with EcNc$^{\Delta lon/\Delta ompT/\mathrm{LLO}+}$ nAg[19] on days 0 and 3. On day 8, tumours were extracted and mechanically homogenized, followed by digestion with collagenase A (1 mg ml^{-1}, Roche) in isolation buffer (RPMI-1640 with 5% FBS, 1% L-glutamine, 1% penicillin–streptomycin and 10 mM HEPES) with gentamicin (40 µg ml^{-1}) for 1 h at 37 °C on a shaker platform at 150 rpm. Tumour homogenates were filtered through 100 µm cell strainers and washed in T cell media. Tumour-infiltrating T cells were isolated from single-cell suspensions of tumours from mice using the EasySep Mouse T Cell Isolation Kit (StemCell Technologies) according to the manufacturer's instructions. Purified T cells were resuspended in T cell media.

CT26-Luc or 4T1-Luc target cells were grown for 12 h in the presence of 100 U ml^{-1} murine IFNγ. Target cells were gathered and plated at 1×10^4 cells per well in a 96-well plate. After 12 h, T cells were added to each well to achieve designated effector-to-target ratios (5:1 or 10:1), with 50 U ml^{-1} IL-2 added to all wells.

Luminescence from each well was quantified after addition of One-Glo Luciferase Assay System (Promega), as per the manufacturer's instructions, after 24–96 h of coculture. Minimum lysis wells contained only the respective luciferase-expressing tumour target cells. In maximum lysis wells, 20 µl of media was replaced with 20 µl of 3% Triton X-100 60 min before luminescence readout. Specific lysis (%) was calculated using the luminescence values of the respective conditions with the following formula: 100 − (100 × ((sample − maximum lysis)/(minimum lysis − maximum lysis))).

IFNγ ELISpot

BALB/c mice with established hind-flank CT26 tumours were treated intravenously with EcNc$^{\Delta lon/\Delta ompT/\mathrm{LLO}+}$ nAg[19] on day 0 and 3. On day 8, tumours were extracted and mechanically homogenized, followed by digestion with collagenase A (1 mg ml^{-1}, Roche) in isolation buffer (RPMI-1640 with 5% FBS, 1% L-glutamine, 1% penicillin–streptomycin and 10 mM HEPES) with gentamicin (40 µg ml^{-1}) for 1 h at 37 °C on a shaker platform at 150 rpm. Tumour homogenates were filtered through 100 µm cell strainers and washed in RPMI containing CTL-Wash Supplement (Immunospot) and 1% L-glutamine. Splenocytes from naive BALB/c mice were isolated in the same way, without digestion. T cells were isolated from single-cell suspensions of tumours from mice using the EasySep Mouse T Cell Isolation Kit (StemCell Technologies) according to the manufacturer's instructions. Purified T cells were resuspended in CTL-Test Medium supplemented with 1% L-glutamine for use in the enzyme-linked immunosorbent spot (ELISpot) assay.

Mouse IFNγ Single-Color ELISpot plates and kits were purchased from Immunospot. ELISpot plates were prepared as per manufacturer's instructions. Here, 5×10^5 naive splenocytes were plated with 2×10^4 TILs per well in 200 µl CTL-Test Medium supplemented with 1% L-glutamine and gentamicin (30 µg ml^{-1}). Then 29-mer synthetic neoantigen or negative control (OVA) peptides were added to each well at a final concentration of 5 µg ml^{-1}. Cells were stimulated overnight in a stationary 37 °C incubator with atmosphere of humidified 5% CO_2. After incubation, plates were developed as per the manufacturer's protocol and spots quantified using a CTL Immunospot S6 Universal machine and CTL ImmunoSpot software v.7.0.24.0.

Flow cytometry immunophenotyping

For CT26 flow-cytometric immunophenotyping, BALB/c mice with hind-flank CT26 tumours received intravenous treatment with the indicated microbial therapeutic or PBS on day 0. Two or 8 days after treatment, TDLNs and/or tumours were extracted. For B16F10 flow-cytometric immunophenotyping, C57BL/6 mice with hind-flank, orthotopic B16F10 tumours received intravenous treatment with the indicated microbial therapeutic or PBS on day 0 and 3. Eight days after treatment, tumours were extracted. Lymphoid and myeloid immune subsets were isolated from tumour tissue by mechanical homogenization of tumour or TDLN tissue, followed by digestion with collagenase A (1 mg ml^{-1}, Roche) and DNase I (0.5 µg ml^{-1}, Roche) in isolation buffer (RPMI-1640 with 5% FBS, 1% L-glutamine, 1% penicillin–streptomycin and 10 mM HEPES) for 1 h at 37 °C for tumours or 30 min at 37 °C for TDLNs, on a shaker platform at 150 rpm. For ex vivo

lymphocyte stimulation with PMA and ionomycin, TDLNs were not digested beforehand. Tumour and TDLN homogenates were filtered through 100 µm cell strainers and washed in isolation buffer. To measure overall cytokine production by T cells, cells were stimulated for 3 h with PMA (50 ng ml^{-1}, Sigma-Aldrich) and ionomycin (1 nM, Calbiochem) in the presence of brefeldin A (1 µg ml^{-1}). To measure neoantigen-specific cytokine production by T cells, cells were stimulated for 5 h with pools of peptides (2 µg ml^{-1}) representing the neoantigens encoded in therapeutic strains in the presence of brefeldin A (1 µg ml^{-1}). Cells were stained in FACS buffer. Ghost Dye cell viability reagent was used to exclude dead cells (diluted 1:1,000 in PBS). Extracellular antibodies for lymphoid immunophenotyping included: CD4 (RM4-5, Biolegend), NKp46 (29A1.4, BD Biosciences), NK1.1 (PK136, Biolegend), CD45 (30-F11, BD Biosciences), B220 (RA3-6B2, BD Biosciences), CD19 (6D5, Biolegend), CD8a (53-6.7, Biolegend), TIM-1 (RMT1-4, BD Biosciences) and CD69 (H1.2F3, BD Biosciences). After extracellular staining, cells were washed with FACS buffer, and fixed using the FOXP3/transcription factor staining buffer set (Tonbo), as per the manufacturer's instructions. Intracellular antibodies for lymphoid immunophenotyping included: Foxp3 (FJK-16s, Thermo), CD3ε (145-2C11, Biolegend), TCRβ (H57-507, BD Biosciences), Ki-67 (SolA15, Thermo), Granzyme-B (QA16A02, Biolegend), TNF (MP6-XT22, Biolegend) and IFNγ (XMG1.2, Biolegend). For myeloid immunophenotyping, extracellular antibodies included: Ly6C (HK1.4, Biolegend), I-A/I-E (M5/114.15.2, BD Biosciences), XCR1 (ZET, Biolegend), CD11b (M1/70, Biolegend), CD103 (2E7, Biolegend), CD45 (30-F11, BD Biosciences), F4/80 (BM8, Biolegend), CD11c (HL3, BD Biosciences), CD172a/SIRPα (P84, Biolegend), Ly6G (1A8, Biolegend and BD Biosciences), PD-L1 (10 F.9G2, Biolegend), CD301b (URA-1, Biolegend), CD3 (145-2C11, Biolegend), CD19 (1D3, Biolegend), NK1.1 (PK136, Biolegend), NKp46 (29A1.4, Biolegend) CD64 (X54-5/7.1, Biolegend), CD80 (16-10A1, Biolegend) and CD86 (GL-1, BD Biosciences). All antibodies for flow cytometry were used at a 1:200 dilution. After staining, cells were washed and resuspended with FACS buffer for flow cytometry analysis using a BD LSRFortessa or Cytek Aurora cell analyser. FACS Diva or SpectroFlo software was used for data acquisition. Collected flow cytometry data were analysed using FlowJo.

Synthetic peptides

Synthetic peptides representing neoantigens for lymphocyte restimulation assays and vaccination were synthesized by and purchased from Peptide v.2.0. All peptides were above or equal to 95% purity.

Statistics and reproducibility

Statistical analyses and *P* value calculations were performed using GraphPad Prism v.9 and v.10. For each experiment, the particular statistical analysis is detailed in the respective figure legend. A two-tailed unpaired Student's *t*-test, one-way analysis of variance (ANOVA) or two-way ANOVA with appropriate post hoc test was used for data that were roughly normally distributed. For analysis of Kaplan–Meier survival experiments, the log-rank (Mantel–Cox) test was used. All analyses were two-tailed. For all statistical analyses, NS denotes not significant, which is $P > 0.05$.

For Fig. 4a and Extended Data Fig. 7b, immunoblot data are representative of four independent experiments. In Extended Data Figs. 1b and 2h, immunoblot data are representative of three independent experiments. Immunofluorescence data in Extended Data Fig. 2i are representative of three independent experiments. Histology data in Extended Data Figs. 5h and 8f are representative of three independent experiments. All other results in the paper were replicated at least two to three times in independent experiments.

Biological materials availability

Reasonable requests for biological materials used in this study will be promptly reviewed by Columbia Technology Ventures to verify whether the request is subject to any intellectual property or confidentiality obligations. Any materials that can be shared will be released through a material transfer agreement.

Reporting summary

Further information on research design is available in the Nature Portfolio Reporting Summary linked to this article.

Data availability

Whole-exome sequencing and RNA sequencing data generated for this study are deposited under umbrella BioProject accession number PRJNA1025007. Whole-exome data are available on the Short Read Archive with BioProject ID PRJNA1024050. RNA sequencing data are available on National Center for Biotechnology Information Gene Expression Omnibus with accession number GSE244808. All other data are available within the article or its Supplementary Information. Datasets used for analyses in this study were: Ensembl release 102 *M. musculus* GRCm38 gene annotations (GRCm38, https://useast.ensembl.org/Mus_musculus/Info/Index, accession GCA_000001635.8) and dbSNP build 142 (ftp.ncbi.nih.gov/snp). Source data are provided with this paper.

56. Gnirke, A. et al. Solution hybrid selection with ultra-long oligonucleotides for massively parallel targeted sequencing. *Nat. Biotechnol.* **27**, 182–189 (2009).
57. Bolger, A. M., Lohse, M. & Usadel, B. Trimmomatic: a flexible trimmer for Illumina sequence data. *Bioinformatics* **30**, 2114–2120 (2014).
58. Miller, N. A. et al. A 26-hour system of highly sensitive whole genome sequencing for emergency management of genetic diseases. *Genome Med.* **7**, 100 (2015).
59. Van der Auwera, G. A. & O'Connor, B. D. *Genomics in the Cloud: Using Docker, GATK, and WDL in Terra* (O'Reilly Media, 2020).
60. Sherry, S. T. et al. dbSNP: the NCBI database of genetic variation. *Nucleic Acids Res.* **29**, 308–311 (2001).
61. Li, H. A statistical framework for SNP calling, mutation discovery, association mapping and population genetical parameter estimation from sequencing data. *Bioinformatics* **27**, 2987–2993 (2011).
62. Dobin, A. et al. STAR: ultrafast universal RNA-seq aligner. *Bioinformatics* **29**, 15–21 (2013).
63. Love, M. I., Huber, W. & Anders, S. Moderated estimation of fold change and dispersion for RNA-seq data with DESeq2. *Genome Biol.* **15**, 550 (2014).
64. Khanna, A. et al. Bam-readcount—rapid generation of basepair-resolution sequence metrics. *J. Open Source Softw.* **7**, 3722 (2022).
65. McLaren, W. et al. The Ensembl Variant Effect Predictor. *Genome Biol.* **17**, 122 (2016).
66. Reynisson, B., Alvarez, B., Paul, S., Peters, B. & Nielsen, M. NetMHCpan-4.1 and NetMHCIIpan-4.0: improved predictions of MHC antigen presentation by concurrent motif deconvolution and integration of MS MHC eluted ligand data. *Nucleic Acids Res.* **48**, W449–W454 (2020).
67. Andreatta, M. & Nielsen, M. Gapped sequence alignment using artificial neural networks: application to the MHC class I system. *Bioinformatics* **32**, 511–517 (2016).
68. Reynisson, B. et al. Improved prediction of MHC II antigen presentation through integration and motif deconvolution of mass spectrometry MHC eluted ligand data. *J. Proteome Res.* **19**, 2304–2315 (2020).
69. Nielsen, M. & Lund, O. NN-align. An artificial neural network-based alignment algorithm for MHC class II peptide binding prediction. *BMC Bioinformatics* **10**, 296 (2009).
70. Danino, T. et al. Programmable probiotics for detection of cancer in urine. *Sci. Transl. Med.* **7**, 289ra84–289ra84 (2015).
71. Gurbatri, C. R. et al. Engineered probiotics for local tumor delivery of checkpoint blockade nanobodies. *Sci. Transl. Med.* **12**, eaax0876 (2020).
72. Datsenko, K. A. & Wanner, B. L. One-step inactivation of chromosomal genes in *Escherichia coli* K-12 using PCR products. *Proc. Natl Acad. Sci. USA* **97**, 6640–6645 (2000).
73. Reisner, A., Krogfelt, K. A., Klein, B. M., Zechner, E. L. & Molin, S. In vitro biofilm formation of commensal and pathogenic *Escherichia coli* strains: impact of environmental and genetic factors. *J. Bacteriol.* **188**, 3572–3581 (2006).
74. Boero, E. et al. Use of flow cytometry to evaluate phagocytosis of *Staphylococcus aureus* by human neutrophils. *Front. Immunol.* **12**, 635825 (2021).
75. Zhang, X., Goncalves, R. & Mosser, D. M. The isolation and characterization of murine macrophages. *Curr. Protoc. Immunol.* **Chapter 14**, 14.1.1–14.1.14 (2008).
76. Inaba, K. et al. Generation of large numbers of dendritic cells from mouse bone marrow cultures supplemented with granulocyte/macrophage colony-stimulating factor. *J. Exp. Med.* **176**, 1693–1702 (1992).
77. Quah, B. J. C., Warren, H. S. & Parish, C. R. Monitoring lymphocyte proliferation in vitro and in vivo with the intracellular fluorescent dye carboxyfluorescein diacetate succinimidyl ester. *Nat. Protoc.* **2**, 2049–2056 (2007).
78. Mengaud, J. et al. Expression in *Escherichia coli* and sequence analysis of the listeriolysin O determinant of *Listeria* monocytogenes. *Infect. Immun.* **56**, 766–772 (1988).
79. Gubin, M. M. et al. Checkpoint blockade cancer immunotherapy targets tumour-specific mutant antigens. *Nature* **515**, 577–581 (2014).
80. Hailemichael, Y. et al. Persistent antigen at vaccination sites induces tumor-specific CD8+T cell sequestration, dysfunction and deletion. *Nat. Med.* **19**, 465–472 (2013).

81. Fu, X. et al. A simple and sensitive method for measuring tumor-specific T cell cytotoxicity. *PLoS ONE* **5**, e11867 (2010).

Acknowledgements Research reported in this publication was performed in the Columbia University Department of Microbiology and Immunology Flow Cytometry core facility, the Columbia Center for Translational Immunology (CCTI) and the Herbert Irving Comprehensive Cancer Center (HICCC) Flow Cytometry core facility. Grant numbers NIH/NCI R01CA249160, NIH/NCI R01CA259634, NIH/NCI U01CA247573, NIH/NIGMS T32GM145766, NIH S10OD030282, Searle Scholars Program SSP-2017-2179, Cancer Research Institute CRI 3446, Pershing Square Foundation PSSCRA CU20-0730 and a Roy and Diana Vagelos Precision Medicine Pilot grant supported the study.

Author contributions A.R., T.D. and N.A. conceived the study. A.R. designed the system and experiments, conducted sequencing analysis and neoantigen selection, constructed all therapeutics and performed most experiments. A.R. and J.I. designed microbial genetic knockouts. A.R. and B.R. designed and performed all in vitro and ex vivo T cell assays, and flow-cytometric immunophenotyping. A.R., J.I., S.H., M.K., Y.J., W.S. and A.V. performed cloning. J.I., S.H., M.K. and Y.J. performed knockouts. M.R., F.L. and J.I. assisted with sample processing for immunophenotyping. J.I., W.S., Z.S., C.R.G., S.H., J.H., E.R.B., R.L.V., M.K. and A.V. assisted with some in vitro, in vivo and/or ex vivo experiments. J.I., Z.S., S.H., M.K. and Y.J. performed blood bactericidal assays and qPCR. A.R. and M.R. performed immunofluorescence studies. A.R., T.D. and N.A. analysed data and wrote the paper with input from all authors.

Competing interests A.R., J.I., T.D. and N.A. have filed a provisional patent application with the US Patent and Trademark Office related to this work. The other authors declare no competing interests.

Additional information

Supplementary information The online version contains supplementary material available at https://doi.org/10.1038/s41586-024-08033-4.

Correspondence and requests for materials should be addressed to Tal Danino or Nicholas Arpaia.

Peer review information *Nature* thanks Paul Robbins and the other, anonymous, reviewer(s) for their contribution to the peer review of this work.

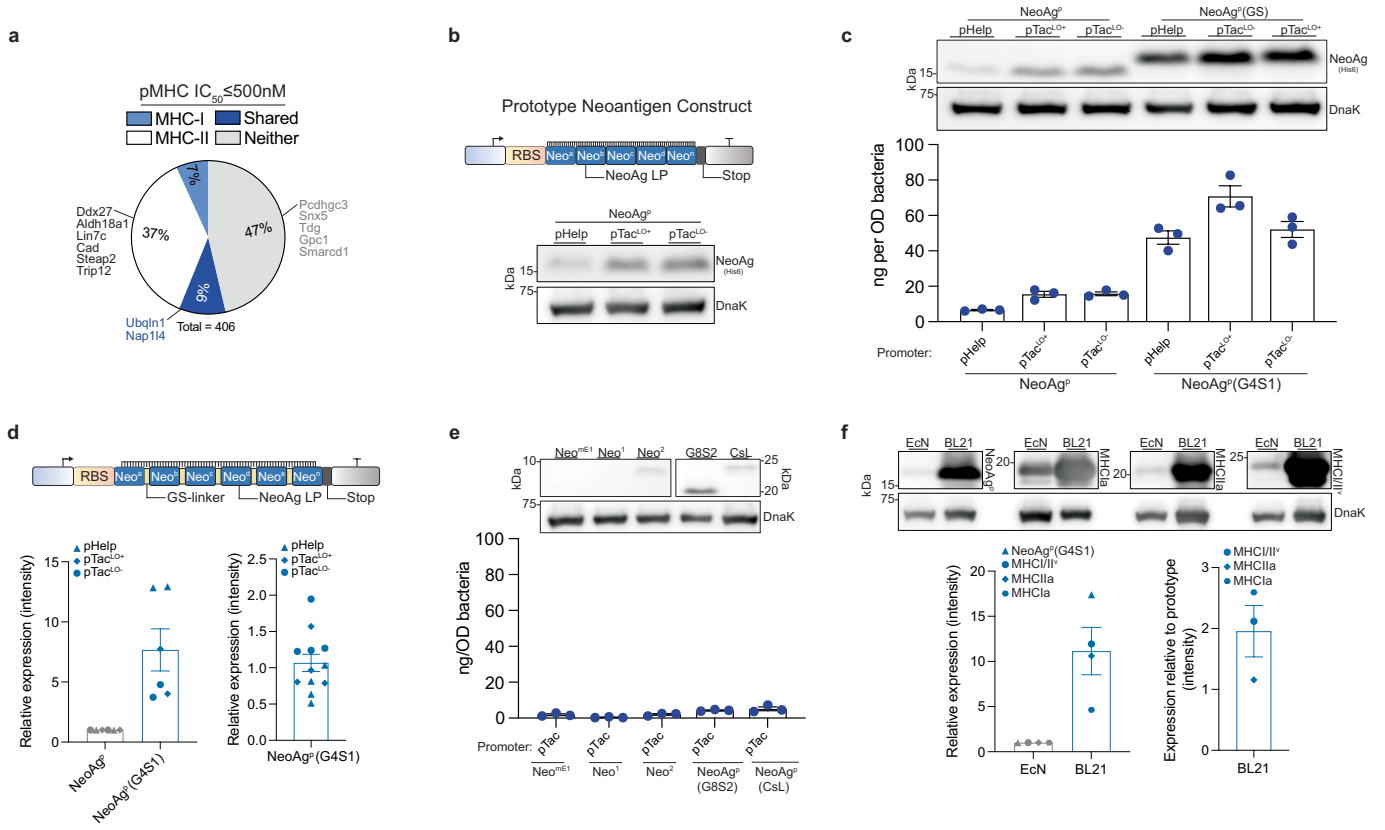

Extended Data Fig. 1 | Neoantigen prediction and synthetic construct design. a, Percentage of predicted CT26 neoantigens containing mutant-epitope(s) with ≤500 nM MHC-I affinity (MHC-I), MHC-II affinity (MHC-II), both MHC-I and MHC-II affinity (Shared), or no epitope meeting affinity criteria (Neither). Previously validated neoantigens within the set are labeled. **b**, Upper: prototype neoantigen construct design, Lower: immunoblot of EcN expressing prototype neoantigen constructs. **c**, Upper: immunoblot of EcN expressing prototype neoantigen constructs with or without GS-linkers. Lower: ELISA quantification of neoantigen construct in soluble fraction with or without GS-linkers in DH5α ($n = 3$ biological replicates per group). $NeoAg^P$ = prototype neoantigen construct, G4S1 = 5-mer GS-linker, $pTac^{LO-}$ = pTac without Lac operator; $pTac^{LO+}$ = with Lac operator. **d**, Upper: neoantigen construct design with GS-linkers, Lower-left: Relative immunoblot chemiluminescent intensity for prototype construct with or without interspersing glycine-serine linkers ($n = 6$ biological replicates per group). Lower-right: relative expression of prototype neoantigen construct with GS-linkers under selected promoters ($n = 12$ biologically independent samples). **e**, Upper: immunoblot of EcN expressing alternate prototype neoantigen constructs. Lower: ELISA quantification of alternative neoantigen construct in soluble fraction in DH5α ($n = 3$ biological replicates per group). Neo^{mE1} = minimal epitope, Neo^1 = 1 neoantigen LP in construct, Neo^2 = 2 neoantigen LP in construct, G8S2 = 10-mer GS-linker, CsL = immunoprotease sensitive linker. **f**, Upper: Immunoblot of neoantigen constructs ($NeoAg^P$, MHCIa, MHCIIa, $MHCI/II^v$), expressed in BL21 or EcN. Lower-left: relative immunoblot chemiluminescent intensity for neoantigen construct expression in EcN vs. BL21 ($n = 4$ biological replicates per group), Lower-right: relative immunoblot chemiluminescent intensity of predicted neoantigen constructs vs. prototype in BL21 ($n = 3$ biologically independent samples). **c**–**f**, Data are mean ± s.e.m. Gel source data in Supplementary Fig. 1.

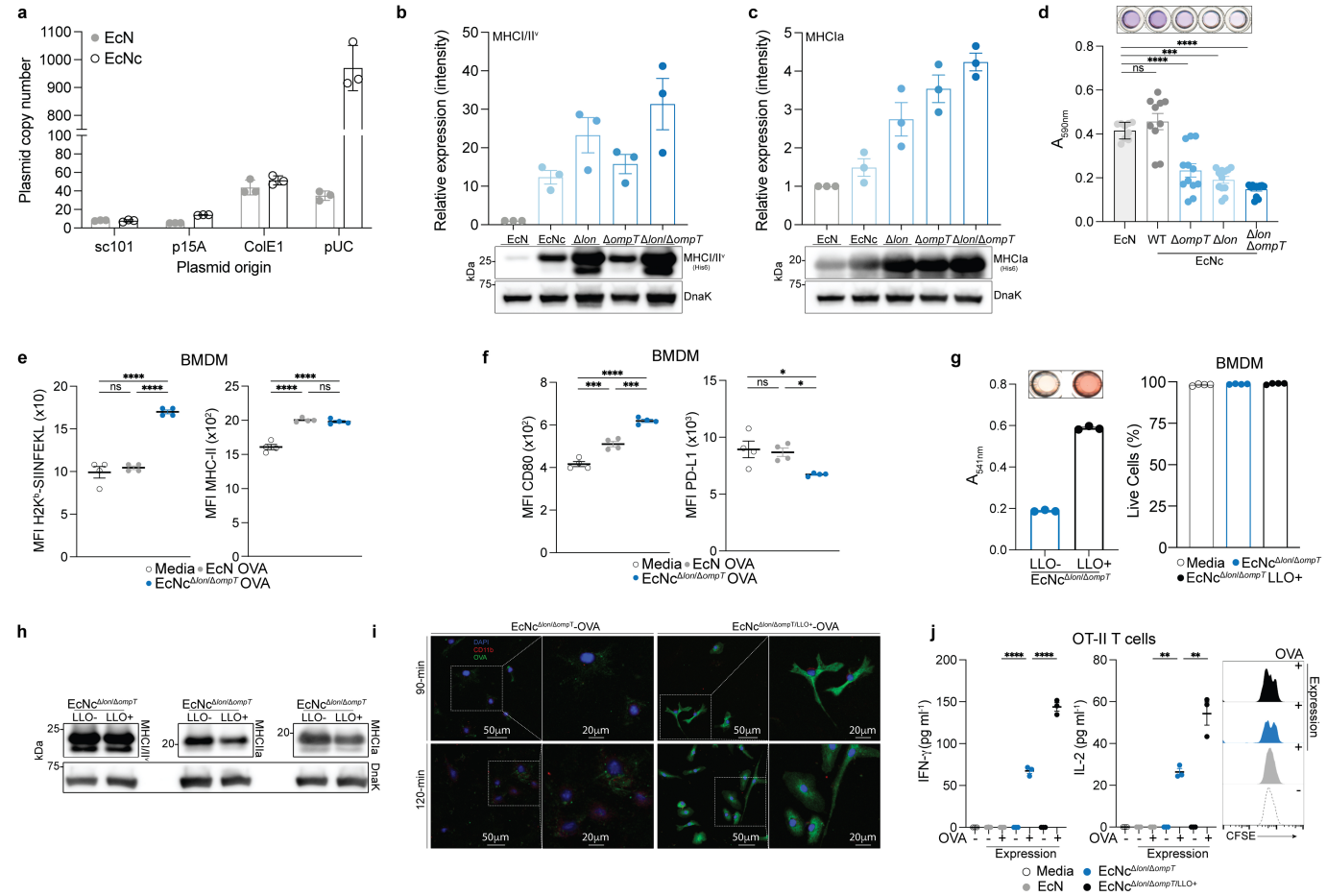

Extended Data Fig. 2 | Evaluation of microbial tumor neoantigen vaccine functioning and immunologic activity in vitro. a, Plasmid copy number in wildtype EcN or cryptic plasmid cured EcNc ($n = 3$ per group). **b**, Upper: relative immunoblot chemiluminescent intensity of synthetic neoantigen construct MHCI/II^{v} expression in wildtype EcN vs. derivative strains ($n = 3$ biological replicates), Lower: representative immunoblot of construct MHCI/II^{v} expressed in wildtype EcN and derivative strains. **c**, Upper: relative immunoblot chemiluminescent intensity of synthetic neoantigen construct MHCIa expression in wildtype EcN vs. derivative strains ($n = 3$ biological replicates), Lower: representative immunoblot of construct MHCIa expressed in wildtype EcN and derivative strains. **d**, Biofilm formation quantified for wildtype EcN, and derivative strains by crystal violet stain assay. (****$P < 0.0001$, ns = $P > 0.05$, One-way ANOVA with Tukey's multiple comparison test, $n = 9$ biological replicates for EcN, 10 for EcNc WT, 12 for other groups). **e**,**f**, MFI of **e**, Left: H2k^{b}-SIINFEKL complex and Right: MHC-II, or **f**, Left: CD80 and Right: PD-L1 for BMDM incubated with the indicated live microbial strain or media for 6 h (*$P = 0.0231$, *$P = 0.0414$, ***$P = 0.0002$, ***$P = 0.0005$, ****$P < 0.0001$, ns = $P > 0.05$, one-way ANOVA with Tukey's multiple comparisons test, $n = 4$ biological replicates per group). **g**, Left: sheep red blood cells (RBCs) were incubated with lysate from EcNc$^{Δlon/ΔompT}$ with (LLO+) or without (LLO−) cytosolic LLO expression. Absorbance at 541 nm ($n = 3$ biological replicates per group). Right: percentage of live BMDM after incubation with indicated live microbial strain or control for 6 h ($n = 4$ biological replicates per group). **h**, Immunoblot depicting expression of neoantigen constructs MHCIa, MHCIIa, and MHCI/II^{v} in EcNc$^{Δlon/ΔompT}$ with (LLO+) or without (LLO−) co-expression of cytosolic LLO. **i**, Immunofluorescence microscopy analysis of BMDM co-incubated with Left: EcNc$^{Δlon/ΔompT}$ OVA or, Right: EcNc$^{Δlon/ΔompT/LLO+}$ OVA. **j**, Naïve OT-II T cells were incubated with BMDC's pulsed with the indicated condition. Left: IFN-γ quantification in supernatant of OT-II cultures (****$P < 0.0001$, one-way ANOVA with Tukey's multiple comparisons test, $n = 3$ biological replicates per group), Middle: IL-2 quantification in supernatant of OT-II culture (****$P < 0.0001$, one-way ANOVA with Tukey's multiple comparisons test, $n = 3$ biological replicates per group). Right: representative histogram depicting CFSE dilution of stimulated OT-II T cells. **a**–**g**,**j**, Data are mean ± s.e.m. Gel source data in Supplementary Figs. 1 and 2.

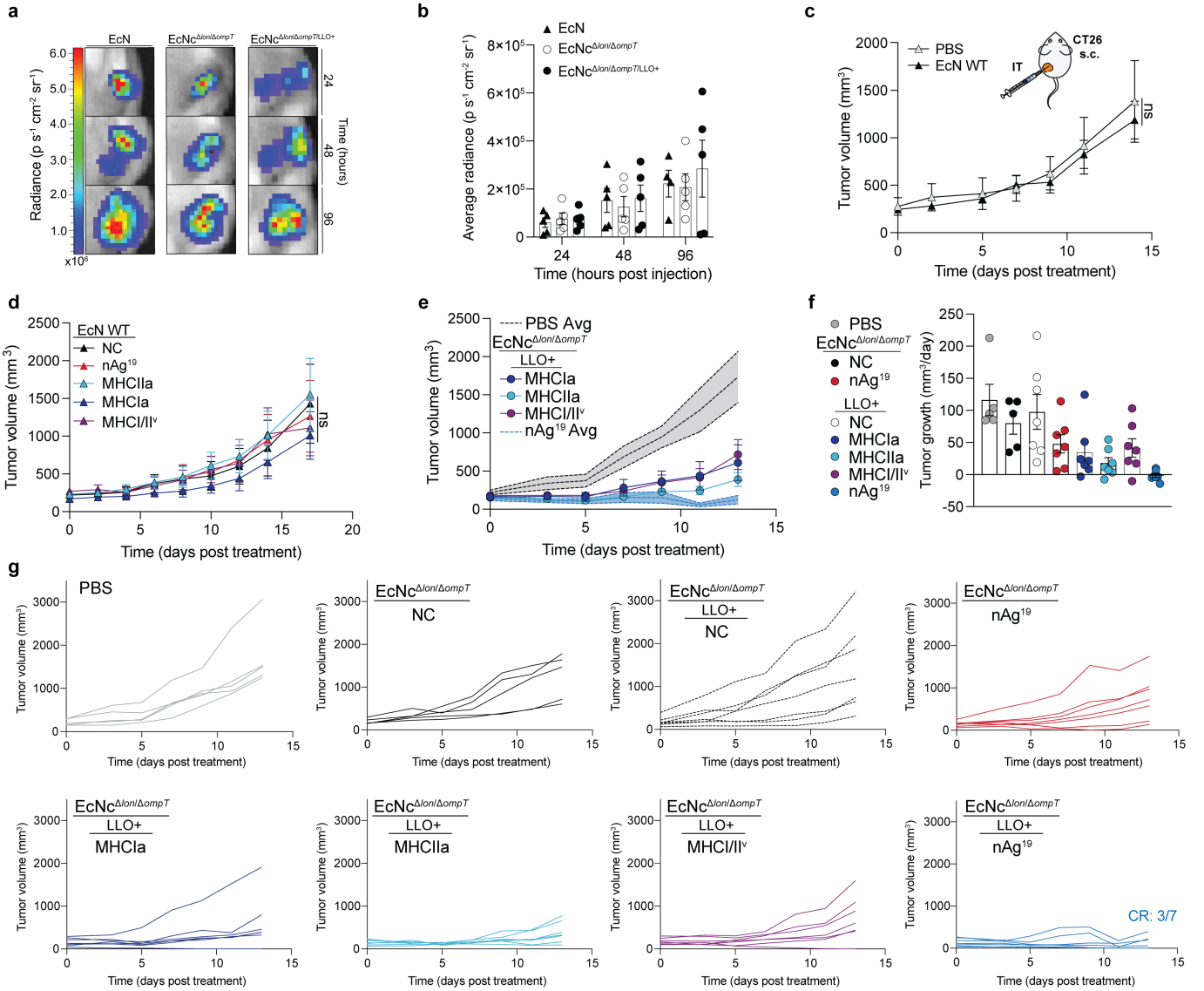

Extended Data Fig. 3 | Characterization of intratumoral treatment with microbial tumor neoantigen vaccines. a–**g**, BALB/c mice with established hind-flank CT26 tumors were treated when average tumor volumes were 150–200mm^3. **a**,**b**, Mice received a single intratumoral injection of EcN WT, EcNc$^{\Delta lon/\Delta ompT}$, or EcNc$^{\Delta lon/\Delta ompT/LLO+}$. **a**, Representative image of tumors colonized by microbes with a genome-integrated luminescence cassette. **b**, Average radiance of microbe colonized tumors in designated ($n = 4$ mice for EcN WT 96 h, 5 for all other groups). **c**, Mice received intratumoral injections of PBS or EcN WT. Tumor growth curves ($n = 5$ mice per group, ns = $P > 0.05$, two-way ANOVA with Tukey's multiple comparisons test). **d**, Mice received intratumoral injections of EcN WT without therapeutic (NC), expressing construct MHCIa, MHCIIa, or MHCI/II^v, or EcN nAg^{19}. Tumor growth curves ($n = 5$ mice per group, ns = $P > 0.05$, two-way ANOVA with Tukey's multiple comparisons test). **e**,**f**, Mice received a single intratumoral injection of PBS, EcNc$^{\Delta lon/\Delta ompT}$ NC, EcNc$^{\Delta lon/\Delta ompT}$ nAg^{19}, or EcNc$^{\Delta lon/\Delta ompT/LLO+}$ expressing construct MHCIa, MHCIIa, or MHCI/II^v, or EcNc$^{\Delta lon/\Delta ompT/LLO+}$ nAg^{19}. **e**, Tumor growth curves ($n = 5$ mice for PBS, 7 for other groups). **f**, Tumor growth rate ($n = 5$ mice for PBS and EcNc$^{\Delta lon/\Delta ompT}$ NC, 7 for other groups) for designated groups. **g**, Individual tumor trajectories after intratumoral treatment with PBS or indicated microbial therapeutic. **b**–**f**, Data are mean ± s.e.m.

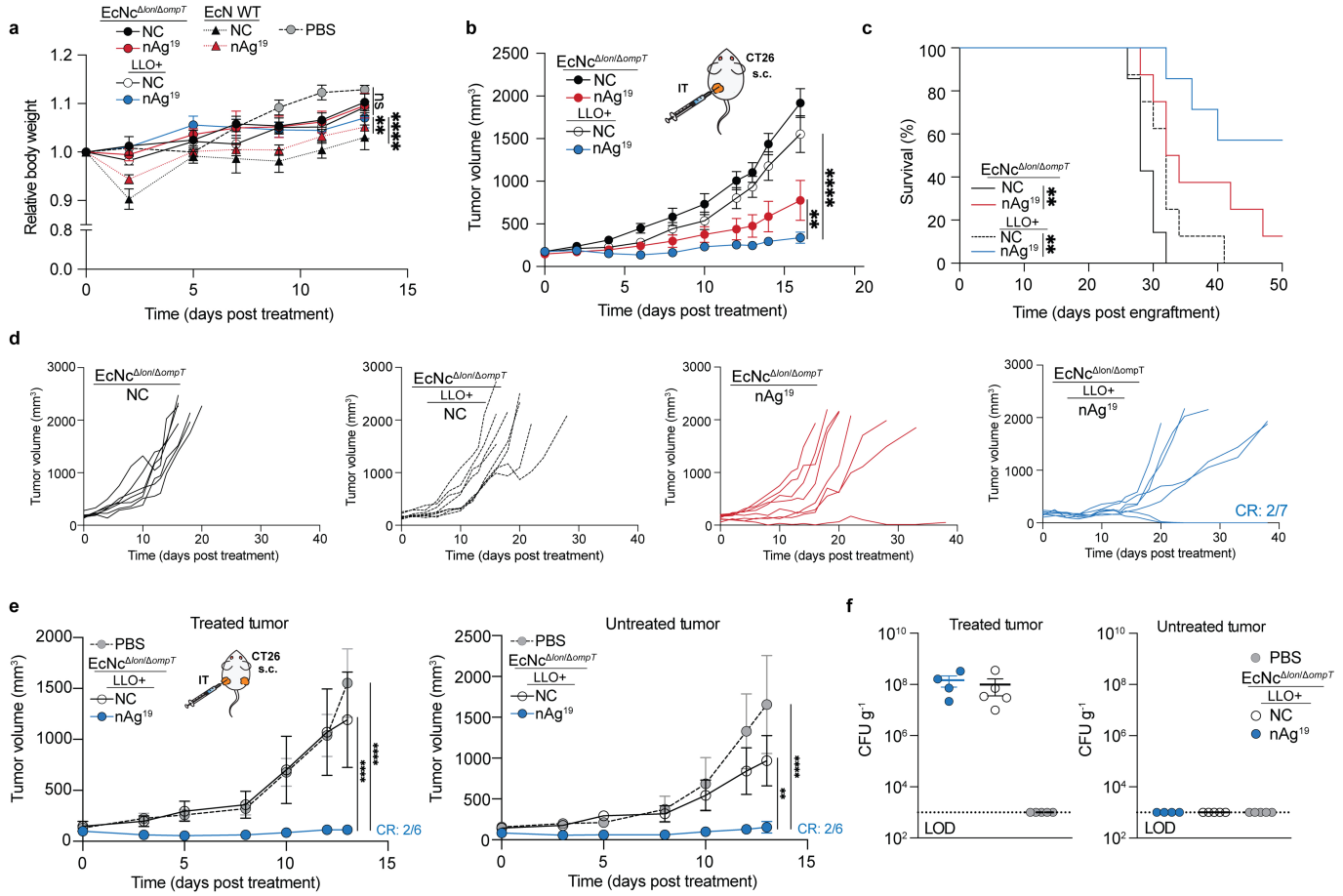

Extended Data Fig. 4 | Comparative profile of intratumoral treatment with engineered microbial neoantigen vaccines. a–**d**, BALB/c mice with established hind-flank CT26 tumors were treated when average tumor volumes were 150–200mm^3. **a**,**b**, Mice received intratumoral injection of wildtype EcN, EcNc$^{\Delta lon/\Delta ompT}$ or EcNc$^{\Delta lon/\Delta ompT/LLO+}$ either without neoantigen expression (NC) or the strain mixture nAg^{19} on day 0. **a**, Relative body weight of CT26 tumor-bearing mice ($n = 5$ mice for PBS, EcN NC, and EcN nAg^{19}, 7 for other groups, $^{**}P = 0.0034$, $^{****}P < 0.0001$, ns = $P > 0.05$, two-way ANOVA with Tukey's multiple comparisons test). **b**–**d**, Mice received intratumoral injection on day 0 and 8 ($n = 7$ mice for EcNc$^{\Delta lon/\Delta ompT}$ NC and EcNc$^{\Delta lon/\Delta ompT/LLO+}$ nAg^{19}, 8 for other groups). **b**, Tumor growth curves ($^{**}P = 0.0020$, $^{****}P < 0.0001$, two-way ANOVA with Tukey's multiple comparisons test). **c**, Kaplan-Meier survival curves for CT26 tumor-bearing mice ($^{**}P = 0.0061$, $^{**}P = 0.0076$, Log-rank Mantel-Cox test). **d**, Individual tumor trajectories after intratumoral treatment with indicated microbial strain. **e**,**f**, BALB/c mice were implanted with CT26 tumors on both hind flanks. When average tumor volumes were 100–150mm^3 mice received an intratumoral injection of PBS, EcNc$^{\Delta lon/\Delta ompT/LLO+}$ (NC), or EcNc$^{\Delta lon/\Delta ompT/LLO+}$ nAg^{19} into a single tumor. **e**, Tumor growth curves ($n = 6$ mice for EcNc$^{\Delta lon/\Delta ompT/LLO+}$ nAg^{19}, 5 for other groups, $^{**}P = 0.0014$, $^{****}P < 0.0001$, two-way ANOVA with Tukey's multiple comparisons test). **f**, CFU g^{-1} of tumor ($n = 4$ mice for EcNc$^{\Delta lon/\Delta ompT/LLO+}$ nAg^{19}, 5 for all other groups), LOD 1 ×103 CFU g^{-1}. **a**,**b**,**e**,**f**, Data are mean ± s.e.m.

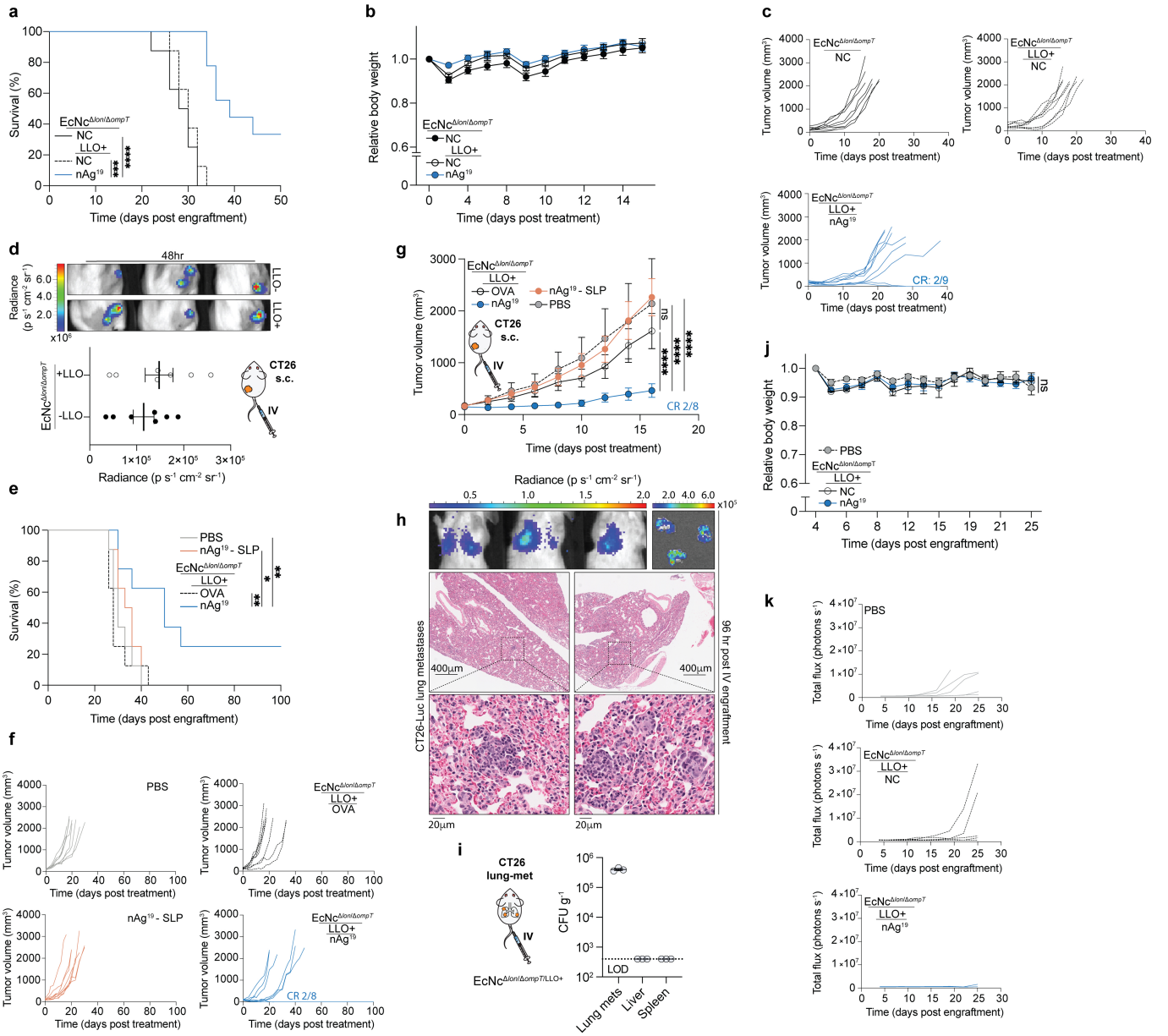

Extended Data Fig. 5 | Intravenous treatment with engineered microbial therapeutics in primary and metastatic solid tumors. a–**c**, BALB/c mice with established hind-flank CT26 tumors were intravenously injected with indicated microbial therapeutics when average tumor volumes were 150–200 mm^3 ($n = 9$ mice for $EcNc^{\Delta lon/\Delta ompT/LLO+}$ nAg^{19}, 8 for other groups). **a**, Kaplan-Meier survival curves for CT26-tumor-bearing mice treated with indicated therapeutic (****$P < 0.0001$, **$P = 0.0021$, Log-rank Mantel-Cox test). **b**, Relative body weight of mice after intravenous treatment with indicated microbial therapeutic. **c**, Individual tumor trajectories after intravenous treatment with the indicated microbial therapeutic. **d**, BALB/c mice with established hind-flank CT26 tumors were intravenously injected with $EcNc^{\Delta lon/\Delta ompT}$ or $EcNc^{\Delta lon/\Delta ompT/LLO+}$. Upper: representative luminescent signature of tumors colonized with $EcNc^{\Delta lon/\Delta ompT}$ (LLO−) or $EcNc^{\Delta lon/\Delta ompT/LLO+}$ (LLO +), 48 h post-injection. Lower: average radiance of colonized tumors ($n = 7$ mice per group). **e**–**f**, BALB/c mice with established hind-flank CT26 tumors were intravenously injected with the indicated microbial therapeutics or PBS, or subcutaneously injected with nAg^{19}-SLP, when average tumor volumes were 100–120 mm^3. **e**, Kaplan-Meier survival curves for CT26 tumor-bearing mice treated with indicated therapeutic ($n = 8$ mice per group, **$P = 0.0055$, **$P = 0.0018$, *$P = 0.0210$, Log-rank Mantel-Cox test). **f**, Individual tumor trajectories ($n = 8$ mice per group) after intravenous treatment with the indicated therapeutic. **g**, Established hind-flank CT26 tumors were intravenously injected with the indicated microbial therapeutics or PBS, or subcutaneously injected with nAg^{19}-SLP, when average tumor volume was 160 mm^3. Tumor growth curves ($n = 5$ mice for PBS, 8 mice for other groups; ****$P < 0.0001$, two-way ANOVA with Tukey's multiple comparisons test). **h**–**k**, BALB/c mice were injected intravenously with CT26-Luc cells. **h**, Upper-left: In vivo, or Upper-right: ex vivo bioluminescent images of mice ($n = 3$) lungs 96 h post-intravenous injection of CT26-Luc cells. Lower: Histology of metastatic lung foci 96-hours post-intravenous injection of CT26-Luc cells. **i**–**k**, Every 3–5 days mice ($n = 5$ per group) received intravenous injection of PBS, $EcNc^{\Delta lon/\Delta ompT/LLO+}$ without therapeutic (NC), or $EcNc^{\Delta lon/\Delta ompT/LLO+}$ nAg^{19} starting 4 days after CT26-Luc engraftment. **i**, Microbial tissue burden quantified as CFU g^{-1}, LOD 4 ×10^2 CFU g^{-1} ($n = 3$ mice). **j**, Relative body weight of mice ($n = 5$ per group) after intravenous treatment with indicated therapeutic. **k**, Individual lung metastases luminescence trajectories ($n = 5$ mice per group). **b**,**d**,**g**,**i**,**j** Data are mean ± s.e.m.

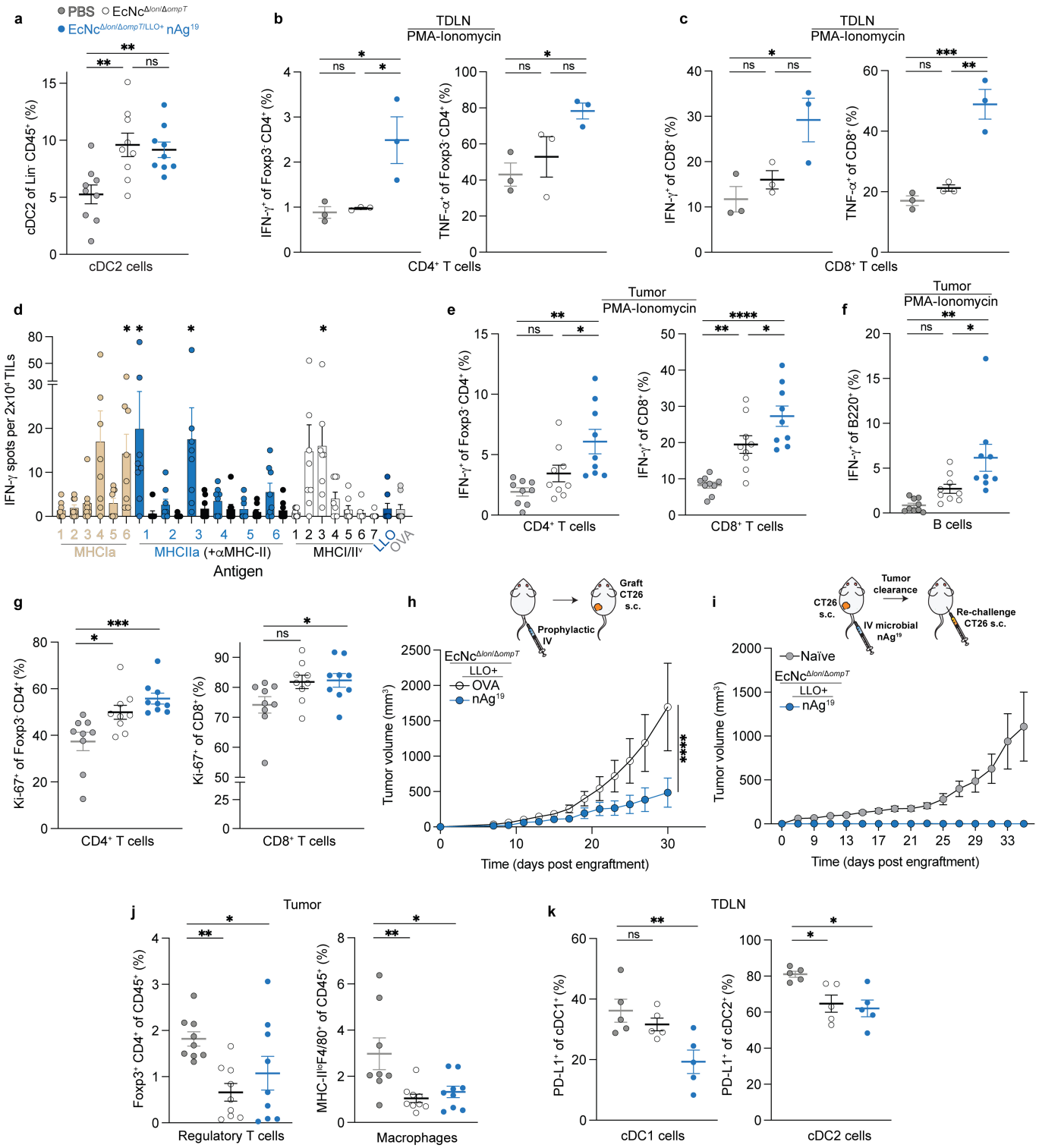

Extended Data Fig. 6 | See next page for caption.

Extended Data Fig. 6 | Modulation of anti-tumor immunity by engineered microbial tumor neoantigen vaccines. a–**f**,**h**–**i**, BALB/c mice with established hind-flank CT26 tumors received intravenous injections of indicated therapeutic or control. **a**, 2 days or **b**–**g**, 8 days after treatment, tumors and TDLNs were extracted. **a**, Frequency of cDC2 in TDLNs ($n = 9$ mice per group, $^{**}P = 0.0042$, $^{**}P = 0.0099$, ns = $P > 0.05$, One-way ANOVA with Tukey's multiple comparisons test). **b**–**c**, Lymphocytes from TDLNs were stimulated ex vivo with PMA and ionomycin in the presence of brefeldin A. **b**, Left: Frequency of IFN-γ$^+$ Foxp3$^-$CD4$^+$ post-stimulation ($n = 3$ mice per group, $^*P = 0.0313$, $^*P = 0.0246$, ns = $P > 0.05$, One-way ANOVA with Tukey's multiple comparisons test). Right: Frequency of TNF-α$^+$ Foxp3$^-$CD4$^+$ T cells post-stimulation ($n = 3$ mice per group, $^*P = 0.0445$, ns = $P > 0.05$, One-way ANOVA with Tukey's multiple comparisons test). **c**, Left: Frequency of IFN-γ$^+$ CD8$^+$ post-stimulation ($n = 3$ mice per group, $^*P = 0.0257$, ns = $P > 0.05$, One-way ANOVA with Tukey's multiple comparisons test). Right: Frequency of TNF-α$^+$ CD8$^+$ T cells post-stimulation ($n = 3$ mice per group, $^{**}P = 0.0017$, $^{***}P = 0.0008$, ns = $P > 0.05$, One-way ANOVA with Tukey's multiple comparisons test). **d**, TILs were stimulated with individual 29-mer neoepitope-containing long peptides. Number IFN-γ spots ($n = 8$ mice per group, $^*P = 0.0439$, $^*P = 0.0364$, $^*P = 0.0281$, $^*P = 0.0200$, Kruskal-Wallis test with Dunn's multiple comparisons test). Data are mean ± s.e.m. of background (medium control) subtracted responses. **e**,**f**, TILs were stimulated ex vivo with PMA and ionomycin in the presence of brefeldin A. **e**, Left: Frequency of IFN-γ$^+$ Foxp3$^-$CD4$^+$ post-stimulation ($n = 9$ mice per group, $^*P = 0.0461$, $^{**}P = 0.0014$, ns = $P > 0.05$, one-way ANOVA with Tukey's multiple comparisons test). Right: frequency of IFN-γ$^+$ CD8$^+$ T cells post-stimulation ($n = 9$ mice per group, $^*P = 0.0486$, $^{**}P = 0.0040$, $^{****}P < 0.0001$, one-way ANOVA with Tukey's multiple comparisons test). **f**, Frequency of IFN-γ$^+$ B220$^+$ B cells post-stimulation ($n = 9$ mice per group, $^*P = 0.0351$, $^{**}P = 0.0010$, ns = $P > 0.05$, One-way ANOVA with Tukey's multiple comparisons test). **g**, Left: Percentage Ki-67$^+$ of Foxp3$^-$CD4$^+$ T cells in tumors ($n = 9$ mice per group, $^*P = 0.0183$, $^{***}P = 0.0008$, one-way ANOVA with Dunnett's multiple comparisons test). Right: Percentage Ki-67$^+$ of CD8$^+$ T cells in tumors ($n = 9$ mice per group, $^*P = 0.0453$, ns = $P > 0.05$, One-way ANOVA with Dunnett's multiple comparisons test). **h**, Naïve, tumor-free BALB/c mice were vaccinated intravenously with the designated treatment. CT26 was engrafted on a single hind-flank after the final vaccination. Tumor growth curves ($n = 8$ mice per group, $^{****}P < 0.0001$, two-way ANOVA with Šídák's multiple comparisons test). **i**, BALB/c mice with established CT26 tumors were treated intravenously with EcNc$^{\Delta lon/\Delta ompT/LLO+}$ nAg^{19} (as in Fig. 2e). Mice that had cleared tumors, and age-matched naïve mice, were subcutaneously rechallenged with CT26 tumor cells. Tumor growth curves ($n = 5$ for naïve mice, 6 for nAg^{19}). **j**, Left: Frequency of FoxP3$^+$CD4$^+$ regulatory T cells in tumors ($n = 9$ mice per group, $^*P = 0.0491$, $^{**}P = 0.0072$, one-way ANOVA with Holm-Šídák's multiple comparisons test), Right: Frequency of MHCII^{lo}F4/80$^+$CD11b$^+$ macrophages in tumors ($n = 8$ mice for PBS, 9 for other groups, $^*P = 0.0173$, $^{**}P = 0.0057$, one-way ANOVA with Dunnett's multiple comparisons test). **k**, Left: Percentage PD-L1$^+$ of cDC1 in TDLN ($n = 5$ mice per group, $^{**}P = 0.0074$, ns = $P > 0.05$, one-way ANOVA with Dunnett's multiple comparisons test), Right: Percentage PD-L1$^+$ of cDC2 in TDLN ($n = 5$ mice per group, $^*P = 0.0103$, $^*P = 0.0244$, one-way ANOVA with Dunnett's multiple comparisons test). **a**–**k**, Data are mean ± s.e.m.

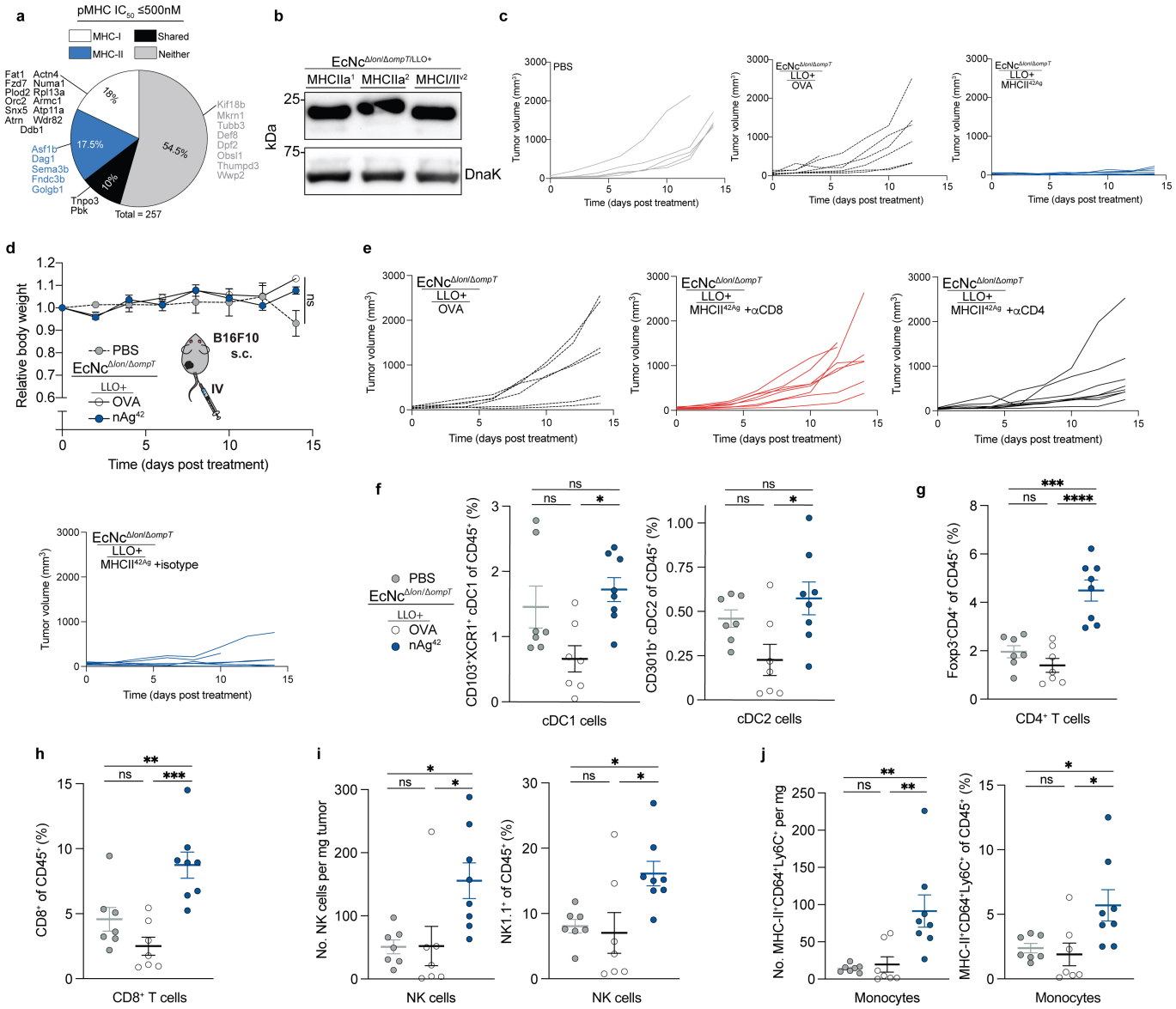

Extended Data Fig. 7 | Assessment of engineered microbial neoantigen therapeutics in B16F10 melanoma. a, Percentage of predicted B16F10 neoantigens containing mutant-epitope(s) with ≤500 nM MHC-I affinity (MHC-I), MHC-II affinity (MHC-II), both MHC-I and MHC-II affinity (Shared), or no epitope meeting affinity criteria (Neither). Previously validated neoantigens within the set are labeled. **b**, Immunoblot of B16F10 neoantigen construct expression in EcNc$^{\Delta lon/\Delta ompT/LLO+}$. **c**–**j**, C57BL/6 mice with established hind-flank B16F10 melanoma tumors were treated 9 days after tumor engraftment. **c**–**e**, Every 3–5 days, mice received an intravenous injection of PBS, EcNc$^{\Delta lon/\Delta ompT/LLO+}$ OVA, or the 7-strain combination EcNc$^{\Delta lon/\Delta ompT/LLO+}$ nAg^{42}. **c**, Individual tumor trajectories after intravenous treatment with indicated therapeutic. **d**, Relative body weight of B16F10-tumor bearing mice ($n = 5$ mice for PBS, 7 for other groups, ns = $P > 0.05$, two-way ANOVA with Tukey's multiple comparisons test). **e**, Individual tumor trajectories after intravenous treatment with indicated therapeutic and intraperitoneal treatment with indicated monoclonal antibody. **f**–**j**, On day 9 and 12 post-engraftment, B16F10 tumor-bearing mice received an intravenous injection of PBS, EcNc$^{\Delta lon/\Delta ompT/LLO+}$ OVA, or EcNc$^{\Delta lon/\Delta ompT/LLO+}$ nAg^{42}. Flowcytometric analysis of TILs was performed 8 days after treatment initiation ($n = 8$ mice for nAg^{42}, 7 for other groups). **f**, Left: Frequency of CD103$^+$XCR1$^+$ cDC1 in tumors (*$P = 0.0132$, ns = $P > 0.05$, one-way ANOVA with Tukey's multiple comparisons test). Right: Frequency of CD301b$^+$ cDC2 in tumors (*$P = 0.0162$, ns = $P > 0.05$, one-way ANOVA with Tukey's multiple comparisons test). **g**, Frequency of Foxp3$^-$CD4$^+$ T cells in tumors (***$P = 0.0001$, ****$P < 0.0001$, ns = $P > 0.05$, one-way ANOVA with Tukey's multiple comparisons test). **h**, Frequency of CD8$^+$ cytotoxic T cells in tumors (**$P = 0.0097$, ***$P = 0.0002$, ns = $P > 0.05$, one-way ANOVA with Tukey's multiple comparisons test). **i**, Left: Number of NK1.1$^+$ NK cells per mg tumor (*$P = 0.0243$, *$P = 0.0224$, ns = $P > 0.05$, one-way ANOVA with Tukey's multiple comparisons test). Right: Frequency of NK1.1$^+$ NK cells in tumors (*$P = 0.0189$, *$P = 0.0389$, ns = $P > 0.05$, one-way ANOVA with Tukey's multiple comparisons test). **j**, Left: Number of MHCII$^+$CD64$^+$Ly6c$^+$ monocytes per mg tumor (**$P = 0.0041$, **$P = 0.0073$, ns = $P > 0.05$, one-way ANOVA with Tukey's multiple comparisons test). Right: Frequency of MHCII$^+$CD64$^+$Ly6c$^+$ monocytes in tumors (*$P = 0.0230$, *$P = 0.0495$, ns = $P > 0.05$, one-way ANOVA with Tukey's multiple comparisons test). **d**,**f**–**j**, Data are mean ± s.e.m. Gel source data in Supplementary Fig. 2.

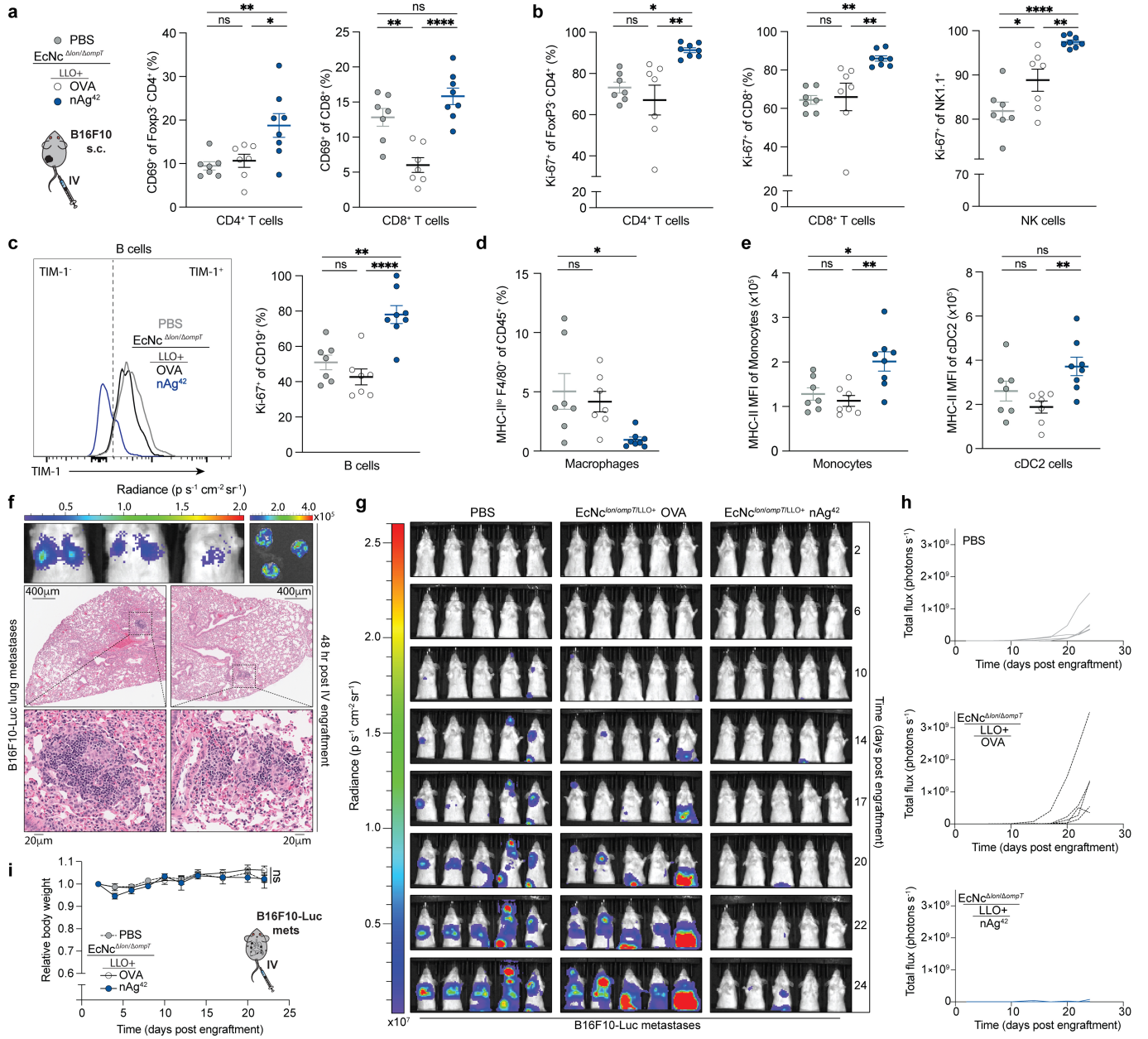

Extended Data Fig. 8 | Mechanisms of anti-tumor immunity and metastases suppression in melanoma. a–**e**, On days 9 and 12 post-engraftment, B16F10 tumor-bearing mice received intravenous injections of PBS, EcNc$^{\Delta lon/\Delta ompT/LLO+}$ OVA, or EcNc$^{\Delta lon/\Delta ompT/LLO+}$ nAg^{42}. Flow cytometric analysis was performed 8 days after treatment initiation ($n = 8$ mice for nAg^{42}, 7 for other groups). **a**, Left: Percentage CD69$^+$ of Foxp3$^-$CD4$^+$ T cells in tumors (*$P = 0.0228$, **$P = 0.0092$, ns = $P > 0.05$, one-way ANOVA with Tukey's multiple comparisons test). Right: Percentage CD69$^+$ of CD8$^+$ T cells in tumors (**$P = 0.0021$, ****$P < 0.0001$, ns = $P > 0.05$, one-way ANOVA with Tukey's multiple comparisons test). **b**, Left: Percentage Ki-67$^+$ of Foxp3$^-$CD4$^+$ T cells in tumors (*$P = 0.0188$, **$P = 0.0020$, ns = $P > 0.05$, one-way ANOVA with Tukey's multiple comparisons test). Middle: Percentage Ki-67$^+$ of CD8$^+$ T cells in tumors (**$P = 0.0048$, **$P = 0.0086$, ns = $P > 0.05$, one-way ANOVA with Tukey's multiple comparisons test). Right: Percentage Ki-67$^+$ of NK1.1$^+$ NK cells in tumors (*$P = 0.0366$, **$P = 0.0070$, ****$P < 0.0001$, ns = $P > 0.05$, one-way ANOVA with Tukey's multiple comparisons test). **c**, Left: Representative histogram of TIM-1 expression on CD19$^+$ B cells. Right: Percentage Ki-67$^+$ of CD19$^+$B cells in tumors (**$P = 0.0015$, ****$P < 0.0001$, ns = $P > 0.05$, one-way ANOVA with Tukey's multiple comparisons test). **d**, Frequency of MHC-II^{lo}F4/80$^+$ macrophages in tumors (*$P = 0.0130$, ns = $P > 0.05$, one-way ANOVA with Dunnett's multiple comparisons test). **e**, Left: MHC-II MFI of CD64$^+$Ly6c$^+$ monocytes in tumors (*$P = 0.0171$, **$P = 0.0041$, ns = $P > 0.05$, one-way ANOVA with Tukey's multiple comparisons test). Right: MHC-II MFI of CD301b$^+$ cDC2 in tumors (**$P = 0.0090$, ns = $P > 0.05$, one-way ANOVA with Tukey's multiple comparisons test). **f**–**i**, C57BL/6 mice were injected intravenously with B16F10-Luc cells. **f**, Upper-left: In vivo, or Upper-right: ex vivo bioluminescent images of mice ($n = 3$) lungs 48-hours post-intravenous injection of B16F10-Luc cells. Lower: Histology of metastatic lung foci 48-hours post-intravenous injection of B16F10-Luc cells. **g**–**i**, Mice received intravenous injection of either PBS, EcNc$^{\Delta lon/\Delta ompT/LLO+}$ OVA or nAg^{42} every 3–5 days starting 2 days post intravenous injection of B16F10-Luc cells. **g**, Images of systemic metastases luminescence in each mouse in all groups over treatment course. **h**, Individual systemic metastases luminescence trajectories ($n = 5$ mice per group). **i**, Relative body weight of mice ($n = 5$ per group) after intravenous treatment with indicated therapeutic. **a**–**e**,**i**, Data are mean ± s.e.m.

Extended Data Table 1 | CT26 peptides in neoantigen constructs

Construct	Number	Gene	AA Mutation	Mutant Sequence in Construct	Mutant MHC-I Epitope	Predicted MHC-I IC50 (nM)	MHC-I Allele	Mutant MHC-II Epitope	Predicted MHC-II IC50 (nM)	MHC-II Allele
NeoAg^{p} (Prototype)	1	Aldh18a1	P154S	LHSGQNHLKEMAISVLEARACAAAGQS	NHLKEMAISV	4355.5	H2Kd	NHLKEMAISVLEARA	48.03	H2IAd
	2	mULV-gp70	ERV antigen	LWPKVTYHSPSYVYHQFERKTKYIR	SPSYVYHQF	98.4	H2Ld	SYVYHQFERKTKYIR	689.64	H2IEd
	3	Ubqln1	A456V	DTLSAMSNPRAMQVLLQIQQGLQTLAT	NPRAMQVLL	284	H2Ld	MSNPRAMQVLLQIQQ	189.26	H2IAd
	4	Gpc1	E165G	YRGANLHLEETLAGFWARLLERLFKQL	GFWARLLERL	5834.18	H2Kd	LEETLAGFWARLLER	556.85	H2IAd
	5	E2f8	I522T	VILPQAPSGPSYATYLQPAQAQMLTPP	SGPSYATYL	36.51	H2Dd	PSYATYLQPAQAQML	82.18	H2IAd
MHCIa	1	Gid8	P7S	MSYAEKSDEITKDEWMEKLNN	SYAEKSDEI	58.46	H2Kd	EKSDEITKDEWMEKLN	16524.89	H2-IAd
	2	Glud1	V546I	NLGLDLRTAAYVNAIEKIFKVYNEAGVTFT	AYVNAIEKI	34.21	H2Kd	IEKIFKVYNEAGVTF	1457.52	H2-IAd
	3	Mia2	A317T	KKLIYAAKLNTSLKALEGERN	IYAAKLNTSL	90.05	H2Kd	KKLIYAAKLNTSLKALE	93.66	H2-IAd
	4	Sel1l	A299T	IAHMILGYRYWTGIGVLQSCESALTHYRLV	RYWTGIGVL	118.72	H2Kd	YWTGIGVLQSCESAL	704.1	H2-IAd
	5	C3	V254I	EPTETFYYIDDPNGLEISIIAKFLYGKNVD	YYIDDPNGLEI	69.16	H2Kd	IDDPNGLEISIIAKF	1629.03	H2-IAd
	6	Hnmpl	I203R	RSVNSVLLFTILNPIYSRTTDVLYTICNPC	IYSRTTDVL	169.83	H2Kd	LFTILNPIYSRTTDV	250.11	H2-IAd
MHCIIa	1	Birc2	E395K	EDVVMMSTPVVKAALKMGFSRSLVRQTVQ	KMGFSRSLV	5116.93	H2Kd	VMMSTPVVKAALKMGFSRS	37.7	H2-IAd
	2	Uvrag	P519L	KRASSENERLQYKTPLPSYNSALTQPGVA	TPLPSYNSAL	650.89	H2Ld	NERLQYKTPLPSYNSALTQ	40	H2-IAd
	3	Aldh18a1	P154S	LHSGQNHLKEMAISVLEARACAAAGQSGL	NHLKEMAISV	4355.5	H2Kd	NHLKEMAISVLEARA	48.03	H2-IAd
	4	Tnks2	A1116V	VTLGKSFLQFSAMKMVHSPPGHHSVTGRP	SFLQFSAMKMV	3314.24	H2Kd	GKSFLQFSAMKMVHSPPGH	46.2	H2-IAd
	5	Tnfaip1	D50N	SLYYTTVRALTRHNTMLKAMFSGRMEVLT	RHNTMLKAM	381.54	H2Kd	SLYYTTVRALTRHNT	58.8	H2-IAd
	6	Rab3ip	C341R	IEPVGLQPIRFVKASAVERGGPKKCALTG	RGGPKKCALT	1067.93	H2Dd	EPVGLQPIRFVKASAVERG	52.2	H2-IAd
MHCI/II^{v}	1	Mtpap	E341K	MSGFQCDLTANNSIALKSSKLLYIYGSLDS	KLLYIYGSL	9045.19	H2Kd	CDLTANNSIALKSSKLLYI	114	H2-IAd
	2	Akap9	V88I	PPYSLEHAKITSETNTQLEHAKITQTELMR	PYSLEHAKI	3350.47	H2Kd	NTQLEHAKITQTELM	978.1	H2-IAd
	3	Gorasp1	G91D	EVEVVPSNMWGDQGLLGASVRFCSFRRAS	VPSNMWGDQGL	454.12	H2Ld	MWGDQGLLGASVRFCSF	1038.2	H2-IAd
	4	Maged1	A169G	GPGTTYNFPQSPSGNEMTNNQPKTAKA	FPQSPSGNEMT	1091.83	H2Ld	TTYNFPQSPSGNEMTN	9693.16	H2-IAd
	5	Top1	T413I	WKEVRHDNKVIWLVSWTENIQGSIKYIML	VIWLVSWTENI	8233.62	H2Kd	DNKVIWLVSWTENIQGSIK	1791.8	H2-IAd
	6	Col8a1	G493D	PKGEPGIPGDQDLQGPPGIPGIVGPSGPI	EPGIPGDQDLQ	11943.12	H2Ld	QDLQGPPGIPGIVGPSGPI	2775.7	H2-IAd
	7	Ciao2b	T134A	AIPSPAVQDGCTHYTRDPRLRACSEQTACR	LRACSEQTA	23017.505	H2Kd	RDPRLRACSEQTACR	4266.04	H2-IAd

For each therapeutic construct 6–7 predicted neoantigens were included. All 3 groups (MHCIa, MHCIIa, MHCI/II^{v}) in combination represent nAg[19]. 5 antigens were included in the production optimization prototype construct (NeoAg^{p}).

Extended Data Table 2 | B16F10 peptides in neoantigen constructs

Construct	Number	Gene	AA Mutation	Mutant Sequence in Construct	Mutant MHC-I Epitope	Predicted MHC-I IC50 (nM)	MHC-I Allele	Mutant MHC-II Epitope	Predicted MHC-II IC50 (nM)	MHC-II Allele
MHCIa[1]	1	Pcmtd1	P222L	ESKNILAVSFAPLVQLSKNDNGTPDSVGLP	VSFAPLVQL	30.93	H2Kb	KNILAVSFAPLVQLSK	269.38	H2-IAb
	2	Hipk3	S702F	WQQVTPMAPAAATLTFEGMAGSQRLGDWGK	ATLTFEGM	107.21	H2Kb	AATLTFEGMAGSQRLG	5250.81	H2-IAb
	3	Map1s	F881V	LPGGGAGHLDQNVFLRVRALCYVISGQGQR	VFLRVRAL	119.32	H2Kb	LDQNVFLRVRALCYVISGQ	3944.2	H2-IAb
	4	Haus6	L176V	PQDMHKCLARSHVARNRFVQILQREHYVMQ	VARNRFVQI	72.41	H2Kb	QDMHKCLARSHVARNRFVQ	3080.52	H2-IAb
	5	Tab2	S77T	QGFNVFGMPSTSGASNTTPHLGFHLGSKGT	SGASNTTPHL	188.87	H2Db	GFNVFGMPSTSGASNT	73.1	H2-IAb
	6	Sec23a	F94L	AKLWACNFCYQRNQLPPTYAGISELNQPAE	CNFCYQRNQL	241.87	H2Kb	RNQLPPTYAGISELNQ	1206.7	H2-IAb
MHCIa[2]	1	Ipo13	E441G	DTLMYVYEMLGAGLLSNLYDKLGRLLT	YVYEMLGAGL	254.77	H2Kb	VYEMLGAGLLSNLYDKLGR	1170.5	H2-IAb
	2	Desi2	N10S	GANQLVVLSVYDMYWMNEYTSSIGIGV	SVYDMYWM	107.59	H2Kb	SVYDMYWMNEYTSSIGIGV	1424.5	H2-IAb
	3	Rnf146	A106V	TLLSPEELKAASRGNGEYVWYYEGRNG	KAASRGNGEYV	178.28	H2Db	TLLSPEELKAASRGNGEYV	7840.8	H2-IAb
	4	Ncor1	H673P	KSEAQCKNFYFNYKRRPNLDNLLQQHK	FNYKRRPNL	21.35	H2Kb	NFYFNYKRRPNLDNLL	5770.7	H2-IAb
	5	Man2b2	D605N	RLVPVMNDCYILLFNQDTNMLHSIQDR	ILLFNQDTNM	524.65	H2Db	YILLFNQDTNMLHSIQ	7182	H2-IAb
	6	Wrap53	S144F	TYSFSQVPRYLSGFWSEFSTRSENFLK	QVPRYLSGF	262.17	H2Kb	YLSGFWSEFSTRSENF	2484.81	H2-IAb
MHCIa[3]	1	Vps13c	S1256P	IDLKAPVIVIPQSSLPTNAVVVDLGLIRVH	SSLPTNAVVV	27.86	H2Db	VIVIPQSSLPTNAVVV	231.5	H2-IAb
	2	Tmem246	L11P	MTTSTSPAAMPLRRLRRLSWGSTAVQLFIL	TSPAAMPL	123.91	H2Kb	MTTSTSPAAMPLRRLR	92.5	H2-IAb
	3	Dop1b	T838I	NHSQSLALVIEDKMKRYKISGNNPFFGKLQ	ISGNNPFFGKL	159.09	H2Kb	MKRYKISGNNPFFGKL	663.4	H2-IAb
	4	Angel2	D144N	RNVDSTCEDREDKFNFSVMSYNILSQDLLE	FNFSVMSYNIL	452.07	H2Kb	REDKFNFSVMSYNILS	654.97	H2-IAb
	5	Chd6	D1602G	TAKHGLNRTDYYIMNGPQLSFLDAYRNYAQ	YYIMNGPQL	503.18	H2Db	TDYYIMNGPQLSFLDA	151	H2-IAb
	6	Smarcc2	G65A	LVVQLLQFQEEVFAKHVSNAPLTKLPIKCF	FAKHVSNAPL	538.04	H2Db	EEVFAKHVSNAPLTKL	230.3	H2-IAb
MHCIIa[1]	1	Wipi2	T304A	SYLPSQVTEMFNQGRAFAAVRLPFCGHKNI	QGRAFAAV	101.34	H2Kb	SQVTEMFNQGRAFAAVRLP	59.7	H2-IAb
	2	Sec16a	S970F	QTPQSPHPNAEKGPFEFVSSPAGNTSVMLV	KGPFEFVSS	4986.04	H2Kb	AEKGPFEFVSSPAGNTSVM	74.8	H2-IAb
	3	Ehbp1l1	P1343A	EGGGGSGTYRVGNAQPSLADCLDAGDLAQR	AQPSLADCL	713.71	H2Db	GGSGTYRVGNAQPSLADCL	80.1	H2-IAb
	4	Atp6v1h	K146T	NRQDPFTVHMAARIIATLAAWGKELMEGSD	MAARIIATL	359.42	H2Kb	RQDPFTVHMAARIIATLAA	190.2	H2-IAb
	5	Pnrc1	T196I	INRQKSKYNLPLTKIISAKRNESDFWQDSA	YNLPLTKII	7072	H2Kb	KSKYNLPLTKIISAK	460.17	H2-IAb
	6	Klhl26	E487A	YDPAADRWEPRAPMRAPRVLHAMLGAAGRI	RAPMRAPRV	484.02	H2Kb	EPRAPMRAPRVLHAML	99.2	H2-IAb
MHCIIa[2]	1	Cnst	G59A	AGDGPAGLTTSEGAMARATVSEQDSLNNNE	GAMARATV	6796.53	H2Kb	DGPAGLTTSEGAMARATVS	198.3	H2-IAb
	2	Ints11	D314N	KHIKAFDRTFANNPGPMVVFATPGMLHAGQ	RTFANNPGPM	591.33	H2Db	TFANNPGPMVVFATPGMLH	54.2	H2-IAb
	3	Hipk1	E413G	YDQIRYISQTQGLPAGYLLSAGTKTTRFFN	AGYLLSAGT	1011.08	H2Kb	TQGLPAGYLLSAGTKTTRF	384.6	H2-IAb
	4	Atf7	G249A	GPPVNNSGSISPSAHPMPSEAKMRLKATLH	ISPSAHPM	272.28	H2Kb	VNNSGSISPSAHPMPSEAK	111	H2-IAb
	5	Gpatch4	G192A	AQEQAFLAQLKGSKALATSQPLTDSEPSQK	KALATSQPL	374.15	H2Db	FLAQLKGSKALATSQP	113	H2-IAb
	6	Heatr5a	T347A	AFLSHILSLVSQSNPKAAQTQIDAVCCRRC	AAQTQIDAV	5195.03	H2Db	SHILSLVSQSNPKAAQTQI	203.4	H2-IAb
MHCI/II[V1]	1	Fig4	F498V	CVDCLDRTNTAQVMVGKCALAYQLYSL	VMVGKCALA	1185.97	H2Kb	DCLDRTNTAQVMVGKCALA	2981.7	H2-IAb
	2	Etv5	E472K	LFSMAFPDNQRPFLKAESKCPLNEEDTL	KCPLNEEDTL	2173.74	H2Db	LFSMAFPDNQRPFLKAESK	1149.5	H2-IAb
	3	Hccs	R199T	PSLVRFGGKAREYSPTARIRSWMGYEL	KAREYSPT	2378.58	H2Kb	LVRFGGKAREYSPTARIRS	297.1	H2-IAb
	4	Cubn	S3211L	LVKLTFNAFTLEEPSLPGKCTFDYVQI	NAFTLEEPSL	3931.28	H2Db	VKLTFNAFTLEEPSLP	738.5	H2-IAb
	5	Dlg5	P666S	PQPSKRVGSLTPPKSPRRSDSIKFQHR	KSPRRSDSI	3310.37	H2Kb	PSKRVGSLTPPKSPRR	1027.3	H2-IAb
	6	Dlg4	R66Q	NDSILFVNEVDVQEVTHSAAVEALKEA	VQEVTHSAAV	5253.65	H2Kb	VDVQEVTHSAAVEALK	323.73	H2-IAb
MHCI/II[V2]	1	Ift52	D43A	LQKRLRSNWKIQSLKAEITSEKLIGVKLWI	KIQSLKAEI	5032.54	H2Kb	RLRSNWKIQSLKAEITSEK	2910.8	H2-IAb
	2	Mta1	P547L	KPLEAVLRYLETHPRLPKPDPVKSSSSVLS	RYLETHPRL	922.68	H2Kb	AVLRYLETHPRLPKPDPVK	544.4	H2-IAb
	3	Rpl12	I82N	NRQAQIEVVPSASALINKALKEPPRDRKKQ	SALINKAL	1058.79	H2Db	QIEVVPSASALINKAL	216.2	H2-IAb
	4	Ctsd	G397S	WILGDVFIGSYYTVFDRDNNRVSFANAVVL	VSFANAVVL	14.98	H2Db	FDRDNNRVSFANAVVL	232.9	H2-IAb
	5	Trrap	K2783R	QAQESYEKAMDKAKREHERSNASPAIFPEY	KAMDKAKRE	19244.21	H2Kb	KAKREHERSNASPAIF	1245.3	H2-IAb
	6	Nsun2	K72M	EELAWHTNLSRKILRMSPLLAKFHQFLVSE	KILRMSPL	39.75	H2Kb	LSRKILRMSPLLAKFH	674.7	H2-IAb

In each construct, 6 predicted neoantigens were included. All 7 groups in combination represent nAg[42].

nature portfolio

Corresponding author(s): Nicholas Arpaia and Tal Danino

Last updated by author(s): Jul 24, 2024

Reporting Summary

Nature Portfolio wishes to improve the reproducibility of the work that we publish. This form provides structure for consistency and transparency in reporting. For further information on Nature Portfolio policies, see our Editorial Policies and the Editorial Policy Checklist.

Statistics

For all statistical analyses, confirm that the following items are present in the figure legend, table legend, main text, or Methods section.

n/a	Confirmed
☐	☒ The exact sample size (*n*) for each experimental group/condition, given as a discrete number and unit of measurement
☐	☒ A statement on whether measurements were taken from distinct samples or whether the same sample was measured repeatedly
☐	☒ The statistical test(s) used AND whether they are one- or two-sided *Only common tests should be described solely by name; describe more complex techniques in the Methods section.*
☒	☐ A description of all covariates tested
☐	☒ A description of any assumptions or corrections, such as tests of normality and adjustment for multiple comparisons
☐	☒ A full description of the statistical parameters including central tendency (e.g. means) or other basic estimates (e.g. regression coefficient) AND variation (e.g. standard deviation) or associated estimates of uncertainty (e.g. confidence intervals)
☐	☒ For null hypothesis testing, the test statistic (e.g. *F*, *t*, *r*) with confidence intervals, effect sizes, degrees of freedom and *P* value noted *Give P values as exact values whenever suitable.*
☒	☐ For Bayesian analysis, information on the choice of priors and Markov chain Monte Carlo settings
☒	☐ For hierarchical and complex designs, identification of the appropriate level for tests and full reporting of outcomes
☒	☐ Estimates of effect sizes (e.g. Cohen's *d*, Pearson's *r*), indicating how they were calculated

Our web collection on statistics for biologists contains articles on many of the points above.

Software and code

Policy information about availability of computer code

Data collection	FACS Diva v8.0 and SpectroFlo v3.0 were used for flow cytometry data collection.
Data analysis	Software used for sequencing data analysis: Illumina bcl2fastq v2.17, Trimmomatic v0.39, bcftools v1.13, Illumina Dragen Bio-IT platform v1.0, Broad Institute GATK v4.2.0.0, pVacTools v2.0.3, STAR aligner v2.5.2b and Subread Package v1.5.2, Bam-readcount v1.0, DESeq2 v1.20.0, VAtools v5.0.0, Ensembl Variant Effect Predictor v104, NetMHCpan v4.1, NetMHC v4.0, NetMHCIIpan v4.1, and NNAlign v2.0. Software used for flow cytometry data anlysis: FlowJo v10. Software used for statistical analysis: GraphPad Prism v9.0 and v10.0.

For manuscripts utilizing custom algorithms or software that are central to the research but not yet described in published literature, software must be made available to editors and reviewers. We strongly encourage code deposition in a community repository (e.g. GitHub). See the Nature Portfolio guidelines for submitting code & software for further information.

Data

Policy information about availability of data

All manuscripts must include a data availability statement. This statement should provide the following information, where applicable:

- Accession codes, unique identifiers, or web links for publicly available datasets
- A description of any restrictions on data availability
- For clinical datasets or third party data, please ensure that the statement adheres to our policy

Whole exome sequencing and RNA-Seq data generated for this study are deposited under umbrella BioProject accession number PRJNA1025007. Whole exome

data are available on the Short Read Archive with BioProject ID PRJNA1024050. RNA-seq data are available on NCBI Gene Expression Omnibus with accession number GSE244808. All other data are available within the article or its Supplementary Information. Source data are provided with this paper. Datasets utilized for analyses in this study: Ensembl release 102 M. musculus GRCm38 gene annotations (GRCm38, https://useast.ensembl.org/Mus_musculus/Info/Index, accession: GCA_000001635.8), and dbSNP build 142 (ftp.ncbi.nih.gov/snp).

Research involving human participants, their data, or biological material

Policy information about studies with human participants or human data. See also policy information about sex, gender (identity/presentation), and sexual orientation and race, ethnicity and racism.

Reporting on sex and gender	N/A
Reporting on race, ethnicity, or other socially relevant groupings	N/A
Population characteristics	N/A
Recruitment	N/A
Ethics oversight	N/A

Note that full information on the approval of the study protocol must also be provided in the manuscript.

Field-specific reporting

Please select the one below that is the best fit for your research. If you are not sure, read the appropriate sections before making your selection.

☒ Life sciences ☐ Behavioural & social sciences ☐ Ecological, evolutionary & environmental sciences

For a reference copy of the document with all sections, see nature.com/documents/nr-reporting-summary-flat.pdf

Life sciences study design

All studies must disclose on these points even when the disclosure is negative.

Sample size	We base our sample size on standards in the field, as well as our prior experience and work involving bacterial and mammalian cell studies, and animal trials (PMCIDs: PMC6688650, PMC7685004, PMC10915968). These previous studies, along with small pilot studies, served as the basis for determination of sample size. Sample size is explicitly stated for each experimental group for individual experiments in figure captions and data descriptions.
Data exclusions	No data were excluded.
Replication	All results in the manuscript were replicated at least 2-3 times in independent experiments.
Randomization	For subcutaneous tumor models: treatment groups were created by selecting from a pool of animals with comparable tumor volume, such that the average tumor between each group was approximately equal at the beginning of all experiments. For metastastic tumor models: animals were randomly distributed between groups after intravenous injection of tumor cells prior to treatment and imaging. For in vitro experiments, equal numbers of cells were seeded or utilized, and randomly allocated between experimental groups.
Blinding	Investigators were not blinded to groups in in vitro or in vivo studies as this was necessary information to carry out studies.

Reporting for specific materials, systems and methods

We require information from authors about some types of materials, experimental systems and methods used in many studies. Here, indicate whether each material, system or method listed is relevant to your study. If you are not sure if a list item applies to your research, read the appropriate section before selecting a response.

Materials & experimental systems

n/a	Involved in the study
☐	☒ Antibodies
☐	☒ Eukaryotic cell lines
☒	☐ Palaeontology and archaeology
☐	☒ Animals and other organisms
☒	☐ Clinical data
☒	☐ Dual use research of concern
☒	☐ Plants

Methods

n/a	Involved in the study
☒	☐ ChIP-seq
☐	☒ Flow cytometry
☒	☐ MRI-based neuroimaging

Antibodies

Antibodies used

The antibodies used in the study are listed below. They are listed in the following format: antigen target, clone name, supplier, catalog number, manufacturer link.

For immunofluorescence:
1. Anti-chicken ovalbumin, EPR27117-90, Abcam, ab306591, https://www.abcam.com/en-us/products/primary-antibodies/ovalbumin-antibody-epr27117-90-ab306591#
2. Anti-CD11b (murine), M1/70, Abcam, ab8878, https://www.abcam.com/en-us/products/primary-antibodies/cd11b-antibody-m1-70-ab8878

For immunoblotting:
1. Anti-6xHis, αTHE, Genscript, A00186S, https://www.genscript.com/antibody/A00186S-THE_His_Tag_Antibody_mAb_Mouse.html
2. Anti-DnaK, 8E2/2, Abcam, ab69617, https://www.abcam.com/en-us/products/primary-antibodies/dnak-antibody-8e2-2-ab69617

For flow cytometry, the fluorochrome-conjugated anti-mouse antibodies used were:
1. CD4-PEDazzle594, RM4-5, Biolegend, 100565, https://www.biolegend.com/en-us/products/pe-dazzle-594-anti-mouse-cd4-antibody-9845
2. NKp46-BV605, 29A1.4, BD Biosciences, 564069, https://www.bdbiosciences.com/en-us/products/reagents/flow-cytometry-reagents/research-reagents/single-color-antibodies-ruo/bv605-rat-anti-mouse-cd335-nkp46.564069
3. NK1.1-BUV395, PK136, BD Biosciences, 564144, https://www.bdbiosciences.com/en-us/products/reagents/flow-cytometry-reagents/research-reagents/single-color-antibodies-ruo/buv395-mouse-anti-mouse-nk-1-1.564144
4. CD45-BV650, 30-F11, Biolegend, 103151, https://www.biolegend.com/en-us/products/brilliant-violet-650-anti-mouse-cd45-antibody-11987
5. CD45-BUV395, 30-F11, BD Biosciences, 564279, https://www.bdbiosciences.com/en-us/products/reagents/flow-cytometry-reagents/research-reagents/single-color-antibodies-ruo/buv395-rat-anti-mouse-cd45.564279
6. B220-BUV496, RA3-6B2, BD Biosciences, 612950, https://www.bdbiosciences.com/en-us/products/reagents/flow-cytometry-reagents/research-reagents/single-color-antibodies-ruo/buv496-rat-anti-mouse-cd45r-b220.612950
7. CD19-APC/Fire810, 6D5, Biolegend, 115577, https://www.biolegend.com/en-us/products/apc-fire-810-anti-mouse-cd19-antibody-20595?GroupID=BLG10556
8. CD8a-AF700, 53-6.7, Biolegend, 100729, https://www.biolegend.com/en-us/products/alexa-fluor-700-anti-mouse-cd8a-antibody-3387
9. TIM1-BV421, RMT1-4, BD Biosciences, 566336, https://www.bdbiosciences.com/en-us/products/reagents/flow-cytometry-reagents/research-reagents/single-color-antibodies-ruo/BV421-Rat-Anti-Mouse-CD365-(TIM-1).566336
10. CD69-BUV563, H1.2F3, BD Biosciences, 741234, https://www.bdbiosciences.com/en-us/products/reagents/flow-cytometry-reagents/research-reagents/single-color-antibodies-ruo/buv563-hamster-anti-mouse-cd69.741234
11. Foxp3-FITC, FJK-16s, Thermo, 11-5773-82, https://www.thermofisher.com/antibody/product/FOXP3-Antibody-clone-FJK-16s-Monoclonal/11-5773-82
12. CD3ε-BV785, 145-2C11, Biolegend, https://www.biolegend.com/en-us/clone-search/brilliant-violet-785-anti-mouse-cd3epsilon-antibody-12081
13. CD3ε-PerCP/Cy5.5, 145-2C11, Biolegend, 100327, https://www.biolegend.com/en-us/products/percp-cyanine5-5-anti-mouse-cd3epsilon-antibody-4191
14. TCRβ-BV711, H57-507, BD Biosciences, 563135, https://www.bdbiosciences.com/en-us/products/reagents/flow-cytometry-reagents/research-reagents/single-color-antibodies-ruo/bv711-hamster-anti-mouse-tcr-chain.563135
15. Ki67-PE, SolA15, Thermo, 12-5698-80, https://www.thermofisher.com/antibody/product/Ki-67-Antibody-clone-SolA15-Monoclonal/12-5698-80
16. GranzymeB-PE-Cy7, QA16A02, Biolegend, 372213, https://www.biolegend.com/en-us/products/pe-cyanine7-anti-humanmouse-granzyme-b-recombinant-antibody-15582
17. TNFα-AF647, MP6-XT22, Biolegend, 506314, https://www.biolegend.com/en-us/products/alexa-fluor-647-anti-mouse-tnf-alpha-antibody-2724
18. IFN -PE, XMG1.2, Biolegend, 505807, https://www.biolegend.com/en-us/products/pe-anti-mouse-ifn-gamma-antibody-997
19. Ly6C-FITC, HK1.4, Biolegend, 128005, https://www.biolegend.com/en-us/products/fitc-anti-mouse-ly-6c-antibody-4896
20. I-A/I-E-BV480, M5/114.15.2, BD Biosciences, 566088, https://www.bdbiosciences.com/en-us/products/reagents/flow-cytometry-reagents/research-reagents/single-color-antibodies-ruo/bv480-rat-anti-mouse-i-a-i-e.566088
21. I-A/I-E-PerCP/Cy5.5, M5/114.15.2, BD Biosciences, 562363, https://www.bdbiosciences.com/en-us/products/reagents/flow-cytometry-reagents/research-reagents/single-color-antibodies-ruo/percp-cy-5-5-rat-anti-mouse-i-a-i-e.562363
22. XCR1-BV605, ZET, Biolegend, 148222, https://www.biolegend.com/en-us/products/brilliant-violet-605-anti-mouse-rat-xcr1-antibody-22025
23. CD11b-AF700, M1/70, Biolegend, 101222, https://www.biolegend.com/en-us/products/alexa-fluor-700-anti-mouse-human-cd11b-antibody-3388

24. CD11b-BV650, M1/70, Biolegend, 101239, https://www.biolegend.com/en-us/products/brilliant-violet-650-anti-mouse-human-cd11b-antibody-7638?GroupID=BLG10599
25. CD103-BV785, 2E7, Biolegend, 121439, https://www.biolegend.com/en-us/products/brilliant-violet-785-anti-mouse-cd103-amtibody-17353
26. F4/80-PE-Cy5, BM8, Biolegend, 123111, https://www.biolegend.com/en-us/products/pe-cyanine5-anti-mouse-f4-80-antibody-4069
27. F4/80-APC, BM8, Biolegend, 123115, https://www.biolegend.com/en-us/products/apc-anti-mouse-f4-80-antibody-4071
28. CD11c-BUV737, HL3, BD Biosciences, 612796, https://www.bdbiosciences.com/en-us/products/reagents/flow-cytometry-reagents/research-reagents/single-color-antibodies-ruo/buv737-hamster-anti-mouse-cd11c.612796
29. CD172a-BUV563, P84, Biolegend, 741349, https://www.bdbiosciences.com/en-us/products/reagents/flow-cytometry-reagents/research-reagents/single-color-antibodies-ruo/buv563-rat-anti-mouse-cd172a.741349
30. Ly6G-APC/Fire810, 1A8, Biolegend, 127669, https://www.biolegend.com/en-us/products/apc-fire-810-anti-mouse-ly-6g-antibody-21380
31. Ly6G-PE-CF594, 1A8, BD Biosciences, 562700, https://www.bdbiosciences.com/en-us/products/reagents/flow-cytometry-reagents/research-reagents/single-color-antibodies-ruo/pe-cf594-rat-anti-mouse-ly-6g.562700
32. PDL1-PE-Cy7, 10F.9G2, Biolegend, 124313, https://www.biolegend.com/en-us/products/pe-cyanine7-anti-mouse-cd274-b7-h1-pd-l1-antibody-6721
33. CD301b-AF647, URA-1, Biolegend, 146805, https://www.biolegend.com/en-us/products/alexa-fluor-647-anti-mouse-cd301b-mgl2-antibody-9657
34. CD19-PerCP/Cy5.5, 1D3, Biolegend, 152405, https://www.biolegend.com/en-us/products/percp-cyanine5-5-anti-mouse-cd19-antibody-13640
35. NK1.1-PerCP/Cy5.5, PK136, Biolegend, 108727, https://www.biolegend.com/en-us/products/percp-cyanine5-5-anti-mouse-nk-11-antibody-4289
36. NKp46-BV510, 29A1.4, Biolegend, 137623, https://www.biolegend.com/en-us/products/brilliant-violet-510-anti-mouse-cd335-nkp46-antibody-9578
37. CD64-PEDazzle594, X54-5/7.1, Biolegend, 139319, https://www.biolegend.com/en-us/products/pe-dazzle-594-anti-mouse-cd64-fcgammari-antibody-12424
38. CD80-PE, 16-10A1, Biolegend, 104707, https://www.biolegend.com/en-us/products/pe-anti-mouse-cd80-antibody-43
39. CD86-BUV805, GL-1, BD Biosciences, 741946, https://www.bdbiosciences.com/en-us/products/reagents/flow-cytometry-reagents/research-reagents/single-color-antibodies-ruo/buv805-rat-anti-mouse-cd86.741946
40. H2Kb-SIINFEKL-PE, 25-D1.16, Biolegend, 141603, https://www.biolegend.com/en-us/products/pe-anti-mouse-h-2kb-bound-to-siinfekl-antibody-7247
41. CD3-PE, 17A2, Biolegend, 100205, https://www.biolegend.com/en-us/products/pe-anti-mouse-cd3-antibody-47

For in-vivo antibody depletion:
1. Anti-mouse CD4, clone GK1.5, BioXcell, #BE0003-1, https://bioxcell.com/invivomab-anti-mouse-cd4-be0003-1
2. Anti-mouse CD8b, clone Ly-3.2, BioXcell, #BE0223, https://bioxcell.com/invivomab-anti-mouse-cd8-beta-lyt-3-2-be0223?queryID=968b7720c10d16b0d5bb810a89b7bd1f&objectID=30662&indexName=bioxcell_live_default_products
3. IgG1 isotype control, clone HRPN, BioXcell, #BE0088, https://bioxcell.com/invivomab-rat-igg1-isotype-control-anti-horseradish-peroxidase-be0088?queryID=c68a9872d06a3d920db5f601de05fe61&objectID=30559&indexName=bioxcell_live_default_products

Validation

All antibodies used in this study are commercially available, and were validated by the manufactures, which can be accessed through the link provided for each antibody listed.

Eukaryotic cell lines

Policy information about cell lines and Sex and Gender in Research

Cell line source(s)	B16F10 (ATCC CRL-6475), CT26 (ATCC CRL-2638), 4T1 (ATCC CRL-2539)
Authentication	Cells were frozen down at early passages after receipt from ATCC and thus did not require re-authetication.
Mycoplasma contamination	Cells were confirmed mycoplasma free.
Commonly misidentified lines (See ICLAC register)	No commonly misidentified cell lines were used.

Animals and other research organisms

Policy information about studies involving animals; ARRIVE guidelines recommended for reporting animal research, and Sex and Gender in Research

Laboratory animals	Mice were housed in a facility with a 12-hour light-dark cycle, and provided unrestricted access to both food and water. The housing facility was maintained at 21–24°C, and kept at 40-60% humidity. Animals used included female 6-7 week old BALB/c, C57BL/6, and B6(Cg)-Tyrc-2J/J mice.
Wild animals	No wild animals were used in this study.
Reporting on sex	Female mice were used in animal studies, as male mice exhibit aggressive behaviors and fight which we noted to cause wounding to the tumors and one another, which can affect experimental outcomes (PMCIDs: PMC9817818, PMC7538892).
Field-collected samples	No field-collected samples were used in this study.

Ethics oversight	Institutional Animal Care and Use Committee (IACUC) of Columbia University (Protocol: AABQ5551)

Note that full information on the approval of the study protocol must also be provided in the manuscript.

Flow Cytometry

Plots

Confirm that:

☒ The axis labels state the marker and fluorochrome used (e.g. CD4-FITC).

☒ The axis scales are clearly visible. Include numbers along axes only for bottom left plot of group (a 'group' is an analysis of identical markers).

☒ All plots are contour plots with outliers or pseudocolor plots.

☒ A numerical value for number of cells or percentage (with statistics) is provided.

Methodology

Sample preparation	Tumors and TDLN were extracted either 2 or 8 days post intravenous treatment for flow cytometry immunophenotyping. Lymphoid and myeloid immune subsets were isolated from tumor tissue by medechanical homogenization of tumor or TDLN tissue, followed by digestion with collagenase A (1mg/ml, Roche) and DNase I (0.5 µg/ml, Roche) in isolation buffer (RPMI 1640 with 5% FBS, 1% L-glutamine, 1% penicillin-streptomycin, and 10mM HEPES) for 1 hour at 37°C for tumors or 30 minutes at 37°C for TDLNs, on a shaker platform at 150rpm. For ex vivo lymphocyte stimulation with PMA and ionomycin, TDLNs were not digested prior. Tumor and TDLN homogenates were filtered through 100 µm cell strainers and washed in isolation buffer. To measure cytokine production by T cells, cells were stimulated for 3-hours with PMA (50ng/ml, Sigma-Aldrich) and ionomycin (1nM, Calbiochem) in the presence of brefeldin A (1µg/ml). To measure neoantigen-specific cytokine production by T cells, cells were stimulated for 5 hours with pools of peptides (2µg/ml) representing the neoantigens encoded in therapeutic strains in the presence of brefeldin A (1µg/ml). Cells were stained in FACS buffer. Ghost Dye cell viability reagent was used to exclude dead cells (diluted 1:1000 in PBS), followed by extracellular staining. After extracellular staining, cells were washed with FACS buffer, and either directly used for flow cytometry analysis, or fixed using the FOXP3/ transcription factor staining buffer set (Tonbo), as per manufacturer's instructions. Cells were then stained intracellularly for lymphoid immunophenotyping panels. After staining, cells were washed and resuspended with FACS buffer for flow cytometry analysis.
Instrument	BD LSRFortessa, Cytek Aurora cell analyzer.
Software	Collection: FACS Diva v8.0. or SpectroFlo v3.0. Analysis: Flowjo v10.0.
Cell population abundance	Cell population abundance depends on the particular cell type, tissue type, and treatment conditions. All cell populations were identifiable by flow cytometry following digestion of either tumor or TDLN.
Gating strategy	Pre-processed FSC files were initially gated on FSC-A and SSC-A to exclude large and small debris or clumps. FSC-H vs. FSC-A, followed by SSC-H vs. SSC-A were used to exclude non-singlet events. CD45 vs. Viability dye were gated to include all live lymphocytes. For myeloid cell analysis: PMNs were defined as CD45+CD11b+Ly6G+ cells. Macrophages were defined as CD45+CD11b +Ly6G-Ly6C-F4/80+ cells. Monocytes were defined as CD45+CD11b+Ly6G-Ly6C+F4/80-Lin-CD64+MHCII+. M-MDSC cells were defined as CD45+CD11b+Ly6G-Ly6c+F4/80-MHCII-CD64- cells. cDC1 were defined as CD45+Ly6G-Ly6c-F4/80-CD11c+MHCII +CD11b-CD172a-Lin-XCR1+ and/or CD103+ cells. cDC2 were defined as CD45+Ly6G-CD11b+CD172a+/-Ly6C-F4/80+/-CD11c +MHCII+Lin-CD103-, and also CD301b+ in the B16 model. Expression markers (PD-L1, CD80, CD86) were gated on major lineage cells ex vivo. For lymphoid cell analysis: B cells were defined as CD45+CD19/B220+NK1.1-CD3-TCRb-. NKp46 was used in place of NK1.1 for BALB/c mice. CD8+ T cells were defined as CD45+CD19/B220-NK1.1-CD3+TCRb+CD4-CD8+. Conventional Foxp3-CD4+ T cells were defined as CD45+CD19/B220-NK1.1-CD3+TCRb+CD8-Foxp3-CD4+ cells. NK cells were defined as CD45+CD19/B220-CD3-TCRb-NK1.1+ cells. Expression markers (CD69, Granzyme-B, Ki67) were gated on major lineage cells ex vivo, while cytokines (IFNy, TNFa) were gated post stimulation.

☒ Tick this box to confirm that a figure exemplifying the gating strategy is provided in the Supplementary Information.